Title: Antimicrobial overproduction sustains intestinal inflammation by inhibiting *Enterococcus* colonization

Kyung Ku Jang[1], Thomas Heaney[1], Mariya London[1], Yi Ding[2], Frank Yeung[1], Defne Ercelen[1], Ying-Han Chen[1], Jordan Axelrad[3], Sakteesh Gurunathan[3], A. Marijke Keestra-Gounder[4], Matthew E. Griffin[5#], Howard C. Hang[5,6], and Ken Cadwell[7,8,9*]

[1]Department of Microbiology, New York University Grossman School of Medicine, New York, NY 10016, USA

[2]Department of Laboratory Medicine, Geisinger Health, Danville, PA 17822, USA

[3]Division of Gastroenterology and Hepatology, Department of Medicine, New York University Grossman School of Medicine, New York, NY 10016, USA

[4]Department of Immunology and Microbiology, University of Colorado School of Medicine, Anschutz Medical Campus, Aurora, CO 80045, USA

[5]Department of Immunology and Microbiology and Department of Chemistry, Scripps Research, 10550 North Torrey Pines Road, La Jolla, CA 92037, USA

[6]Department of Chemistry, Scripps Research, 10550 North Torrey Pines Road, La Jolla, CA 92037, USA

[7]Division of Gastroenterology and Hepatology, Department of Medicine, University of Pennsylvania Perelman School of Medicine, Philadelphia, PA 19104, USA

[8]Department of Systems Pharmacology and Translational Therapeutics, University of Pennsylvania Perelman School of Medicine, Philadelphia, PA 19104, USA

[9]Department of Pathology and Laboratory Medicine, University of Pennsylvania Perelman School of Medicine, Philadelphia, PA 19104, USA

#Present address: Department of Chemistry, University of California, Irvine, Irvine, CA 92617, USA

[*]Correspondence:

Ken Cadwell

Professor

Email: Ken.Cadwell@Pennmedicine.upenn.edu

Office: 212-263-8891

SUMMARY

Loss of antimicrobial proteins such as REG3 family members compromises the integrity of the intestinal barrier. Here, we demonstrate that overproduction of REG3 proteins can also be detrimental by reducing a protective species in the microbiota. Patients with inflammatory bowel disease (IBD) experiencing flares displayed heightened levels of secreted REG3 proteins that mediated depletion of *Enterococcus faecium* (*Efm*) from the gut microbiota. *Efm* inoculation of mice ameliorated intestinal inflammation through activation of the innate immune receptor NOD2, which was associated with the bacterial DL-endopeptidase SagA. Microbiota sensing by NOD2 in myeloid cells mediated IL-1β secretion and increased the proportion of IL-22-producing $CD4^+$ T helper cells and innate lymphoid cells. Finally, *Efm* was unable to protect mice carrying a *NOD2* gene variant commonly found in IBD patients. Our findings demonstrate that inflammation self-perpetuates by causing aberrant antimicrobial activity that disrupts symbiotic relationships with gut microbes.

Keywords: Enterococci, antimicrobial proteins, REG3, NOD2, and inflammatory bowel disease

INTRODUCTION

Secretion of antimicrobial proteins (AMPs) at barrier surfaces represents a ubiquitous and evolutionarily ancient defense strategy. AMPs such as defensins, cathelicidins, lysozyme, and C-type lectins are abundant in the mammalian gastrointestinal tract where they limit the overgrowth or invasion of microbes, typically by disrupting membrane integrity of their targets[1-3]. Although certain AMPs recognize structures associated with invasive microbes such as flagellin[4], many display broad-spectrum activity, reflecting the diversity of pathogenic and non-pathogenic infectious agents in the gut. Regenerating family member 3 (REG3) C-type lectins REG3A and REG3G bind to the peptidoglycan cell wall of Gram-positive (+) bacteria and are essential for maintaining a balanced relationship with the gut microbiota[5,6]. *Reg3γ* expression in mice is induced by toll-like receptor (TLR) signaling in the intestinal epithelium to achieve spatial segregation between the host and the microbiota[7-9]. REG3A (also known as HIP/PAP) is the main paralog that has been characterized in humans and may have a similar role as murine REG3G because transgenic expression of the human gene in mice alters microbiota composition[10]. In addition to inducing lysis of microbes, REG3 proteins contribute to intestinal homeostasis by regulating crypt regeneration and scavenging reactive oxygen species[10,11]

Dysregulated AMP production exacerbates intestinal injury in animal models and is associated with human inflammatory bowel disease (IBD)[12-17], a chronic immune-mediated disorder of the gut involving complex interactions between genetic and environmental factors. IBD affects more than 6 million worldwide, and although immunomodulatory medications can offer substantial relief to patients, maintaining disease remission remains a major clinical challenge. Consistent with the link between AMPs and intestinal inflammation, an altered microbiota composition is a common feature of IBD[18-20]. Also, population genetic studies have implicated genes associated with host-microbe interactions[21,22]. Coding region variants of the intracellular microbial sensor nucleotide-binding oligomerization domain-containing protein 2 (NOD2) are among the strongest genetic risk factors for IBD[23,24]. In the presence of peptidoglycan byproducts, NOD2 mediates production of AMPs and cytokines downstream of NFκB activation[23]. Accordingly, *Nod2*-deficient mice are susceptible to enteric bacterial infections and display an altered microbiota composition depending on the animal facility[25-34], and IBD patients harboring *NOD2* variants display impaired production of AMPs, especially defensins[35-37]. However, *NOD2* variants are found in only a subset of IBD patients, indicating that additional mechanisms may be involved. Also, IBD is associated with increased *REG3* expression[38,39], suggesting a different role for this family of AMPs in disease pathogenesis.

97 The *Enterococcus* genus includes Gram+ bacterial members of the gut microbiota that activate
98 and are controlled by NOD2[40-42], and are highly sensitive to killing by REG3A and REG3G[6,9].
99 However, the relationship between enterococci and IBD is obfuscated by contradictory
100 observations. *Enterococcus* species are opportunistic pathogens in hospital settings that cause
101 life-threatening bloodstream infections[43] and induce intestinal inflammation in *Il10* deficient
102 mice[44,45]. Yet, enterococci are consumed as probiotics for treatment of diarrheal diseases[46,47].
103 Recent studies have provided a mechanistic basis for their probiotic properties by identifying a
104 DL-endopeptidase, SagA, secreted by certain enterococci including *Enterococcus faecium*
105 (*Efm*)[48-50]. Processing of peptidoglycan by SagA generates muropeptides, which potently activate
106 NOD2 to induce an antimicrobial and inflammatory gene expression program that enhances
107 colonization resistance towards enteric pathogens and antitumor immunity[41,50,51]. Interventions
108 that promote antitumor immunity typically exacerbate intestinal inflammation[52]. Therefore, it is
109 unclear whether NOD2 activation by enterococci would worsen or improve IBD.
110 In this study, we found IBD patients displayed uncontrolled production of REG3 proteins that
111 deplete enterococci from the gut microbiota. Inoculation with *Efm* or a *Lactococcus* strain
112 engineered to express *SagA* protected mice from intestinal injury. Protection was dependent on
113 NOD2 activity in myeloid cells, which mediated an increase in lymphoid cells producing the
114 regenerative cytokine IL-22. This beneficial effect of *Efm* colonization was abrogated in mice
115 harboring the R702W variant of NOD2 associated with IBD. Our findings uncover a mechanism
116 of perpetuating intestinal inflammation initiated by a harmful feedback loop involving excess AMP
117 production and depletion of protective enterococci, which renders the host functionally NOD2-
118 deficient.
119

RESULTS

REG3 proteins overproduced by IBD patients inhibit enterococci

Although *REG3A* mRNA was shown to be increased in inflamed intestinal tissues from IBD patients[38,39], only a small number of samples were analyzed in these prior studies, and it is unclear whether gene expression is associated with REG3 protein secretion and activity. Thus, the functional consequence has not been investigated. To measure antimicrobial activity in the gut, we collected stool from 56 IBD patients experiencing disease flares (Supplemental table 1). An equal number of non-IBD patients (NIBD) experiencing gastrointestinal symptoms, such as diarrhea, were used as a control cohort (Supplemental table 2). Stool extracts were prepared by 2-step filtrations (see METHOD DETAILS) and subjected to Western blot analysis of the two human REG3 family members, REG3A and REG3G (Figure 1A). We also examined two additional paralogs: REG1A, which is a pancreatic growth factor and should not be co-regulated with REG3 proteins[53], and REG4, a potential AMP that is less characterized[54,55]. As we expected, pancreatic growth factor REG1A is equally present in NIBD and IBD (Figure 1B and C). In contrast, REG3A was detected in a higher proportion of IBD patients compared with NIBD patients, and REG3G and REG4 were exclusively present in IBD samples (Figure 1B and C). An ELISA assay confirmed higher REG3A concentration in stool extracts from IBD compared with those of NIBD (Figure 1D). These results indicate that the presence of REG3 proteins is more prevalent and enriched in IBD patients.

Next, we examined the antimicrobial activity of the IBD and NIBD-derived stool extracts against *Enterococcus faecalis* (*Efl*) and *Salmonella* Typhimurium (*S*Tm) as representative Gram+ and –enteric bacteria, respectively. The number of *Efl* colonies recovered after culturing in IBD stool extracts was significantly lower compared with NIBD stool extracts, whereas *S*Tm numbers were similar in both groups. (Figure 1E). We confirmed this antimicrobial activity of IBD stool extracts with another *Enterococcus* species, *Efm* (Figure 1E). Consistent with Gram+ bacterial targeting, REG3A concentration negatively correlated with *Efl* and *Efm* colony forming units (CFUs) following treatment with NIBD and IBD stool extracts, but not with *S*Tm CFUs (Figure 1F). To determine whether the antimicrobial activity in stool samples was dependent on REG3 proteins, we added anti-REG3A or -REG3G antibodies, individually or together, to *Efm* cultured in the stool extracts. Less *Efm* was recovered when grown in IBD stool extracts compared with PBS control, and this antimicrobial activity was inhibited by antibodies against REG3A or REG3G, but not REG1A control antibodies (Figure 1G). Unlike IBD samples, an increased number of *Efm* was recovered when cultured in NIBD stool extracts compared with PBS control, and adding anti-

154 REG3A and REG3G antibodies together (but not individually) enhanced growth, suggesting low
155 levels of antimicrobial activity was present in these samples (Figure 1G). Thus, *Efm* growth
156 impairment in human stool extracts is attributed to REG3A and REG3G.
157 We next segregated the data based on sex, disease type and severity, and age. IBD stool
158 extracts from both males and females displayed higher amounts of REG3A compared with NIBD
159 samples (Supplemental figure 1A). IBD consists of two major forms, Crohn's disease (CD) and
160 ulcerative colitis (UC); REG3A concentrations were similar in stool from CD and UC patients
161 (Supplemental figure 1B). REG3A concentration did not differ among age groups in NIBD patients,
162 however, displayed a modest but significant inverse relationship with age among IBD patients
163 (Supplemental figure 1C). When controlling for age, we found that IBD patients younger than age
164 60 displayed increased levels of REG3A compared with matched NIBD controls, and this
165 difference was lost in the older age group (Supplemental figure 1D). Disease severity
166 measurements of CD (Crohn's disease activity index, CDAI) and UC (total Mayo) displayed a
167 positive correlation with REG3A concentrations (Figure 1H). Thus, the combined results suggest
168 that the increase in REG3 in stool from IBD patients, proportional to disease severity, inhibits
169 *Enterococcus* species.
170
171 ***Enterococcus* and *Efm* are lost from the gut microbiota in IBD patients**
172 The above results raise the possibility that *Enterococcus* is depleted in the gut microbiota of
173 IBD patients. Analysis of stool by 16S rRNA sequencing indicated that the overall microbiota
174 composition of NIBD and IBD were indistinguishable according to multiple metrics of alpha and
175 beta diversities (Figure 2A and B). These results further confirm that our NIBD cohort is an
176 appropriate control for IBD patients. However, >80% of the sequencing reads aligned to
177 *Enterococcus* in one of the NIBD samples, indicating that this individual had an overabundance
178 of *Enterococcus* and thus, we excluded this patient from subsequent analyses. Consistent with
179 our *in vitro* findings (Figure 1), the relative abundance of *Enterococcus* in IBD patients was lower
180 than that in NIBD patients (Figure 2C).
181 To confirm our 16S sequencing result, we plated NIBD and IBD stool on media that allows
182 enumeration of enterococci or that is selective for *Efm*. The burden and detection rate of total
183 *Enterococcus* and *Efm* in IBD stools were lower than in NIBD stools (Figure 2D and Supplemental
184 figure 1E). *Efm* accounted for less than 20% of the total enterococci present in IBD stool compared
185 with 49% in NIBD stool, indicating that *Efm* was particularly vulnerable to depletion in IBD patients.
186 (Supplemental figure 1F). REG3A concentration displayed a negative correlation with total
187 *Enterococcus* and *Efm* burden in IBD patient-derived stool (Figure 2E) as well as with CDAI and

188 total Mayo score (Figure 2F). These results, combined with *in vitro* bacterial culturing data,
189 indicate that levels of enterococci including *Efm* are reduced by the increased REG3 proteins in
190 IBD patients.
191
192 **Enterococci protect against intestinal injury in mice**
193 We next wanted to examine the relationship between *Enterococcus* dynamics and intestinal
194 inflammation. While performing experiments to determine the appropriate conditions for
195 administering dextran sulfate sodium (DSS) in drinking water, a widely used model of intestinal
196 chemical injury, we observed extreme differences in susceptibility between wild-type (WT)
197 C57BL/6J (B6) mice bred in two rooms within the same institutional vivarium. Mice bred in room
198 6 receiving 5% DSS displayed higher lethality, weight loss, and disease score compared with
199 mice raised in room 13 (Figure 3A-C). Lipocalin-2 (LCN2), a marker of inflammation[56], was also
200 more abundant in stool from DSS-treated room 6 mice compared with room 13 mice (Figure 3D).
201 Susceptibility to DSS can diverge between B6 mice, even those bred in the same animal facility,
202 due to differences in microbiota composition that arise from separate parental lineages[57,58].
203 Because we were performing these experiments with the goal of investigating enterococci, we
204 plated stool specimens to examine their presence in the microbiota and observed a 2-log higher
205 burden of endogenous enterococci in room 13 mice than room 6 mice (Figure 3E). Similar to the
206 inverse relationship with inflammation observed in human samples, *Enterococcus* levels
207 decreased following DSS-induced intestinal inflammation in mice (Figure 3F). In all subsequent
208 experiments, we used mice from room 6.
209 To determine whether *Enterococcus* colonization protects against intestinal injury, we
210 inoculated mice by administering *Efm* in the drinking water (10^9 CFU/ml) for 2 weeks[59] and then
211 switched to water containing 5% DSS for an additional 6 days. Body weight and fecal LCN2
212 concentration were unchanged in mice inoculated with *Efm* in the absence of DSS treatment
213 (Supplemental figure 2A and B), confirming that *Efm* colonization does not induce inflammation.
214 In mice receiving DSS, both total *Enterococcus* and *Efm* levels decreased during the treatment
215 and partially recovered after cessation (Supplemental figure 2C and D). *Efm*-colonized WT B6
216 mice treated with DSS displayed less body weight reduction, disease score, and fecal LCN2
217 compared with DSS-treated mice that were not inoculated with *Efm* (Figure 3G and H and
218 Supplemental figure 2E and F). Mice were sacrificed on day 23 to determine whether
219 improvement of these disease features reflected reduced intestinal inflammation. *Efm*-colonized
220 mice displayed less shortening of the colon (a marker of intestinal inflammation) and
221 histopathologic changes compared with uncolonized WT mice (Figure 3I-K and Supplemental

222 table 3). Inoculating mice with *Efm* after DSS treatment also mitigated these signs of disease
223 (Supplemental figure 3A-G and Supplemental table 3). Therefore, *Efm* colonization confers
224 protection against DSS-induced inflammation.
225 Given that *Efm* protects against enteric pathogens in a NOD2-dependent manner[41], we asked
226 whether *Efm* would lose its beneficial properties when administered to *Nod2*-deficient mice during
227 intestinal injury. The colonization patterns of *Efm* in *Nod2*$^{+/-}$ and *Nod2*$^{-/-}$ mice were consistent with
228 those in WT mice (Supplemental figure 2G). In contrast to *Nod2*$^{+/-}$ mice in which we reproduced
229 the protective effect of the bacterium, *Efm* administration to *Nod2*$^{-/-}$ mice did not improve weight
230 loss, disease score, fecal LCN2 concentration, colon shortening, and intestinal histopathology
231 (Figure 3L-P, Supplemental figure 2H and I, and Supplemental table 3). These findings indicate
232 that the anti-inflammatory effect of *Efm* is dependent on *Nod2*.
233
234 **SagA mediates NOD2-dependent protection against intestinal injury**
235 *Efm* encodes a secreted DL-endopeptidase SagA that processes peptidoglycan to generate
236 NOD2-stimulating muropeptides[41,50]. Because SagA is essential for growth of *Efm*[60], we tested
237 the role of SagA by orally inoculating mice with *Lactococcus lactis* (*Lls*) strains expressing wild-
238 type SagA (*Lls-SagA*^{WT}) or catalytically inactive (C443A) SagA (*Lls-SagA*^{C443A}), then treating with
239 3% DSS (Supplemental figure 4A). A lower concentration of DSS was used because mice were
240 pre-treated with antibiotics (abx) to facilitate *Lls* colonization, and abx increases susceptibility to
241 DSS [61,62]. We included conditions in which mice were inoculated with PBS or the parental
242 unmodified *Lls* strain to control for effects of abx treatment and *Lls* colonization, respectively. *Lls*
243 strains displayed a similar degree of colonization (Supplemental figure 4B and D). Mice given *Lls-*
244 *SagA*^{WT} displayed enhanced survival compared with all the other conditions, and other disease
245 parameters were generally improved (Figure 4A-D and Supplemental figure 4C). *Lls-SagA*^{WT}
246 ameliorated disease in *Nod2*$^{+/-}$ mice but not *Nod2*$^{-/-}$ mice (Figure 4E-H and Supplemental figure
247 4E). If protection is mediated through peptidoglycan processing by secreted SagA, bacterial
248 colonization would potentially be dispensable. To test this possibility, we administered filtered
249 culture supernatants from *Lls* strains to mice without abx treatment for a week and then switched
250 to water containing 5% DSS (Supplemental figure 4F). In contrast to supernatant collected from
251 the parental *Lls* and *Lls-SagA*^{C443A} cultures, or sterile broth, supernatant from *Lls-SagA*^{WT} was
252 sufficient for increasing survival, lessening body weight reduction, and decreasing disease score
253 and fecal LCN2 concentration of DSS-treated mice (Figure 4I and J and Supplemental figure 4G
254 and H). These protective effects of *Lls-SagA*^{WT} culture supernatant were all NOD2-dependent

255 (Figure 4K and L and Supplemental figure 4I and J). Taken together, our findings indicate that
256 activating NOD2 downstream of SagA protects against intestinal injury.
257
258 **NOD2 in myeloid cells is indispensable for *Efm*-mediated protection**
259 Myeloid and intestinal epithelial cells are among the cell types in which NOD2 function has been
260 most extensively investigated[63-65]. Therefore, we developed *Nod2*$^{fl/fl}$*;LysM-Cre* and *Villin-Cre* mice
261 that are *Nod2*-deficient in myeloid and intestinal epithelial cells, respectively, and confirmed the
262 presence of *Efm* in stool samples following inoculation in all groups (Supplemental figure 5A and
263 C). Unlike *Nod2*$^{fl/fl}$ controls in which signs of disease were ameliorated, *Efm* colonization of
264 *Nod2*$^{fl/fl}$*;LysM-Cre*$^{+}$ mice did not improve lethality, body weight reduction, disease score, and
265 LCN2 present in stool samples (Figure 5A-D and Supplemental figure 5B). In contrast, *Efm*
266 colonization reduced mortality, body weight reduction, disease score, and fecal LCN2
267 concentration in *Nod2*$^{fl/fl}$*;Villin-Cre*$^{+}$ mice to a similar extent as *Nod2*$^{fl/fl}$ controls (Figure 5E-H and
268 Supplemental figure 5D). These findings indicate that NOD2 is required in myeloid cells and
269 dispensable in the intestinal epithelium for *Efm*-mediated protection.
270
271 ***Efm* induces IL-22 production by lymphoid cells downstream of myeloid NOD2 to protect**
272 **against intestinal injury**
273 Activation of NOD2 in myeloid cells is frequently associated with pro-inflammatory cytokine
274 production[63-65], which is counterintuitive when considering the anti-inflammatory function
275 observed in the above experiments. One way to reconcile these observations would be if myeloid
276 cells, following NOD2 activation, act on other cell types in the gut to produce factors involved in
277 tissue repair. For example, IL-22 is a major tissue regenerative cytokine and is protective in
278 models of DSS-induced intestinal inflammation similar to the one used here[66,67]. We observed
279 increased IL-22 production in colon explants harvested from WT mice on day 14 following *Efm*
280 administration in the drinking water (prior to DSS) and day 20 (with DSS) compared with mice
281 that did not receive *Efm* (Figure 6A and B). IL-22 secretion was not enhanced by *Efm* colonization
282 in *Nod2*$^{-/-}$ and *Nod2*$^{fl/fl}$*;LysM-Cre*$^{+}$ mice on days 14 and 20 (Figure 6A and B), indicating that *Efm*-
283 mediated induction of IL-22 is dependent on myeloid *Nod2* expression.
284 IL-22 in the gut is typically produced by group 3 innate lymphoid cells (ILC3s) and CD4^{+} T cells.
285 To identify the subset of immune cells that induce IL-22 secretion responding to *Efm* colonization,
286 we isolated colonic lamina propria of WT mice inoculated with *Efm* on day 14 to analyze the
287 immune cell compartment by flow cytometry. Bacterial colonization increased the proportion of
288 both IL-22^{+} ILCs and CD4^{+} T cells in WT mice, and not *Nod2*$^{-/-}$ and *Nod2*$^{fl/fl}$*;LysM-Cre*$^{+}$ mice (Figure

289 6C-F). NOD2 in antigen-presenting cells can induce IL-10 production from regulatory T cells
290 (Tregs)[68]. However, *Efm* did not alter the proportion of IL10$^+$ CD4$^+$ T cells, CD4$^+$ T helper 1 (Tbet$^+$)
291 and 2 (GATA3$^+$) cells, and Tregs (Supplemental figure 6C-F). Also, consistent with ILC3s being a
292 source of IL-22, *Efm* colonization increased the proportion of ILC3s and not ILC1s and ILC2s in
293 a NOD2-dependent manner (Figure 6G and H and Supplemental figure 6G and H). Therefore,
294 *Efm* induces expansion of IL-22-producing CD4$^+$ T cells and ILCs in a myeloid NOD2-dependent
295 manner.
296 Secretion of IL-1β from intestinal myeloid cells induces IL-22 production from ILC3s[69,70]. Also,
297 myeloid cell-derived IL-1β secretion in the gut in response to the microbiota depends on NOD2[71].
298 The secretion of IL-1β, but not the related cytokine IL-18, was induced in *Efm*-colonized WT,
299 *Nod2*$^{+/-}$, and *Nod2*$^{fl/fl}$*;LysM-Cre*$^-$ mice on days 14 and 20 (Figure 6I and J and Supplemental figure
300 6I and J). This *Efm*-mediated IL-1β induction did not occur in *Nod2*$^{-/-}$ and *Nod2*$^{fl/fl}$*;LysM-Cre*$^+$ mice,
301 indicating that *Nod2*-dependent sensing of *Efm* in myeloid cells is required for the upregulated IL-
302 1β secretion (Figure 6I and J and Supplemental figure 6I and J). Therefore, NOD2 in myeloid cells
303 mediates IL-1β secretion in response to *Efm* colonization.
304 To confirm whether IL-22 is required for *Efm*-mediated protection, we developed *Il22ra1*$^{fl/fl}$*;Villin-*
305 *Cre* mice in which *Il22ra1* encoding IL-22 receptor subunit α is deficient in intestinal epithelial cells
306 and confirmed the *Efm* shedding in stool samples following inoculation in all groups
307 (Supplemental figure 6K). *Il22ra1*$^{fl/fl}$*;Villin-Cre*$^+$ mice displayed exacerbated signs of intestinal
308 injury compared with *Il22ra1*$^{fl/fl}$*;Villin-Cre*$^-$ mice regardless of *Efm* colonization (Figure 6K and L
309 and Supplemental figure 6L). In contrast, *Efm* colonization improves mortality, body weight
310 reduction, and disease score in *Il22ra1*$^{fl/fl}$*;Villin-Cre*$^-$ mice (Figure 6K and L and Supplemental
311 figure 6L). Therefore, epithelial response to IL-22 is necessary for *Efm*-mediated protection.
312
313 **The NOD2 R702W equivalent impairs *Efm*-mediated protection in mice**
314 The three major NOD2 variants linked to IBD – R702W, G908R, and a frameshift deletion
315 mutation at L1007 (L1007fs) – result in the loss of muropeptide recognition and NF-κB signaling
316 *in vitro*[72,73]. L1007fs has received the bulk of attention, and mice harboring a similar frameshift
317 mutation display a compromised cytokine response during bloodstream infection by *Efl*[42],
318 confirming that it results in loss-of-function. The R702W variant, despite being the most common
319 and detected in up to 5% of individuals of European descent (Supplemental figure 7A), has not
320 been studied using an *in vivo* model (Figure 7A). Thus, we introduced a knock-in mutation to
321 generate mice harboring the equivalent of the human R702W variant (Q675W, Supplemental
322 figure 7B). We confirmed the absence of other mutations in *Nod2,* and that NOD2 Q675W protein

323 was produced (Supplemental figure 7C and D). After backcrossing with WT B6 mice, we used
324 heterozygous mice (*Nod2*$^{Q675W/+}$) as littermate controls. Like other mice, *Efm* was detected in stool
325 collected from *Nod2*$^{Q675W/+}$ and *Nod2*$^{Q675W/Q675W}$ following administration in drinking water
326 (Supplemental figure 7E). In the absence of *Efm*, *Nod2*$^{Q675W/+}$ and *Nod2*$^{Q675W/Q675W}$ mice displayed
327 modest mortality, weight loss, or disease score following DSS treatment (Figure 7B-D), likely due
328 to the high levels of endogenous *Enterococcus* colonization at the outset of the experiment
329 compared with the other mice raised in the same room (Supplemental figure 7G). Nevertheless,
330 we were able to detect significant differences between *Nod2*$^{Q675W/+}$ and *Nod2*$^{Q675W/Q675W}$ mice. *Efm*
331 colonization did not improve survival, body weight reduction, disease score, fecal LCN2
332 concentration, colon shortening, and intestinal histopathology in *Nod2*$^{Q675W/Q675W}$ mice, and as
333 such, *Efm* colonized mice were more susceptible to DSS than similarly treated *Nod2*$^{Q675W/+}$ mice
334 (Figure 7B-H, Supplemental figure 7F, and Supplemental table 3). These results indicate that the
335 NOD2 R702W equivalent in mice impairs *Efm*-mediated protection.
336

337 **DISCUSSION**

338 In patients with IBD, previous small studies demonstrated excessive *REG3* gene expression
339 despite that AMP secretion is generally associated with an improved mucosal barrier[39]. Here, we
340 revisited this unresolved counterintuitive observation. Functional assays showed increased REG3
341 antimicrobial activity in IBD patients compared with controls matched for gastrointestinal
342 symptoms, indicating that REG3 overproduction is not a general byproduct of diarrheal disease
343 and more likely IBD itself. Based on prior studies demonstrating that enterococci are among the
344 most sensitive bacteria to REG3-mediated killing[6,9], we focused our analysis on this group and
345 showed their reduced presence in IBD patients. Recent findings indicating that *Enterococcus*
346 species activate the IBD susceptibility gene NOD2 led us to hypothesize that these bacteria have
347 anti-inflammatory properties, which we tested in an animal model of intestinal injury. The results
348 from these experiments support a model in which SagA-secreting enterococci such as *Efm*
349 activate NOD2 in myeloid cells to induce IL-1β, leading to an increase in lymphoid cell types that
350 produce the protective cytokine IL-22. Once the inflammation has been resolved, this enhanced
351 IL-22 may maintain optimal REG3 expressions through STAT3 activation[74], perpetuating gut
352 homeostasis. In IBD, either depletion of enterococci due to REG3 overproduction or genetic
353 deficiency in NOD2 function disrupts this anti-inflammatory circuit (Supplemental figure 7H). This
354 model helps explain how IBD patients with intact NOD2 can develop disease presentations similar
355 to those observed in individuals with NOD2 variants once inflammation is established.

356 Excess REG3 likely acts in concert with other mechanisms to disrupt the microbiota of IBD
357 patients. Altered availability of oxygen and nitrate in the inflamed gut favors colonization by
358 facultative anaerobic Enterobacteriaceae species over the strictly anaerobic *Firmicutes*, the
359 phylum that includes enterococci[75,76]. A recent study identified additional *Firmicutes* that encode
360 NOD2-activating DL-endopeptidases such as *Streptococcus cristatus*, *Lactobacillus rhamnosus*,
361 and *Bacteroides caccae*, which are reduced in IBD patients[40]. It is possible that AMP
362 dysregulation exacerbates the depletion of NOD2-activating species that are already vulnerable
363 due to imbalanced redox status of the inflamed environment. Notably, antimicrobial activity was
364 greater in the IBD cohort compared with individuals experiencing gastrointestinal symptoms
365 without IBD. REG3 overproduction may explain why individuals who experience transient
366 gastroenteritis recover while individuals with IBD remain susceptible to disease flare.

367 Our findings have relevance to other disease settings such as cancer. Probiotics engineered to
368 secrete SagA were shown to improve the efficacy of immune checkpoint blockade therapy in
369 reducing tumors in mice[50]. Although adverse events such as colitis have been a major concern
370 for strategies that improve antitumor therapies, our results predict that inducing NOD2 through

371 SagA would promote checkpoint inhibitor efficacy while also reducing intestinal inflammation.
372 However, our findings with the *Nod2 Q675W* knock-in mice suggest that this approach will fail in
373 individuals homozygous for analogous loss-of-function variants of NOD2. Genetic information
374 may be useful in determining eligibility of patients for microbiota-targeting therapies. Additionally,
375 in treating various diseases, administration of live bacteria is associated with substantial safety
376 concerns. In this context, it is notable that we achieved a similar degree of protection against
377 intestinal injury by administering sterile supernatant collected from SagA-producing bacterial
378 cultures. Postbiotic strategies using bacterial products may be a safe alternate to beneficially
379 trigger NOD2.
380
381 **Limitations of the study**
382 The consequence of *Enterococcus* depletion on intestinal inflammation and the immune
383 mechanism was investigated in an animal model. A long-term goal would be to determine whether
384 NOD2 activation by enterococci leads to similar immune responses in humans and ultimately
385 tests the efficacy of therapies designed based on such findings. However, there are significant
386 safety concerns when considering interventions that target these pathways. For instance, IL-1β
387 production promotes intestinal inflammation in the IL-10-deficient setting[77]. Also, our proposed
388 immune circuit induced by NOD2 in myeloid cells is not mutually exclusive with the multitude of
389 other ways in which NOD2 has been shown to protect the intestinal barrier.
390

391 **Figure legend**

392

393 **Figure 1. Increased REG3A and REG3G in IBD patient stool inhibit *Enterococcus*. A)**
394 Schematic of stool extract preparation and analysis. **B)** Western blots of REG1A, REG3A, REG3G,
395 and REG4 in stool extracts from representative 3 non-IBD (NIBD) and 5 IBD patients. **C)**
396 Proportion of stool specimens from individual NIBD (n = 23) and IBD (n = 26) patients in which
397 REG1A, REG3A, REG3G, or REG4 were detectable by western blot. **D)** Quantification of REG3A
398 in NIBD and IBD patients-derived stool extracts by ELISA. **E)** Fold changes in colony forming
399 units (CFU) of *Enterococcus faecalis* (*Efl*) and *Salmonella* Typhimurium (*S*Tm) following 24 hrs
400 of culture in stool extracts from NIBD (n = 56) and IBD (n = 56) patients. Results obtained with *Efl*
401 were confirmed with *E. faecium* (*Efm*) (n = 18 for NIBD and n = 19 for IBD). **F)** Correlation between
402 REG3A concentration and CFU fold changes of *Efl* (upper), *S*Tm (middle), and *Efm* (lower)
403 cultured in stool extract from NIBD and IBD patients. **G)** Fold change in *Efm* CFU at 24 hr-post
404 culture in NIBD (left) and IBD (right) patient-derived stool extract or PBS in the presence of anti-
405 REG1A, REG3A, and REG3G antibodies. N = 13 for NIBD and IBD. **H)** Correlation between
406 REG3A concentration and Crohn's disease activity index (CDAI) for CD patients (n = 31, left) or
407 total Mayo score for ulcerative colitis (UC) patients (n = 24, right). Data points in D-H represent
408 individual patients. Bars represent mean ± SEM and at least three independent experiments were
409 performed. NIBD, non-IBD; *Efl*, *E. faecalis*; *S*Tm, *S.* Typhimurium; *Efm*, *E. faecium*; CDAI, Crohn's
410 disease activity index; UC, ulcerative colitis; r, Pearson correlation coefficient. Indicated *p* values
411 by Fisher's exact test in C, unpaired *t* test, two-tailed in D, E, and G, and simple linear regression
412 analysis in F and H.

413

414 **Figure 2. *Enterococcus* and *Efm* are depleted in gut microbiota from IBD patients. A and**
415 **B)** 16S rRNA sequencing of stool from NIBD and IBD patients from Figure 1. Alpha diversity
416 values calculated as Shannon (right), Faith's phylogenetic diversity (PD) (middle), and Pielou-
417 evenness (right) indices (A). Principle coordinate analyses of beta diversity determined by Bay-
418 Curtis, Jaccard, and Unweighted and Weighted unifrac methods (B). **C)** Proportion of sequencing
419 reads representing *Enterococcus* in NIBD and IBD patient stool. One NIBD sample contained
420 >80% *Enterococcus* indicative of an overabundance, which is shown as a reference on the graph
421 but excluded from statistical analysis and downstream assays. **D)** Total *Enterococcus* (left) and
422 *Efm* (right) CFUs in stool from NIBD (n = 39) and IBD (n = 43) patients. **E)** Correlation between
423 REG3A concentration and the burden of total *Enterococcus* and *Efm* in IBD stool. **F)** Correlation
424 between the burden of total *Enterococcus* and CDAI of CD patients (n = 24, left) and total Mayo

425 score of UC patients (n = 18, right). Data points represent individual patients. Bars represent
426 mean ± SEM and at least three independent experiments were performed. r, Pearson correlation
427 coefficient. Indicated *p* values by Kruskal-Wallis test in A, unpaired *t* test, two-tailed in C and D,
428 and simple linear regression analysis in E and F.
429
430 **Figure 3. *Enterococcus* protects against intestinal injury in a NOD2-dependent manner. A-**
431 **F)** Dextran sulfate sodium (DSS)-induced intestinal injury of wild-type (WT) B6 mice bred in room
432 6 or 13 in the NYU animal facility. The mice were examined for survival (A), changes in body
433 weight (B) and disease score (C), and lipocalin-2 (LCN2) in stool samples at the indicated time
434 points (D). Endogenous *Enterococcus* burden was measured on day 0 (E) and changes in the
435 *Enterococcus* burden on day 3 (F). **G-I)** DSS-treatment of WT mice from room 6 following
436 administration of *Efm* in drinking water or control. The mice were examined for changes in disease
437 score (G), LCN2 in stool at the indicated time points (H), and colon length (I) on day 23. **J and K)**
438 Representative images of hematoxylin and eosin (H&E)-stained sections of the colon (J) and
439 quantification of the proportion of colon affected (K). In the left panel of J, black arrow indicates
440 destroyed colonic epithelium replaced with a diffuse ulcer and pus, and red arrow indicates acute
441 inflammation with primary neutrophils, lymphocytes, plasma cells, and debris of dead cells. A
442 breakdown of histological signs of inflammation by individual mice is listed in Supplemental table
443 3 for this and other figures. **L-N)** DSS-treatment of *Nod2*$^{+/-}$ and *Nod2*$^{-/-}$ mice from room 6 following
444 administration of *Efm* in drinking water or control were examined for changes in disease score (L),
445 LCN2 in stool at the indicated time points (M), and colon length on day 23 (N). **O and P)**
446 Representative images of H&E-stained sections of the colon (O) and quantification of the
447 proportion of colon affected (P). Bars, 200 μm. Data points in D-F, H, I, K, M, N, and P represent
448 individual mice. Data points in B, C, G, and L represent mean ± SEM. Bars represent mean ±
449 SEM and at least three independent experiments were performed. DSS, dextran sulfate sodium;
450 Rm 6, room 6; Rm 13, room 13; WT, wild type. Indicated *p* values by log-rank Mantel-Cox test in
451 A, two-way ANOVA test in B, C, G, and L, unpaired *t* test, two-tailed in D, E, H, I, K, M, N, and P,
452 and paired *t* test, two-tailed in F.
453
454 **Figure 4. SagA mediates NOD2-dependent protection against intestinal injury. A-D)**
455 Antibiotics (ampicillin + streptomycin, abx)-treated WT mice orally inoculated with PBS,
456 *Lactococcus lactis* (*Lls*), *Lls-SagA*^{WT}, or *Lls-SagA*^{C443A} and then given DSS were examined for
457 survival (A), changes in body weight (B) and disease score (C), and LCN2 presence in stool
458 samples at the indicated time points (D). **E-H)** Abx-treated *Nod2*$^{+/-}$ and *Nod2*$^{-/-}$ mice inoculated

459 with *Lls* or *Lls-SagA*^{WT} and then given DSS were examined for survival (E), changes in body
460 weight (F) and disease score (G), and fecal LCN2 at the indicated time points (H). **I and J)** DSS-
461 treated WT mice receiving broth or culture supernatants of *Lls* (S-*Lls*), *Lls-SagA*^{WT} (S-*Lls-SagA*^{WT}),
462 or *Lls-SagA*^{C443A} (S-*Lls-SagA*^{C443A}) as drinking water were examined for survival (I) and changes
463 in body weight (J). **K and L)** DSS-treated *Nod2*$^{+/-}$ and *Nod2*$^{-/-}$ mice receiving S-*Lls* or S-*Lls-SagA*^{WT}
464 as drinking water were examined for survival (K) and changes in disease score (L). All mice were
465 bred in room 6. Data points in D and H represent individual mice. Lines in B, C, and J represent
466 mean. Data points in F, G, and L represent mean ± SEM. Bars represent mean ± SEM and at
467 least two independent experiments were performed. *Lls*, *L. lactis*; S, supernatant. Indicated *p*
468 values by log-rank Mantel-Cox test in A, E, I, and K, two-way ANOVA test in B, C, F, G, J, and L,
469 and unpaired *t* test, two-tailed in D and H.
470
471 **Figure 5. NOD2 in myeloid cells is required for *Efm*-mediated protection. A-H)** DSS-
472 treatment of *Nod2*$^{fl/fl}$*;LysM-Cre*$^{-}$ and *Cre*$^{+}$ mice (A-D) or *Nod2*$^{fl/fl}$*;Villin-Cre*$^{-}$ and *Cre*$^{+}$ mice (E-H)
473 from room 6 following administration of *Efm* in drinking water or control. The mice were examined
474 for survival (A and E), changes in body weight (B and F) and disease score (C and G), and LCN2
475 presence in stool samples at the indicated time points (D and H). Data points in H represent
476 Individual mice. Data points in B-D, F, and G represent mean ± SEM. Bars represent mean ±
477 SEM and at least three independent experiments were performed. Indicated *p* values by log-rank
478 Mantel-Cox test in A and E, two-way ANOVA test in B, C, F, and G, and unpaired *t* test, two-tailed
479 in D and H.
480
481 **Figure 6. *Efm* induces IL-1β and increases the proportion of IL-22-producing lymphoid**
482 **cells to prevent intestinal injury. A and B)** Quantification of IL-22 on days 14 (A) and 20 (B)
483 in the supernatants of gut explants from WT, *Nod2*$^{+/-}$, *Nod2*$^{-/-}$, and *Nod2*$^{fl/fl}$*;LysM-Cre*$^{-}$ and *Cre*$^{+}$
484 mice with and without *Efm* inoculation. **C-F)** Representative flow cytometry plots and
485 quantification of proportion of IL-22^{+} innate lymphoid cells (ILCs) (C and D) and CD4^{+} T helper
486 cells (E and F) of WT, *Nod2*$^{+/-}$, *Nod2*$^{-/-}$, and *Nod2*$^{fl/fl}$*;LysM-Cre*$^{-}$ and *Cre*$^{+}$ mice with and without
487 *Efm* inoculation. **G and H)** Representative flow cytometry plots and quantification of group 3
488 ILCs (ILC3s) from mice in C-F. **I and J)** Quantification of IL-18 (I) and IL-1β (J) in the
489 supernatants of gut explants from A. **K and L)** DSS treatment of *Il22ra1*$^{fl/fl}$*;Villin-Cre*$^{-}$ and *Cre*$^{+}$
490 mice from room 6 following 2-week administration of *Efm* in drinking water or control. The mice
491 were examined for survival (K) and changes in disease score (L). Data points in A, B, D, F, H,
492 I, and J represent individual mice. For A, I, and J, n = 8 (WT), 8 (WT *Efm*), 9 (*Nod2*$^{+/-}$), 10

493 (*Nod2*$^{+/-}$ *Efm*), 10 (*Nod2*$^{-/-}$), 10 (*Nod2*$^{-/-}$ *Efm*), 4 (*Nod2*$^{fl/fl}$*;LysM-Cre*$^{-}$), 3 (*Nod2*$^{fl/fl}$*;LysM-Cre*$^{-}$ *Efm*),
494 4 (*Nod2*$^{fl/fl}$*;LysM-Cre*$^{+}$), and 3 (*Nod2*$^{fl/fl}$*;LysM-Cre*$^{+}$ *Efm*). For B, n = 8 (WT), 8 (WT *Efm*), 6 (*Nod2*$^{+/-}$
495), 8 (*Nod2*$^{+/-}$ *Efm*), 8 (*Nod2*$^{-/-}$), 7 (*Nod2*$^{-/-}$ *Efm*), 8 (*Nod2*$^{fl/fl}$*;LysM-Cre*$^{-}$), 8 (*Nod2*$^{fl/fl}$*;LysM-Cre*$^{-}$ *Efm*),
496 9 (*Nod2*$^{fl/fl}$*;LysM-Cre*$^{+}$), and 8 (*Nod2*$^{fl/fl}$*;LysM-Cre*$^{+}$ *Efm*). For D and F, n =13 (WT), 12 (WT *Efm*),
497 7 (*Nod2*$^{+/-}$), 11 (*Nod2*$^{+/-}$ *Efm*), 10 (*Nod2*$^{-/-}$), 9 (*Nod2*$^{-/-}$ *Efm*), 7 (*Nod2*$^{fl/fl}$*;LysM-Cre*$^{-}$), 7
498 (*Nod2*$^{fl/fl}$*;LysM-Cre*$^{-}$ *Efm*), 8 (*Nod2*$^{fl/fl}$*;LysM-Cre*$^{+}$), and 9 (*Nod2*$^{fl/fl}$*;LysM-Cre*$^{+}$ *Efm*). For H, n = 8
499 (WT), 7 (WT *Efm*), 5 (*Nod2*$^{+/-}$), 7 (*Nod2*$^{+/-}$ *Efm*), 8 (*Nod2*$^{-/-}$), 6 (*Nod2*$^{-/-}$ *Efm*), 7 (*Nod2*$^{fl/fl}$*;LysM-Cre*$^{-}$
500), 7 (*Nod2*$^{fl/fl}$*;LysM-Cre*$^{-}$ *Efm*), 8 (*Nod2*$^{fl/fl}$*;LysM-Cre*$^{+}$), and 9 (*Nod2*$^{fl/fl}$*;LysM-Cre*$^{+}$ *Efm*). Data
501 points in L represent mean ± SEM. Bars represent mean ± SEM and at least two independent
502 experiments were performed. Indicated *p* values by unpaired *t* test, two-tailed in A, B, D, F, H,
503 and J, log-rank Mantel-Cox test in K, and two-way ANOVA test in L.
504
505 **Figure 7. NOD2 Q675W impairs *Efm*-mediated protection. A)** NOD2 protein region targeted
506 by mutagenesis. Arginine at position 702 in human NOD2 and the corresponding glutamine at
507 position 675 in mouse NOD2 are indicated in the red box. Numbers refer to human amino acid
508 positions. **B-F)** DSS-treated *Nod2*$^{Q675W/+}$ and *Nod2*$^{Q675W/Q675W}$ mice with and without *Efm*
509 inoculation were examined for survival (B), changes in body weight (C) and disease score (D),
510 and LCN2 presence in stool samples at the indicated time points (E), and colon length (F) on day
511 23. **G and H)** Representative images of H&E-stained sections of the colon (G) and quantification
512 of the proportion of colon affected (H). Bars, 200 μM. Data points in E, F, and H represent
513 individual mice. Data points in C and D represent mean ± SEM. Bars represent mean ± SEM and
514 at least two independent experiments were performed. CARD, caspase recruitment domain; NBD,
515 nucleotide-binding domain; LRR, leucine-rich repeat domain; Het, heterozygotes; Homo,
516 homozygotes. Indicated *p* values by log-rank Mantel-Cox test in B, two-way ANOVA test in C and
517 D, and unpaired *t* test, two-tailed in E, F, and H.
518
519

520 **Supplemental figure 1. Contribution of patient demographics to REG3A levels and**
521 **antimicrobial activity. A)** REG3A concentration in stool extracts from NIBD and IBD patients
522 from Figure 1 separated by sex. **B)** REG3A concentration in stool extracts from Crohn's disease
523 (CD) or ulcerative colitis (UC) patients. **C)** Correlation between age of NIBD and IBD patients and
524 REG3A concentration. **D)** REG3A concentration in stool extracts segregated into indicated age
525 groups. **E)** Proportion of patients in which *Enterococcus* and *E. faecium* (*Efm*) were detected in
526 stool. **F)** Proportion of *Enterococcus* that are *Efm* in NIBD and IBD stools. Data points in A-D and
527 F represent individual patients. Bars represent mean ± SEM and at least two independent
528 experiments were performed. r, Pearson correlation coefficient. Indicated *p* values by unpaired *t*
529 test, two-tailed in A, D, and F, simple linear regression analysis in C, and Fisher's exact test in E.
530
531 **Supplemental figure 2. *Efm* colonization levels and disease parameters in wild-type and**
532 ***Nod2*-deficient mice. A and B)** Changes in body weight (A) and lipocalin-2 (LCN2) concentration
533 in stool samples at the indicated time points (B) in wild-type (WT) B6 mice following administration
534 of *Efm* in drinking water or control. **C-F)** Dextran sulfate sodium (DSS)-induced intestinal injury of
535 WT mice from room 6 following administration of *Efm* in drinking water or control. The mice were
536 examined for the burden of total *Enterococcus* (C) and *Efm* (D) in the stool, changes in body
537 weight (E), and fecal LCN2 concentration (F) at the indicated time points. **G-I)** DSS-treatment of
538 *Nod2*$^{+/-}$ and *Nod2*$^{-/-}$ mice from room 6 following administration of *Efm* in drinking water or control.
539 The mice were examined for the burden of *Efm* (G) in the stools, changes in body weight (H), and
540 fecal LCN2 concentration (I) at the indicated time points. Data points in B, F, and I and lines in D
541 and G represent individual mice. Data points in A, C, E, and H represent mean ± SEM. Bars
542 represent mean ± SEM and at least three independent experiments were performed. Indicated *p*
543 values by two-way ANOVA test in E and H and unpaired *t* test, two-tailed in F and I.
544
545 **Supplemental figure 3. *Efm* inoculation after DSS administration ameliorates intestinal**
546 **injury. A-E)** WT B6 mice from room 6 received *Efm* in drinking water or control following DSS
547 treatment. The mice were examined for survival (A), changes in body weight (B) and disease
548 score (C), and LCN2 concentration (D) in stool samples at the indicated time points, colon length
549 on days 10 and 20 (E). **F and G)** Representative images of hematoxylin and eosin (H&E)-stained
550 sections of the colon (F) and quantification of the proportion of colon affected (G) on day 10 from
551 mice in A-E. Bars, 200 μM. Data points in D, E, and G represent individual mice from mice in A-
552 C. Data points in B and C represent mean ± SEM. Bars represent mean ± SEM and at least three

553 independent experiments were performed. Indicated *p* values by log-rank Mantel-Cox test in A,
554 two-way ANOVA test in C, unpaired *t* test, two-tailed in D, E, and G.
555
556 **Supplemental figure 4. *L. lactis* expressing SagA promotes NOD2-dependent protection**
557 **against intestinal injury. A)** Schematic of experimental procedure for mice inoculation with *L.*
558 *lactis* (*Lls*) strains. Mice received antibiotics (ampicillin + streptomycin, abx) in drinking water for
559 7 days, and were orally gavaged with PBS or *Lls* strains twice on days 8 and 14 to coincide with
560 the initiation and cessation of DSS administration. **B and C)** Abx-treated WT mice given PBS,
561 parental *Lls*, *Lls* expressing catalytic mutant SagA (*Lls-SagA*^{C443A}), or *Lls* expressing WT SagA
562 (*Lls-SagA*^{WT}) were treated with DSS as in A and examined for the burden of *Lls* strains (B) and
563 LCN2 concentration in stool samples at the indicated time points (C). **D and E)** Abx-treated
564 *Nod2*$^{+/-}$ and *Nod2*$^{-/-}$ mice given parental *Lls* or *Lls-SagA*^{WT} were treated with DSS and examined
565 for the burden of *Lls* strains (D) and LCN2 concentration in stool samples at the indicated time
566 points (E). **F)** Schematic of experimental procedure for DSS treatment of mice that received broth
567 or culture supernatants of *Lls* strains as drinking water. **G and H)** DSS-treatment of WT mice
568 inoculated with broth or culture supernatants of *Lls* (S-*Lls*), *Lls-SagA*^{C443A} (S-*Lls-SagA*^{C443A}), or
569 *Lls-SagA*^{WT} (S-*Lls-SagA*^{WT}) were examined for changes in body weight (G) and LCN2 presence
570 in stool samples at the indicated time points (H). **I and J)** DSS-treatment of *Nod2*$^{+/-}$ and *Nod2*$^{-/-}$
571 mice inoculated with S-*Lls* or S- *Lls-SagA*^{WT}. The mice were examined for changes in body weight
572 (I) and LCN2 presence in stool samples on day 13 (J). All mice were bred in room 6. Data points
573 in C, E, H, and J represent individual mice. Data points in B, D, and I represent mean ± SEM.
574 Lines in G represent mean. Bars represent mean ± SEM and at least two independent
575 experiments were performed. Indicated *p* values by unpaired *t* test, two-tailed in C, H, and J and
576 two-way ANOVA test in G and I.
577
578 **Supplemental figure 5. *Efm*-mediated protection is dependent on myeloid and not**
579 **intestinal epithelial *Nod2* expression. A-D)** DSS-treatment of *Nod2*$^{fl/fl}$*;LysM-Cre*$^{-}$ and *Cre*$^{+}$ mice
580 (A and B) or *Nod2*$^{fl/fl}$*;Villin-Cre*$^{-}$ and *Cre*$^{+}$ mice (C and D) from room 6 following administration of
581 *Efm* in drinking water or control. The mice were examined for *Efm* burden in stool samples (A and
582 C) and fecal LCN2 concentration at the indicated time points (B and D). Lines in A and C and data
583 points in B and D represent individual mice. Bars represent mean ± SEM and at least three
584 independent experiments were performed. Indicated *p* values by unpaired *t* test, two-tailed in B
585 and D.
586

587 **Supplemental figure 6. Immune cell and cytokine analysis of colons from *Efm*-colonized**
588 **mice and analysis of *Efm*-colonized *Il22ra1$^{fl/fl}$;Villin-Cre* mice. A and B)** Flow cytometry gating
589 strategies for T cells and innate lymphoid cells (ILCs) (A, transcription factors), and cytokine
590 production (B). **C-F)** Flow cytometry graph depicting the proportion of IL10^{+} (C), Tbet^{+} (D), and
591 GATA3^{+} (E) CD4^{+} T cells and regulatory T cells (Treg, F) in WT, *Nod2$^{+/-}$*, *Nod2$^{-/-}$*, and
592 *Nod2$^{fl/fl}$;LysM-Cre^{-}* and *Cre^{+}* mice following 2-week administration of *Efm* in drinking water or
593 control. **G and H)** Flow cytometry graph depicting the proportion of group 1 (ILC1, G) and group
594 2 (ILC2, H) ILCs in WT, *Nod2$^{+/-}$*, *Nod2$^{-/-}$*, and *Nod2$^{fl/fl}$;LysM-Cre^{-}* and *Cre^{+}* mice following 2-week
595 administration of *Efm* in drinking water or control. **I and J)** Quantification of secreted IL-18 (I) and
596 IL-1β (J) in the supernatants of gut explants from *Efm*-colonized WT, *Nod2$^{+/-}$*, *Nod2$^{-/-}$*, and
597 *Nod2$^{fl/fl}$;LysM-Cre^{-}* and *Cre^{+}* mice on day 20. **K and L)** DSS treatment of *Il22ra1$^{fl/fl}$;Villin-Cre^{-}* and
598 *Cre^{+}* mice from room 6 following 2-week administration of *Efm* in drinking water or control. The
599 mice were examined for the burden of *Efm* (K) and changes in body weight (L). Data points in C-
600 J and lines in K represent individual mice. For C, n = 13 (WT), 12 (WT *Efm*), 7 (*Nod2$^{+/-}$*), 11
601 (*Nod2$^{+/-}$ Efm*), 10 (*Nod2$^{-/-}$*), 9 (*Nod2$^{-/-}$ Efm*), 7 (*Nod2$^{fl/fl}$;LysM-Cre^{-}*), 7 (*Nod2$^{fl/fl}$;LysM-Cre^{-} Efm*), 8
602 (*Nod2$^{fl/fl}$;LysM-Cre^{+}*), and 9 (*Nod2$^{fl/fl}$;LysM-Cre^{+} Efm*). For D-H, n = 8 (WT), 7 (WT *Efm*), 5 (*Nod2$^{+/-}$*),
603 7 (*Nod2$^{+/-}$ Efm*), 8 (*Nod2$^{-/-}$*), 6 (*Nod2$^{-/-}$ Efm*), 7 (*Nod2$^{fl/fl}$;LysM-Cre^{-}*), 7 (*Nod2$^{fl/fl}$;LysM-Cre^{-} Efm*), 8
604 (*Nod2$^{fl/fl}$;LysM-Cre^{+}*), and 9 (*Nod2$^{fl/fl}$;LysM-Cre^{+} Efm*). For I and J, n = 8 (WT), 8 (WT *Efm*), 6
605 (*Nod2$^{+/-}$*), 8 (*Nod2$^{+/-}$ Efm*), 8 (*Nod2$^{-/-}$*), 7 (*Nod2$^{-/-}$ Efm*), 8 (*Nod2$^{fl/fl}$;LysM-Cre^{-}*), 8 (*Nod2$^{fl/fl}$;LysM-Cre^{-}*
606 *Efm*), 9 (*Nod2$^{fl/fl}$;LysM-Cre^{+}*), and 8 (*Nod2$^{fl/fl}$;LysM-Cre^{+} Efm*). Data points in L represent mean ±
607 SEM. Bars represent mean ± SEM and at least two independent experiments were performed.
608 Indicated *p* values by unpaired *t* test, two-tailed in C-J and two-way ANOVA test in L.
609
610 **Supplemental figure 7. Characterization of mice carrying a *Nod2* knock-in mutation**
611 **equivalent to the human R702W**. **A)** *NOD2 R702W* allele frequency according to ethnic groups.
612 The frequencies were retrieved from 1000 Genomes Project and Allele Frequency Aggregator. **B)**
613 Schematic of genotyping PCR product (left) and representative genotyping gel image (right) for
614 *Nod2 Q675W* knock-in mouse. **C)** Sequencing of the *Nod2* locus from the above mice confirmed
615 successful gene targeting. Figure shows exon 4 DNA and amino acid sequences from *Nod2*
616 *Q675W* knock-in mouse sequencing results aligned to the WT sequences. Red boxes indicate
617 the mutated region. **D)** Western blot image of NOD2 and β-actin (ACTB) in colonic tissue lysates
618 from *Nod2$^{-/-}$*, *Nod2$^{Q675W/+}$*, and *Nod2$^{Q675W/Q675W}$* mice. **E and F)** DSS treatment of *Nod2$^{Q675W/+}$ and*
619 *Nod2$^{Q675W/Q675W}$* mice from room 6 following 2-week administration of *Efm* in drinking water or
620 control. The mice were examined for the burden of *Efm* (E) and LCN2 concentration (F) in the

621 stool samples at the indicated time points. **G)** Endogenous *Enterococcus* burden among mice
622 with different genotypes on day 0 (upper). The *p*-values relative to *Nod2*$^{Q675W/+}$ or *Nod2*$^{Q675W/Q675W}$
623 mice were indicated in lower table. **H)** Schematic of the mechanism by which *Efm* activates NOD2
624 to suppress inflammation, and how this process is disrupted when either REG3A is overproduced
625 or NOD2 is genetically inactivated. Lines in E and data points in F and G represent individual
626 mice. Bars in F and G represent mean ± SEM and at least three independent experiments were
627 performed. Het, heterozygotes; Homo, homozygotes. Indicated *p* values by unpaired *t* test, two-
628 tailed in F and G.
629
630

631 **STAR METHODS**

632 Detailed methods are provided in the online version of this paper and include the following:

633 - KEY RESOURCES TABLE
634 - RESOURCE AVAILABILITY
635 - Lead contact
636 - Materials availability
637 - Data and code availability
638 - EXPERIMENTAL MODEL AND SUBJECT DETAILS
639 - Mice
640 - Generation of *Nod2 Q675W* knock-in mice
641 - Human stool samples and data collection
642 - METHOD DETAILS
643 - Bacterial species
644 - Preparation of human stool extract, antimicrobial activity and REG3A measurement
645 - Western blotting
646 - DNA extraction and 16S rRNA sequencing analysis
647 - Enumeration of total *Enterococcus* and *Efm* in human stool samples
648 - Bacterial inoculation and DSS treatment of mice
649 - Quantification of bacterial burden and lipcalin-2 (LCN2) in murine stool samples
650 - Histology
651 - Colon explant culture and cytokine detection
652 - Isolation of lamina propria (LP) cells
653 - Flow cytometry
654 - *Nod2* sequencing
655 - Statistical analyses

656 **KEY RESOURCES TABLE**

REAGENT or RESOURCE	SOURCE	IDENTIFIER
Antibodies		
Rat anti-Human Reg1A antibody	R&D Systems	Cat#: MAB4937; RRID: AB_2102139; Clone: 431202
Mouse anti-Human Reg3A antibody	R&D Systems	Cat#: 62257S; RRID: AB_1964697; Clone: 512124
Rabbit anti-REG3G antibody	Abcam	Cat#: ab233480
Rabbit anti-REG4 antibody	Abcam	Cat#: ab255820; Clone: EPR22810-327
Mouse anti-NOD2 antibody	Invitrogen	Cat#: MA1-16611; RRID: AB_568643; Clone: 2D9
Mouse anti-β-Actin antibody	Sigma	Cat#: A5441; RRID: AB_476744; Clone: AC-15
IRDye 680RD Goat anti-Rabbit IgG Secondary Antibody	LI-COR	Cat# 925-68071; RRID: AB_2721181;
IRDye 800CW Goat anti-Mouse IgG Secondary Antibody	LI-COR	Cat#: 925-32210; RRID: AB_2687825;
IRDye 800CW Goat anti-Rat IgG Secondary Antibody	LI-COR	Cat#: 925-32219; RRID: AB_2721932;
PerCP/Cyanine5.5 anti-mouse/human CD11b Antibody	Biolegend	Cat#: 101228; RRID: AB_893232; Clone: M1/70
PerCP/Cyanine5.5 anti-mouse CD11c Antibody	Biolegend	Cat#: 117328; RRID: AB_2129641; Clone: N418
PerCP/Cyanine5.5 anti-mouse Ly-6G/Ly-6C (Gr-1) Antibody	Biolegend	Cat#: 108428; RRID: AB_893558; Clone: RB6-8C5
PerCP/Cyanine5.5 anti-mouse TER-119/Erythroid Cells Antibody	Biolegend	Cat#: 116228; RRID: AB_893636; Clone: TER-119
PerCP/Cyanine5.5 anti-mouse NK-1.1 Antibody	Biolegend	Cat#: 108728; RRID: AB_2132705; Clone: PK136
PE anti-T-bet Antibody	Biolegend	Cat#: 644810; RRID: AB_2200542; Clone: 4B10
PE- Cyanine7 anti-mouse/human CD44 antibody	Biolegend	Cat#: 103030; RRID: AB_830787; Clone: IM7
APC/Cyanine7 anti-mouse CD4 Antibody	Biolegend	Cat#: 100414; RRID: AB_312699; Clone: GK1.5
Brilliant Violet 570 anti-mouse CD62L Antibody	Biolegend	Cat#: 104433; RRID: AB_10900262; Clone: MEL-14

Brilliant Violet 605 anti-mouse CD127 (IL-7Ra) Antibody	Biolegend	Cat#: 135041; RRID: AB_2572047; Clone: A7R34
Brilliant Violet 650 anti-mouse NK-1.1 Antibody	Biolegend	Cat#: 108736; RRID: AB_2563159; Clone: PK136
Alexa Fluor 700 anti-mouse CD8a Antibody	Biolegend	Cat#: 100730; RRID: AB_493703; Clone: 53-6.7
Brilliant Violet 711 anti-mouse TCR β chain Antibody	Biolegend	Cat#: 109243; RRID: AB_2629564; Clone: H57-597
PerCP/Cyanine5.5 anti-mouse CD19	eBioscience	Cat#: 45-0193-82; RRID: AB_1106999; Clone: 1D3
PE anti-mouse IL-22 Antibody	eBioscience	Cat#: 12-7221-82; RRID: AB_10597428; Clone: 1H8PWSR
APC anti-mouse FOXP3 Antibody	eBioscience	Cat#: 17-5773-82; RRID: AB_469457; Clone: FJK-16s
PE-CF594 anti-mouse γδ T-Cell Receptor Antibody	BD Bioscience	Cat#: 563532; RRID: AB_2661844; Clone: GL3
BUV395 anti-mouse CD45 Antibody	BD Bioscience	Cat#: 564279; RRID: AB_2651134; Clone: 30-F11
BV421 anti-mouse RORgt Antibody	BD Bioscience	Cat#: 562894; RRID: AB_2687545; Clone: Q31-378
BV421 anti-mouse IL-10 Antibody	BD Bioscience	Cat#: 566295; RRID: AB_2739668; Clone: JES5-16E3
Alexa Fluor 488 anti-mouse GATA3 Antibody	BD Bioscience	Cat#: 560163; RRID: AB_1645302; Clone: L50-823
Bacterial strains		
Enterococcus faecalis OG1RF	Dr. Hang (Scripps Research Institutes), originally acquired from ATCC 47077.	
Enterococcus faecium Com15	Dr. Hang (Scripps Research Institutes), originally acquired Dr. Gilmore (Harvard Medical School).	
Salmonella Typhimurium SL1344	Gift from Dr. Littman (NYU)	
Lactococcus lactis thyA auxotroph	Dr. Hang (Scripps Research Institutes)[50], generated in collaboration with Rise Therapeutics	

Lactococcus lactis thyA expressing wild-type SagA	Dr. Hang (Scripps Research Institutes)[50], generated in collaboration with Rise Therapeutics	
Lactococcus lactis thyA expressing catalytic mutant SagA	Dr. Hang (Scripps Research Institutes)[50], generated in collaboration with Rise Therapeutics	
Chemicals, Peptides, and Recombinant Proteins		
Bacto Brain Heart Infusion	BD	Cat#: 237500
M17 Broth	BD	Cat#: 218561
M17 Agar	BD	Cat#: 218571
Bile esculin azide agar	Millipore	Cat#: 06105
HiCrome Enterococcus faecium Agar Base	HIMEDIA	Cat#: M1580
Enterococcus faecium Selective Supplement	HIMEDIA	Cat#: FD226
Lactose	Sigma-Aldrich	Cat#: 17814
Thymidine	Sigma-Aldrich	Cat#: T9250
Phosphate-buffer saline	Corning	Cat#: 21040CV
Triton X-100	Sigma-Aldrich	Cat#: T8787
Glycerol	Sigma-Aldrich	Cat#: G5516
Halt Protease and Phosphatase Inhibitor Cocktail	Thermo Fisher	Cat#: 78440
Bolt 4-12% Bis-Tris Plus Gels	Invitrogen	Cat#: NW04120BOX
Intercept (TBS) Blocking Buffer	LI-COR	Cat#: 927-60003
Dextran sulfate sodium	TdB Consultancy	Cat#: DB001
Ampicillin	Amercian Bioanalytical	Cat#: 69-52-3
Streptomycin	Sigma-Aldrich	Cat#: S6501
Low melting point agar	Promega	Cat#: V2111
10% Formalin	Thermo Fisher	Cat#: SF99-4
RPMI 1640 Medium	Gibco	Cat#: 61870127
L-glutamine	Corning	Cat#: 25-005-CI
Penicillin-Streptomycin Solution	Corning	Cat#: 30-002-CI
HEPES	Corning	Cat#: 25-060-CI
MEM Nonessential Amino Acids	Corning	Cat#: 25-025-CI
Sodium pyruvate	Corning	Cat#: 25-000-CI
β-mercaptoethanol	Gibco	Cat#: 21985023
HBSS	Gibco	Cat#: 14175103
DL-dithiothreitol	Sigma Aldrich	Cat#: D0632
Collagenase	Sigma Aldrich	Cat#: C2139
Deoxyribonuclease I	Sigma Aldrich	Cat#: DN25
Percoll	Sigma-Aldrich	Cat#: P1644
Fetal bovine serum	Peak Serum	Cat#: PS-FB2
Cell Stimulation Cocktail (plus protein transport inhibitors)	eBioscience	Cat#: 00-4975-93
Bovine Serum Albumin	Thermo Fisher	Cat#: BP1600-100
Fixation Buffer	Biolegend	Cat#: 420801
Intracellular Staining Permeabilization Wash Buffer	Biolegend	Cat#: 421002
Foxp3 / Transcription Factor Staining Buffer Set	Thermo Fisher	Cat#: 00-5523-00
Zombie UV Fixable Viability Kit	Biolegend	Cat#: 423108

Critical commercial assays		
10 ml syringe	BD	Cat#: 302995
Gauze pad	4MD Medical	Cat#: PROP157025
Millex-GS Syringe Filter Unit, 0.22 µm	Millipore	Cat#: SLGL0250S
Nalgene Rapid-Flow Sterile Disposable Filter Units with PES Membranes	Thermo Fisher	Cat#: 567-0020
Human Reg3A DuoSet ELISA	R&D systems	Cat#: DY5940-05
Mouse Lipocalin-2/NGAL DuoSet ELISA	R&D systems	Cat#: DY1857-05
Mouse IL-22 DuoSet ELISA	R&D systems	Cat#: DY582-05
Mouse IL-18 DuoSet ELISA	R&D systems	Cat#: DY7625-05
Mouse IL-1 beta/IL-1 F2 DuoSet ELISA	R&D systems	Cat#: DY401-05
DNeasy PowerSoil Pro Kit	Qiagen	Cat#: 47016
RNeasy Mini Kit	Qiagen	Cat#: 74106
RNase-Free DNase Set	Qiagen	Cat#: 79256
70 µm nylon mesh	ELKO Filtering	Cat#: 03-70/33
High-Capacity cDNA Reverse Transcription Kit	Thermo Fisher	Cat#: 4368814
TOPO TA Cloning Kit	Invitrogen	Cat#: 450002
Experimental Models: Organisms/Strains		
Mouse: *Nod2*$^{-/-}$	Jackson Laboratory	Cat#: 005763
Mouse *Nod2*$^{fl/fl}$	Dr. Keestra-Gounder (University of Colorado Anschutz Medical Campus)	N/A
Mouse: *Il22ra1*$^{fl/fl}$	Dr. Sergei Koralov (New York University Grossman school of medicine), originally acquired from Jackson Laboratory (Cat#: 031003)	
Mouse: *LysM-Cre*	Jackson Laboratory	Cat#: 004781
Mouse: *Villin-Cre*	Jackson Laboratory	Cat#: 004586
Mouse: *Nod2*$^{Q675W/Q675W}$	This study	N/A
Software and Algorithms		
Prism 9	GraphPad Software	https://www.graphpad.com/scientific-software/prism/
FlowJo	BD	https://www.flowjo.com
NCBI Gene and Protein Data Base	NCBI	http://www.ncbi.nlm.nih.gov
Nucleotide blast	NCBI	https://blast.ncbi.nlm.nih.gov/Blast.cgi
Blastx	NCBI	https://blast.ncbi.nlm.nih.gov/Blast.cgi

657

658 **RESOURCE AVAILABILITY**

659

660 **Lead contact**

661 Further information and requests for resources and reagents should be directed to and will be
662 fulfilled by the Lead Contact, Ken Cadwell (Ken.Cadwell@nyulangone.org).
663
664 **Materials availability**
665 The materials in the current study are available from the Lead Contact with a completed
666 Materials Transfer Agreement.
667
668 **Data and code availability**
669 The 16S sequencing data are deposited in the NCBI Sequence Read Archive under BioProject
670 accession number PRJNA915760.
671
672 **EXPERIENTAL MODEL AND SUBJECT DETAILS**
673
674 **Mice**
675 Age- and gender-matched 7 to 10-week-old mice on the C57BL/6J (B6) background were used.
676 All mice were bred on-site. Mice harboring gene deletions were compared to their respective
677 littermate control mice indicated in the results section. *Nod2*$^{-/-}$, *LysM-Cre*, and *Villin-Cre* mice were
678 purchased from The Jackson Laboratory. *Il22ra1*$^{fl/fl}$ and *Nod2*$^{fl/fl}$ mice were obtained from Sergei
679 Koralov (New York University Grossman School of Medicine) and A. Marijke Keestra-Gounder
680 (University of Colorado Anschutz School of Medicine)[78], respectively. To generate cell type-
681 specific knock-out mice, *Nod2*$^{fl/fl}$ mice were bred with *LysM-Cre* and *Villlin-Cre* mice and *Il22ra1*$^{fl/fl}$
682 mice were bred with *Villin-Cre* mice. Mice were assigned numbers to facilitate blind data collection
683 and distributed randomly to treatment groups. All animal studies were performed according to
684 approved protocols by the NYU Grossman School of Medicine Animal Care and Use Committee
685 (IACUCs).
686
687 **Generation of *Nod2 Q675W* knock-in mice**
688 CRISPR–Cas9 gene-targeting mixture containing sgRNA (5'-AGCGGGCACGTGCCTGACGC-
689 3') targeting exon 4 of B6 *Nod2* and template (5'-
690 TCACAGCAGCCTTCCTAGCAGGTCTGTTGTCCCAGCAGCATCGGGACCTGTTGGCTGCAT
691 GCCAGGTCTCCGAGAGGGTACTTCTATGGCGTCAGGCACGTGCCCGCTCGTGTCTGGCC
692 CACAGCCT-3') (synthesized at Integrated DNA Technologies) and Cas9 mRNA were injected
693 into the cytoplasm of zygotes generated from B6 females impregnated by B6 males, and then the
694 microinjected embryos were incubated in potassium-supplemented simplex optimized medium

695 (KSOM) at 37°C for one day and subsequently transferred into pseudopregnant CD-1 female
696 mice at the two-cell stage by the Rodent Genetic Engineering Laboratory at NYU Grossman
697 School of Medicine. The resulting F0 chimeras were screened through genotyping PCR.
698 Amplicons were generated using a pair of primers (Fwd 5'-CTTTTCAGCTGTGGCCGGCT-3' and
699 Rev 5'-TTTGCCACAGGCCCAATCGG-3') flanking the targeting sites from tail DNA from
700 chimeras and wild-type mice and cut by BsaHI (NEB) (Supplemental figure 7A). A 3042-bp region
701 containing the *Nod2* coding region was sequenced to verify correct gene targeting (Supplemental
702 figure 7C). All mice used in experiments were backcrossed with B6 mice at least 3 generations.
703
704 **Human stool samples and data collection**
705 Stool samples were collected with consent from hospitalized adult non-IBD (NIBD) and IBD
706 patients with gastrointestinal symptoms (Supplemental tables 1 and 2) with consent. The protocol
707 has been approved by the New York University School of Medicine Institutional Review Board
708 (Mucosal Immune Profiling in Patients with Inflammatory Bowel Disease; S12-01137). The clinical
709 data of NIBD and IBD patients were collected using EPIC EHR and REDCap 9.3.6 software. At
710 the time of sample acquisition and processing, investigators were blinded to the patient clinical
711 status.
712
713 **METHOD DETAILS**
714 **Bacterial species**
715 *Enterococcus faecalis* OG1RF (*Efl*), *E. faecium* Com15 (*Efm*), and *Lactococcus lactis thyA*
716 auxotroph (*Lls*) expressing wild-type SagA (*Lls-SagA*^{WT}) and catalytic mutant SagA (*Lls-SagA*^{C443A})
717 were previously described[50]. *Salmonella* Typhimurium SL1344 (*S*Tm) was provided by Dan
718 Littman (NYU). *Efl* and *Efm* were grown at 37°C under ambient atmosphere in autoclaved
719 antibiotics-free Bacto Brain Heart Infusion (BHI) broth (BD). *Lls* strains and *S*Tm were cultured at
720 the above condition in M17 broth (BD) supplemented with 2% (v/v) lactose (Sigma-Aldrich) and
721 20 µg/ml of thymidine (Sigma-Aldrich) (LM17 broth) and Luria Bertani (LB) broth (NYU Reagent
722 Preparation Core), respectively. Colony forming unit (CFU) of *Efl*, *Efm*, *Lls* strains, and *S*Tm was
723 enumerated on bile esculin azide (BEA) agar (Millipore), HiCrome *Enterococcus faecium* Agar
724 with Selective Supplement (HIMEDIA), M17 agar (BD) supplemented with 2% (v/v) lactose and
725 20 µg/ml of thymidine (LM17 agar), and LB agar (NYU Reagent Preparation Core), respectively.
726
727 **Preparation of human stool extract, antimicrobial activity assay, and REG3A measurement**

728 1 g of human stools from NIBD and IBD patients were homogenized in 5 ml of phosphate-
729 buffered saline (PBS, Corning) using TissueRuptor (Qiagen). 0.5-1 ml of human stool slurries
730 were taken for quantification of bacterial burden. The remaining stool slurries were filtered using
731 a 10 ml syringe (BD) with gauze (4MD Medical). Human stool extracts were collected by
732 centrifugation at 15,000 x *g* for 20 min at 4°C and filter-sterilized using a 10 ml syringe with Millex-
733 GS Syringe Filter Unit, 0.22 µm (Millipore).
734 For quantifying the antimicrobial activity of the human stool extracts, overnight cultures of *Efl*,
735 *Efm*, and *S*Tm were harvested, resuspended in 50 µl of PBS, and mixed with one volume of
736 human stool extracts or PBS. The mixture of bacteria and human stool extract was incubated in
737 a 37°C static incubator for 24 h and then plated in serial dilution on selective agars as mentioned
738 above for enumerating *Efl*, *Efm*, and *S*Tm.
739 Quantification of REG3A in human stool extracts was performed using Human Reg3A DuoSet
740 ELISA (R&D systems) according to the manufacturer's instructions.
741
742 **Western blotting**
743 Mouse colonic tissues were processed for immunoblotting as previously described[79,80]. Briefly,
744 proximal colonic tissues (2 mm) were cut open and washed with PBS, then suspended in lysis
745 buffer (20 mM Tris-HCl (pH 7.4, NYU Reagent Preparation Core), 150 mM NaCl (NYU Reagent
746 Preparation Core), 1% Triton X-100 (Sigma-Aldrich), 10% glycerol (Sigma-Aldrich), and 2x Halt
747 Protease and Phosphatase Inhibitor Cocktail (Thermo Fisher)) and homogenized using FastPrep-
748 24 Classic bead beating grinder and lysis system (MP Biomedicals). Tissue homogenate was
749 then pelleted twice at 10,000 x *g* for 10 min at 4°C to collect the lysates. human stool extracts and
750 mouse colonic tissue lysates were resolved on Bolt 4-12% Bis-Tris Plus Gels (Invitrogen),
751 transferred onto polyvinylidene difluoride membranes, and blocked using Intercept (TBS) blocking
752 buffer (LI-COR). Membranes were probed with primary antibody overnight at 4°C. The following
753 primary antibodies were used for western blotting studies: anti-REG1A (R&D systems, MAB4937),
754 REG3A (R&D systems, MAB5965), REG3G (Abcam, ab233480), REG4 (Abcam, ab255820),
755 NOD2 (Invitrogen, MA1-16611), and β-actin (Sigma-Aldrich, A5441). After incubation with the
756 primary antibody, the membrane was washed and probed with the secondary antibody for 1 h at
757 room temperature (RT). As for secondary antibodies, IRDye 680RD Goat anti-Rabbit (925-68071),
758 IRDye 800CW Goat anti-Mouse (925-32210), and IRDye 800CW Goat anti-Rat (925-32219) were
759 purchased from LI-COR. After additional washing, the protein was then detected with Image
760 Studio for Oddyseey CLx (LI-COR).
761

762 **DNA extraction and 16S rRNA sequencing analysis**

763 DNA from human stool samples was extracted with DNeasy PowerSoil Pro kit (Qiagen)
764 according to the manufacturer's instruction. Bacterial 16S rRNA gene was amplified at the V4
765 region using primer pairs and paired-end amplicon sequencing was performed on the Illumina
766 MiSeq system at NYU Genome Technology Core. Sequencing reads were processed using the
767 DADA2 pipeline in the QIIME2 software package. Taxonomic assignment was performed against
768 the Greengenes 13_8 99% OTUs full-length sequences database[81]. Alpha diversity analysis was
769 done using observed OTUs[82]. Beta diversity was calculated using Bay-Curtis, Jaccard,
770 unweighted UniFrac, and weighted UniFrac distance and visualized with EMPeror[83].

771

772 **Enumeration of total *Enterococcus* and *Efm* in human stool samples**

773 The human stool slurries (200 mg/ml) were plated in serial dilution on selective agars mentioned
774 above for enumerating CFU of total *Enterococcus* and *Efm*, respectively.

775

776 **Bacterial inoculation and DSS treatment of mice**

777 *Efm* drinking water was prepared as described previously[59]. Briefly, overnight culture of *Efm*
778 was harvested and resuspended in filter-sterilized drinking water to 10^9 CFU/ml, herein referred
779 as *Efm* water, and administered to mice for 14 days. This drinking water was then replaced with
780 one containing 5% dextran sulfate sodium (DSS, TdB Consultancy) for 6 days and then switched
781 to regular drinking water for the remainder of the experiment when examining intestinal injury
782 following *Efm* colonization. For experiments in which *Efm* was administered after the initiation of
783 intestinal injury, mice were treated with 5% DSS for 6 days and received *Efm* water or control
784 water for the remainder of the experiment. Drinking water was exchanged with freshly prepared
785 ones every 2-3 days for all types of treatment.

786 Overnight cultures of *Lls* strains were harvested and resuspended in PBS to 10^9 CFU/100 µl.
787 Water containing ampicillin (1 mg/ml, American Bioanalytical) and streptomycin (0.5 mg/ml,
788 Sigma-Aldrich) was filter-sterilized using Nalgene Rapid-Flow Sterile Disposable Filter Units with
789 PES Membranes (Thermo Fisher) for the antibiotic (abx) treatment. The mice treated with abx-
790 containing water for 7 days were given 3% DSS for 6 days. On days 8 and 14, the mice were
791 orally administered 100 µl inoculum of *Lls* strains (approximately 10^9 CFU).

792 For treatment of *Lls* culture supernatant, overnight cultures of *Lls* strains were centrifuged at
793 6,000 x *g* for 15 min at 4°C to collect the culture supernatant. The supernatants and LM17 broth
794 control were filter-sterilized using Nalgene Rapid-Flow Sterile Disposable Filter Units with PES

795 Membranes to avoid bacterial contamination. The mice receiving the filter-sterilized supernatants
796 of *Lls* strains or LM17 broth as drinking water for 7 days were given 5% DSS for 6 days.
797 The mice were monitored daily for survival and weight loss. Disease score was quantified based
798 on five parameters in which eight was the maximum score: diarrhea (0-2), bloody stool (0-1),
799 hunched posture (0-2), mobility (0-2), and fur ruffling (0-1).
800
801 **Quantification of bacterial burden and lipocalin-2 (LCN2) in murine stool samples**
802 Stool pellets from individual mice were weighed, homogenized in PBS, and plated in serial
803 dilution on selective agars as mentioned above for enumerating CFU of total *Enterococcus*, *Efm*,
804 and *Lls* strains, respectively. The remaining stool homogenates were centrifuged at 15,000 x *g*
805 for 5 min to collect clear supernatants. LCN2 in the clear supernatants was quantified using Mouse
806 Lipocalin-2/NGAL DuoSet ELISA (R&D systems) according to the manufacturer's instructions.
807
808 **Histology**
809 Quantification of colon histology data was performed blind. Colonic tissues were cut open along
810 the length, pinned on black wax, and fixed in 10% formalin (Thermo Fisher). Tissues were
811 embedded in 3% low melting point agar (Promega). Formalin embedding, cutting, and
812 hematoxylin and eosin (H&E) staining were performed by the NYU Histopathology core. Sections
813 were imaged on a Nikon Eclipse Ci microscope. Pathologic changes in colonic mucosa evaluated
814 by Y.D. included colonic epithelium, lamina propria, muscularis mucosa, and submucosa. It was
815 based on the state of the changes (acute or chronic) and the degree of involvement. Acute
816 changes primarily included neutrophils in the crypt lumen, erosions, ulcers, pus, and the formation
817 of polyps. Features of chronic changes included the following: crypt distortion (sideways crypts,
818 branching, tortuous), crypt loss, crypt atrophy, basal plasmacytosis, and lymphoid aggregates.
819 The involvement pattern included focal distal involvement, patchy involvement with skipping areas,
820 diffuse involvement, and pancolonic (no skip areas) involvement. The percentage of involvement
821 was calculated as 100 x (Length of disease involved colon / Total length of the colon).
822
823 **Colon explant culture and cytokine detection**
824 Colon explant culture was performed as previously described[66]. The proximal colon tissue (1
825 cm) was opened longitudinally, washed with PBS and cultured for 48 h in 1ml of complete Roswell
826 Park Memorial Institute (RPMI) 1640 (Gibco) containing 2 mM L-glutamine (Corning),
827 penicillin/streptomycin solution (Corning), 20 mM N-2-hydroxyethylpiperazine-N'-2-ethane
828 sulfonic acid (HEPES, Corning), Minimum Essential Medium (MEM) non-essential amino acids

829 (Corning), 1 mM sodium pyruvate (Corning), and β-mercaptoethanol (Gibco). Cytokines in
830 supernatants were measured using the Mouse IL-22, IL-18, and IL-1 beta/IL-1 F2 DuoSet ELISA
831 (R&D systems) according to the manufacturer's instructions.
832
833 **Isolation of lamina propria (LP) cells**
834 LP cells were harvested as before[84]. Briefly, colonic tissue including caecum was cut open and
835 washed with PBS, and fat was removed. The tissues were incubated first with 20 ml of Hank's
836 Balanced Salt Solution (HBSS, Gibco) with 2% HEPES, 1% sodium pyruvate, 5 mM
837 Ethylenediaminetetraacetic acid (EDTA, NYU Reagent Preparation Core), and 1mM DL-
838 dithiothreitol (Sigma-Aldrich) for 15 min at 37°C with 220 rpm and then with new 20 mL of HBSS
839 with 2% HEPES, 1% sodium pyruvate, 5mM EDTA for 10 min at 37°C with 210 rpm. The tissue
840 bits were washed with HBSS, minced, and then enzymatically digested with collagenase (0.5
841 mg/ml, Sigma-Aldrich) and Deoxyribonuclease I (0.01 mg/ml, Sigma-Aldrich) for 30 min at 37°C
842 with 200 rpm. Digested solutions were passed through 70 µm nylon mesh (ELKO Filtering) and
843 isolated cells were resuspended in 40% Percoll (Sigma-Aldrich), layered onto 80% Percoll, and
844 centrifuged at RT at 2,200 rpm for 22 min. Cells were recovered from the interphase and washed
845 with RPMI containing 10% fetal bovine serum (FBS, Peak Serum) (cRPMI). For the analysis of
846 the cytokine production, LPLs were plated in cRPMI and stimulated with 1X Cell Stimulation
847 Cocktail (plus transport inhibitors) (eBiosciecne) for 4 h at 37°C.
848
849 **Flow cytometry**
850 Surface and intracellular cytokine staining was performed per manufacturer's instruction in PBS
851 with 0.5% bovine serum albumin (BSA, Thermo Fisher) (BSA/PBS) for 20 min on ice. Two staining
852 panels were prepared as described previously[84]. The following antibodies were used for the first
853 panel: CD11b (101228, 1:200), CD11c (117328, 1:200), CD127 (135041, 1:33), CD4 (100414,
854 1:150), CD44 (103030, 1:100), CD62L (104433, 1:100), CD8 (100730, 1:100), GR1 (108428,
855 1:300), NK1.1 (108736, 1:150), Tbet (644810, 1:50), TCRβ (109243, 1:100), TER119 (116228,
856 1:200) from Biolegend, CD19 (45-0193-82, 1:100) and FOXP3 (17-5773-82, 1:100) from
857 eBioscience, and CD45 (564279, 1:200), GATA3 (560163, 1:40), RORγt (562894, 1:100), TCRγδ
858 (563532, 1:100) from BD Bioscience. The following antibodies were used for the second panel:
859 CD11b (101228, 1:200), CD11c (117328, 1:200), CD127 (135041, 1:33), CD4 (100414, 1:150),
860 CD8 (100730, 1:100), GR1 (108428, 1:300), NK1.1 (108728, 1:200), TCRβ (109243, 1:100),
861 TER119 (116228, 1:200) from Biolegend, IL-22 (12-7221-82, 1:100) from eBioscience, and
862 CD45 (564279, 1:200), IL-10 (566295, 1:100) and TCRγδ (563532, 1:100) from BD Bioscience.

863 Samples were fixed with either Fixation Buffer (Biolegend) or Foxp3/Transcription Factor Staining
864 Buffer Set (Thermo Fisher). For intracellular staining of the transcription factor, cells were
865 permeabilized with the Foxp3/Transcription Factor Staining Buffer Set at RT for 45 min in the
866 presence of antibodies. For intracellular staining of cytokines, cells were permeabilized with
867 Intracellular Staining Permeabilization Wash Buffer (Biolegend) at RT for 20 min in the presence
868 of antibodies. Zombie UV Fixable Viability Kit (Biolegend) was used to exclude dead cells.
869 Samples were acquired on a BD LSR II (BD Biosciences) and analyzed using FlowJo software
870 (BD).
871
872 ***Nod2* sequencing**
873 *Nod2* mRNA was sequenced as previously described [85]. Briefly, total RNA was extracted from
874 proximal colonic tissues (2 mm) using RNeasy Mini Kit with DNase treatment (QIAGEN), and
875 synthesis of cDNA was conducted with High-Capacity cDNA Reverse Transcription Kit (Thermo
876 Fisher) according to the manufacturer's protocol. A 3042-bp region containing the *Nod2* coding
877 region was amplified from cDNA by PCR using a pair of primers (Fwd 5'-
878 ATGTGCTCACAGGAAGAGTTC C-3' and Rev 5'-TCACAACAAGAGTCTGGCGTCCC-3').
879 Amplicons were cloned into pCR2.1-TOPO (Invitrogen). The plasmids were sequenced by Oxford
880 Nanopore from SNPsaurus.
881
882 **Statistical analyses**
883 Statistical differences were determined as described in the figure legend using GraphPad Prism
884 9 software. $p < 0.05$ was considered statistically significant for all assays, and individual p values
885 are indicated in the figure panels.
886
887 **ACKNOWLEDGEMENT**
888 We would like to acknowledge NYU Grossman School of Medicine Flow Cytometry and Cell
889 Sorting, Microscopy, Genome Technology, Rodent Genetic Engineering, and Histology Cores
890 and Clinical Microbiology Laboratory for use of their instruments and technical assistance
891 (supported by National Institutes of Health [NIH] grants P31CA016087, S10OD01058, and
892 S10OD018338). This work was supported in part by NIH grants DK093668 (K.C.), AI121244
893 (K.C.), HL123340 (K.C.), AI130945 (K.C.), AI140754 (K.C.), DK124336 (K.C.), AI164154 (A.M.K-
894 G.), AI173121 (A.M.K-G.), DK122698 (F.Y.), and DK132908 (M.L.); Faculty Scholar grant from
895 the Howard Hughes Medical Institute (K.C.), Crohn's & Colitis Foundation (K.C.), Kenneth Rainin

Foundation (H.C.H. and K.C.), Bernard Levine Postdoctoral Research Fellowship in Immunology (Y.H.C.) and the Charles H. Revson Senior Fellowships in Biomedical Science (Y.H.C.).

COMPETING INTERESTS

K.C. has received research support from Pfizer, Takeda, Pacific Biosciences, Genentech, and Abbvie. K.C. has consulted for or received an honoraria from Puretech Health, Genentech, and Abbvie. K.C. is an inventor on U.S. patent 10,722,600 and provisional patent 62/935,035 and 63/157,225. H.C.H. has received research support from Rise Therapeutics and LISCure Biosciences. U.S. patents PCT/US16/28836 (H.C.H.) and PCT/US2020/019038 (H.C.H. and M.E.G.) were obtained for the commercial use of SagA-engineered bacteria. Rise Therapeutics has licensed these patents to develop SagA-probiotics as therapeutics. J.A. reports consultancy fees, honoraria, or advisory board fees from Abbvie, Adiso, Bristol Myers Squibb, Janssen, Pfizer, Fresnius, and BioFire Diagnostics.

AUTHOR CONTRIBUTIONS

K.K.J. and K.C. conceived the study and designed the experiments. K.K.J. contributed to all the experiments and data analysis. T.H., M.L., and Y.C. helped perform mouse experiments. Y.D. performed histopathology analysis. F.Y. generated *Nod2 Q675W* mice. D.E. performed 16S rRNA sequencing analysis. J.A. and S.G. assisted with the design, analysis, and interpretation of clinical data. M.E.G. and H.C.H. provided *Lls* and *Efm* strains and associated technical assistance. A.M.K-G. provided *NOD2*$^{fl/fl}$ mice. K.C. oversaw the analysis and interpretation of all experiments. K.K.J., Y. D., and K.C. wrote the manuscript, and all authors commented on the manuscript, data, and conclusion.

921 **Table S1**

Name	Sex	Age	Disease	CDAI	Total Mayo
IBD1	F	24	CD	250	
IBD2	F	28	CD	192	
IBD3	M	49	CD	234	
IBD4	M	33	CD	258	
IBD5	F	49	CD	180	
IBD6	M	26	CD	265	
IBD7	F	43	CD	260	
IBD8	F	60	CD	176	
IBD9	F	36	CD	310	
IBD10	F	56	CD	323	
IBD11	M	36	CD	268	
IBD12	M	21	CD	397	
IBD13	M	19	CD	261	
IBD14	M	36	CD	251	
IBD15	F	35	CD	187	
IBD16	F	78	CD	235	
IBD17	F	36	CD	275	
IBD18	F	62	CD	313	
IBD19	F	20	CD	104	
IBD20	M	28	CD	298	
IBD21	F	58	CD	275	
IBD22	F	33	CD	300	
IBD23	F	51	CD	372	
IBD24	M	25	CD	292	
IBD25	M	42	CD	236	
IBD26	M	36	CD	301	
IBD27	F	56	CD	358	
IBD28	M	30	CD	87	
IBD29	F	58	CD	264	
IBD30	M	28	CD	337	
IBD31	M	69	CD	341	
IBD32	M	30	UC		10
IBD33	M	41	UC		7
IBD34	F	58	UC		8

IBD35	M	40	UC		10
IBD36	M	42	UC		9
IBD37	M	30	UC		10
IBD38	M	65	UC		10
IBD39	M	34	UC		10
IBD40	M	28	UC		7
IBD41	M	34	UC		10
IBD42	M	78	UC		11
IBD43	M	33	UC		10
IBD44	F	28	UC		11
IBD45	F	26	UC		9
IBD46	F	35	UC		11
IBD47	M	62	UC		4
IBD48	F	27	UC		11
IBD49	F	28	UC		10
IBD50	F	36	UC		10
IBD51	F	58	UC		3
IBD52	F	35	UC		11
IBD53	M	41	UC		9
IBD54	F	48	UC		9
IBD55	F	18	UC		7
IBD56	M	66	UC		N/A

Supplemental Table 1. Information for IBD patients. M; male, F; female; CD; Crohn's disease; UC; ulcerative colitis; CDAI, Crohn's disease activity index; N/A, not available.

926 **Table S2**

Name	Sex	Age	GI-related medical history	GI symptoms
NIBD1	F	83		Diarrhea for 7 days
NIBD2	M	61	*Clostridia difficile* infection	Intermittent diarrhea for 3 months.
NIBD3	M	37	Irritable bowel syndrome	Intermittent diarrhea with urgency, bloating and chest discomfort every 2 weeks
NIBD4	F	50	Hirschsprung's disease, type 2 diabetes mellitus	Vomiting and watery diarrhea and for 4 days
NIBD5	F	40		Nausea, Vomiting, and diarrhea for 5 days
NIBD6	M	86	Whipple procedure	Diarrhea and abdominal pain for 3 days
NIBD7	M	56		Diarrhea and abdominal pain
NIBD8	F	42		Bloody diarrhea and abdominal pain
NIBD9	M	9		Diarrhea
NIBD10	M	35		Right Lower Quadrant pain, Nausea, Vomiting, and diarrhea for 1 day
NIBD11	F	29		Abdominal pain
NIBD12	F	58		Vomiting and abdominal tenderness
NIBD13	F	44		Nausea, vomiting, and diarrhea for 4 days
NIBD14	M	23		Nausea, vomiting, and diarrhea with fever for 2 days
NIBD15	M	75		Diarrhea for 2 weeks
NIBD16	M	51		Diarrhea for 10 days
NIBD17	M	70		Diarrhea
NIBD18	F	49		Diarrhea for 5 days
NIBD19	F	53		Abdominal pain
NIBD20	F	54		Constipation and rectal pain
NIBD21	M	79		Bloody stool
NIBD22	F	69		Diarrhea
NIBD23	M	71		Diarrhea

NIBD24	F	65	*C. difficile* infection	Nausea, vomiting, and diarrhea for 4 days
NIBD25	F	53		Nausea and diarrhea for 4 days
NIBD26	F	49		Diarrhea for 2 weeks
NIBD27	F	23	Recurrent *C. difficile* infection	Diarrhea and abdominal pain for 1 week
NIBD28	M	86		Diarrhea and abdominal pain
NIBD29	F	74		Diarrhea and abdominal pain with fever for 2 days
NIBD30	F	63		Vomiting, diarrhea, abdominal pain, neutropenic fever
NIBD31	M	52	Pancreatic cancer	Unclear
NIBD32	F	36		Abdominal pain
NIBD33	F	73		Abdominal pain and bloating
NIBD34	F	55		Antibiotic associated diarrhea
NIBD35	F	33		Vomiting and watery diarrhea
NIBD36	M	29		Rectal bleeding and bloating
NIBD37	M	55		Diarrhea for 3 days
NIBD38	F	72		Constipation with rectal bleeding
NIBD39	F	38		Nausea, diarrhea, and bloating
NIBD40	F	76		Diarrhea and abdominal pain
NIBD41	F	82		Diarrhea
NIBD42	F	69		Nausea, vomiting, and Diarrhea for 5 days
NIBD43	F	74	Microscopic colitis	Diarrhea
NIBD44	F	29		Rectal bleeding and abdominal pain
NIBD45	F	55		Diarrhea
NIBD46	M	37		Loose stools
NIBD47	M	39		Nausea, vomiting, and diarrhea for 4 days
NIBD48	M	54		Nausea and watery diarrhea for 6 days
NIBD49	F	45		Diarrhea
NIBD50	F	91	Gastro-Esophageal Reflux Disease	Nausea, vomiting, and diarrhea for 1 day

NIBD51	M	91		Nausea, vomiting, and diarrhea for 3 days
NIBD52	M	38	Chronic norovirus infection	Diarrhea and abdominal pain for 1 week
NIBD53	F	0		Diarrhea with fever
NIBD54	F	58		Diarrhea and hematuria for 2 days
NIBD55	F	75	*C. difficile* infection and diverticulitis	Nausea and diarrhea for 1 day
NIBD56	F	51		Abdominal pain

927

928 **Supplemental Table 2. Information for non-IBD (NIBD) patients.**

929

930 **Table S3**

Genotype	*Efm*	Histological findings	% of colon affected
WT	-	Epithelial erosion with depletion of goblet cells and mixed acute and chronic inflammatory cells throughout the sample with heterogenous epithelial regrowth and mucosal edema; Focal lymphoid hyperplasia.	70%
WT	-	Epithelial erosion with subepithelial lymphoid aggregate, mixed inflammatory reaction in a skipping pattern; Focal low-grade dysplasia.	40%
WT	-	Small focal epithelial erosion.	5%
WT	-	Small focal epithelial erosion.	10%
WT	-	Epithelial erosion with goblet cell depletion, abscess formation and focal submucosal lymphoid aggregate	50%
WT	-	Epithelial erosion with goblet cell depletion from the distal end with skipping pattern	25%
WT	-	Epithelial erosion with depletion of goblet cells and mixed acute and chronic inflammatory cells throughout the sample with heterogenous epithelial regrowth and mucosal edema; Low grade dysplasia noted in the epithelium adjacent to lesion	40%
WT	-	Epithelial erosion with goblet cell depletion from the distal end with skipping pattern, focal abscess formation	25%
WT	-	Epithelial erosion with goblet cell depletion from the distal end with skipping pattern with associated lymphoid aggregates	10%
WT	-	Epithelial erosion with goblet cell depletion from the distal end with skipping pattern	25%
WT	-	Small focal epithelial erosion	5%
WT	-	Epithelial erosion with depletion of goblet cells throughout the sample with heterogenous epithelial regrowth, mucosal edema, and submucosal lymphoid aggregates	65%
WT	-	Epithelial erosion with depletion of goblet cells throughout the sample with heterogenous epithelial regrowth, focal mucosal hyperplasia, and dysplasia and submucosal lymphoid aggregates	80%
WT	-	Very small focal epithelial erosion at the distal end of colon/rectum, otherwise within normal limit	10%
WT	-	Epithelial erosion with goblet cell depletion from the distal end with skipping pattern with heterogenous epithelial regeneration	50%
WT	-	Epithelial erosion with skipping(proximal) and continuous (distal) pattern with associated lymphoid aggregates and heterogenous epithelial regeneration	80%
WT	-	Epithelial erosion with skipping(proximal) and continuous (distal) pattern with associated lymphoid aggregates	60%
WT	-	Distal portion with decrease to depletion of epithelial colonic glands with mild chronic inflammation; Mid and proximal portion with skipping pattern of similar change	40%
WT	-	Distal portion with decrease to depletion of epithelial colonic glands with mild chronic inflammation; Mid and proximal portion with skipping pattern of similar change	35%
WT	-	Distal portion with decrease to depletion of epithelial colonic glands; Mid and proximal portion with skipping pattern of similar change	30%
WT	-	Distal portion with decrease to depletion of epithelial colonic glands with mild chronic inflammation; Mid and proximal portion with skipping pattern of above change; A few lymphoid aggregates noted	30%
WT	-	within normal limit	0%
WT	-	Distal end with decrease to depletion of epithelial colonic glands	10%
WT	-	Distal portion with significant decrease to depletion of epithelial colonic glands without associated lymphoid aggregates; Mid and proximal portions with epithelial erosion and goblet cell depletion in a skipping pattern	45%
WT	+	Epithelial erosion with depletion of goblet cells and mixed acute and chronic inflammatory cells at distal end; Multiple foci of epithelial lymphoid aggregates. Mucosal edema. No overt dysplasia	50%
WT	+	Small foci of epithelial erosion in a skipping pattern, majority of colonic mucosa unaffected	10%
WT	+	Epithelial erosion with depletion of goblet cells, repairment and mixed acute and chronic inflammatory cells at distal end and mid portion; Multiple foci of epithelial lymphoid aggregates. Mucosal edema. No overt dysplasia	67%

WT	+	Epithelial erosion with goblet cell depletion; Focal submucosal lymphoid aggregate. Majority of colonic mucosa unaffected	20%
WT	+	Epithelial erosion with goblet cell depletion and associated lymphoid aggregates	25%
WT	+	Epithelial erosion with goblet cell depletion at distal end only	15%
WT	+	Epithelial erosion with goblet cell depletion	30%
WT	+	Epithelial erosion with goblet cell depletion at distal end only	15%
WT	+	Focal epithelial erosion with goblet cell depletion. Multifocal lymphoid aggregates	5%
WT	+	Focal epithelial erosion with goblet cell depletion	5%
WT	+	Epithelial erosion with goblet cell depletion and associated lymphoid aggregates	15%
WT	+	Epithelial erosion with goblet cell depletion and associated lymphoid aggregates	55%
WT	+	Epithelial erosion with goblet cell depletion and associated lymphoid aggregates	50%
WT	+	Epithelial erosion with goblet cell depletion and associated lymphoid aggregates with a skipping pattern; Moderate dysplasia present	30%
WT	+	Epithelial erosion with goblet cell depletion	22%
WT	+	Epithelial erosion with skipping pattern with associated lymphoid aggregates, epithelial regeneration, and low-grade dysplasia	37%
WT	+	Epithelial erosion with goblet cell depletion from the distal end with skipping pattern with heterogenous epithelial regeneration	10%
WT	+	Epithelial erosion with skipping pattern with associated lymphoid aggregates, epithelial regeneration, and low-grade dysplasia	33%
WT	+	Epithelial erosion with skipping(proximal) and continuous (distal) pattern with associated lymphoid aggregates and heterogenous epithelial regeneration	25%
WT	+	Epithelial erosion with skipping(proximal) and continuous (distal) pattern with associated lymphoid aggregates and heterogenous epithelial regeneration	18%
WT	+	Focal epithelial erosion with goblet cell depletion with a skipping pattern through the entire colon	5%
WT	+	Focal epithelial erosion with goblet cell depletion with a skipping pattern through the entire colon	25%
WT	+	Focal epithelial erosion with goblet cell depletion with a skipping pattern through the entire colon	15%
WT	+	Distal portion with decrease to depletion of epithelial colonic glands with mild chronic inflammation. Mid and proximal portion with skipping pattern of above change; A few lymphoid aggregates noted	30%
WT	+	Distal portion with decrease to depletion of epithelial colonic glands. Focal similar changes in proximal end	5%
WT	+	Distal portion with decrease to depletion of epithelial colonic glands	10%
WT	+	Distal portion with decrease to depletion of epithelial colonic glands. Multiple lymphoid aggregates noted	10%
WT	+	Very mild change	5%
WT	+	Very mild change in distal end	1%
WT	+	Distal portion with significant decrease to depletion of epithelial colonic glands without associated lymphoid aggregates; Mid and proximal portions with epithelial erosion and goblet cell depletion in a skipping pattern; Epithelial repair and regeneration	50%
WT	+	Epithelial erosion with goblet cell depletion and associated lymphoid aggregates in a skipping pattern, epithelial regeneration and dysplastic changes noted	25%
WT (post)	-	Epithelial erosion with skipping pattern with associated lymphoid aggregates and heterogenous epithelial regeneration	50%
WT (post)	-	Epithelial erosion with skipping pattern with associated lymphoid aggregates and heterogenous epithelial regeneration	12%
WT (post)	-	Epithelial erosion with skipping pattern with associated lymphoid aggregates, epithelial regeneration, and low-grade dysplasia	40%
WT (post)	-	Epithelial erosion with skipping pattern with heterogenous epithelial regeneration	70%
WT (post)	-	Epithelial erosion with skipping pattern with associated lymphoid aggregates and heterogenous epithelial regeneration	50%
WT (post)	-	Epithelial erosion with skipping pattern with associated lymphoid aggregates and heterogenous epithelial regeneration	20%

WT (post)	-	Epithelial erosion with skipping pattern with associated lymphoid aggregates and heterogenous epithelial regeneration	30%
WT (post)	-	Epithelial erosion with skipping pattern with associated lymphoid aggregates and heterogenous epithelial regeneration	10%
WT (post)	-	Epithelial erosion with skipping pattern with associated lymphoid aggregates and heterogenous epithelial regeneration	55%
WT (post)	-	Epithelial erosion with skipping pattern with associated lymphoid aggregates and heterogenous epithelial regeneration	75%
WT (post)	+	a small portion of epithelial is affected however the tissue is partially lost	5%
WT (post)	+	Skipping lesion of epithelial damage with regrowth and loss of goblet cells	5%
WT (post)	+	Within normal limit; Two small lymphoid aggregate	0%
WT (post)	+	Very small focal epithelial erosion at the distal end of colon/rectum, otherwise within normal limit	1%
WT (post)	+	Epithelial erosion with goblet cell depletion and associated lymphoid aggregates	35%
WT (post)	+	Epithelial erosion with goblet cell depletion	7%
WT (post)	+	Within normal limit	0%
WT (post)	+	Epithelial erosion with goblet cell depletion from the distal end with skipping pattern with associated lymphoid aggregates and heterogenous epithelial regeneration	30%
WT (post)	+	Epithelial erosion with skipping pattern with associated lymphoid aggregates and heterogenous epithelial regeneration	10%
WT (post)	+	Epithelial erosion with goblet cell depletion	5%
Nod2$^{+/-}$	-	Epithelial erosion with depletion of goblet cells from the distal end with mucosal edema, associated lymphoid aggregates and heterogenous epithelial regeneration	40%
Nod2$^{+/-}$	-	Epithelial erosion with depletion of goblet cells from the distal end with mucosal edema, associated lymphoid aggregates and heterogenous epithelial regeneration	67%
Nod2$^{+/-}$	-	Epithelial erosion with skipping pattern with associated lymphoid aggregates, epithelial regeneration, and low-grade dysplasia	40%
Nod2$^{+/-}$	-	Epithelial erosion with skipping(proximal) and continuous (distal) pattern with associated lymphoid aggregates	27%
Nod2$^{+/-}$	-	Distal portion with decrease to depletion of epithelial colonic glands with mild chronic inflammation; Mid and proximal portion with skipping pattern of similar change	40%
Nod2$^{+/-}$	-	Epithelial erosion with goblet cell depletion and associated lymphoid aggregates with a skipping pattern	20%
Nod2$^{+/-}$	-	Epithelial erosion with goblet cell depletion and associated lymphoid aggregates with a skipping pattern; Repair and regeneration associated colonic adenoma	30%
Nod2$^{+/-}$	-	Distal and mid portions with decrease to depletion of epithelial colonic glands with mild chronic inflammation and lymphoid aggregates; Proximal portion with skipping pattern of above change	55%
Nod2$^{+/-}$	-	Distal and mid portions with decrease to depletion of epithelial colonic glands with mild chronic inflammation and lymphoid aggregates; Proximal portion with skipping pattern of above change	60%
Nod2$^{+/-}$	-	Distal and mid portions with decrease to depletion of epithelial colonic glands with mild chronic inflammation and lymphoid aggregates; Proximal portion with skipping pattern of above change	60%
Nod2$^{+/-}$	-	Distal and mid portions with decrease to depletion of epithelial colonic glands with mild chronic inflammation and lymphoid aggregates; Proximal portion with skipping pattern of above change	50%
Nod2$^{+/-}$	+	Epithelial erosion with skipping(proximal) and continuous (distal) pattern with associated lymphoid aggregates and heterogenous epithelial regeneration	35%
Nod2$^{+/-}$	+	Epithelial erosion with skipping(proximal) and continuous (distal) pattern with associated lymphoid aggregates and heterogenous epithelial regeneration	42%
Nod2$^{+/-}$	+	Epithelial erosion with skipping pattern with associated lymphoid aggregates and epithelial regeneration	25%
Nod2$^{+/-}$	+	Distal portion with decrease to depletion of epithelial colonic glands; Mid and proximal portion with skipping pattern of similar change	20%
Nod2$^{+/-}$	+	Distal portion with decrease to depletion of epithelial colonic glands; Mid and proximal portion with skipping pattern of above change. A few lymphoid aggregates noted	35%
Nod2$^{+/-}$	+	Two focal area with colonic adenomatous changes	10%
Nod2$^{+/-}$	+	Small foci of epithelial erosion with chronic inflammatory cell infiltration	5%

Nod2$^{+/-}$	+	Epithelial erosion with goblet cell depletion and associated lymphoid aggregates, epithelial regeneration and dysplastic changes note	10%
Nod2$^{+/-}$	+	Distal and proximal portions with significant decrease to depletion of epithelial colonic glands without associated lymphoid aggregates; Mid portion is generally within normal limit	40%
Nod2$^{+/-}$	+	Distal portion with significant decrease to depletion of epithelial colonic glands without associated lymphoid aggregates; Mid portion with epithelial erosion and goblet cell depletion in a skipping pattern	40%
Nod2$^{+/-}$	+	Within normal range	0%
Nod2$^{+/-}$	+	Distal and mid portions with decrease to depletion of epithelial colonic glands with mild chronic inflammation and lymphoid aggregates; Proximal portion with skipping pattern of above change	35%
Nod2$^{-/-}$	-	Epithelial erosion with goblet cell depletion from the distal end with skipping pattern with heterogenous epithelial regeneration	50%
Nod2$^{-/-}$	-	Epithelial erosion with goblet cell depletion from the distal end with skipping(proximal) and continuous (distal) pattern; associated lymphoid aggregates and heterogenous epithelial regeneration	67%
Nod2$^{-/-}$	-	Epithelial erosion with goblet cell depletion from the distal end with skipping(proximal) and continuous (distal) pattern, abscess, submucosal lymphoid aggregates and heterogenous epithelial regeneration	67%
Nod2$^{-/-}$	-	Epithelial erosion with skipping(proximal) and continuous (distal) pattern with associated lymphoid aggregates	40%
Nod2$^{-/-}$	-	Epithelial erosion with skipping(proximal) and continuous (distal) pattern with associated lymphoid aggregates	35%
Nod2$^{-/-}$	-	Epithelial erosion with skipping(proximal) and continuous (distal) pattern with associated lymphoid aggregates	25%
Nod2$^{-/-}$	-	Distal and mid portion with decrease to depletion of epithelial colonic glands with mild chronic inflammation. Proximal end with skipping pattern of above change; Mild dysplastic changes in remaining colonic epithelium	40%
Nod2$^{-/-}$	-	Distal and mid portion with decrease to depletion of epithelial colonic glands with mild chronic inflammation; Skipping pattern getting to proximal end; Single lymphoid aggregate noted	50%
Nod2$^{-/-}$	-	Distal and mid portion with decrease to depletion of epithelial colonic glands with mild chronic inflammation. Skipping pattern getting to proximal end; No thickening of colonic wall. Single lymphoid aggregate noted	60%
Nod2$^{-/-}$	+	Epithelial erosion with depletion of goblet cells from the distal end with mucosal edema, associated lymphoid aggregates and heterogenous epithelial regeneration	65%
Nod2$^{-/-}$	+	Epithelial erosion with depletion of goblet cells from the distal end with mucosal edema, associated lymphoid aggregates and heterogenous epithelial regeneration	50%
Nod2$^{-/-}$	+	Epithelial erosion with depletion of goblet cells from the distal end with mucosal edema, associated lymphoid aggregates and heterogenous epithelial regeneration	63%
Nod2$^{-/-}$	+	Epithelial erosion with skipping pattern with associated lymphoid aggregates and heterogenous epithelial regeneration	25%
Nod2$^{-/-}$	+	Epithelial erosion with skipping(proximal) and continuous (distal) pattern with associated lymphoid aggregates	60%
Nod2$^{-/-}$	+	Epithelial erosion with skipping(proximal) and continuous (distal) pattern with associated lymphoid aggregates	57%
Nod2$^{-/-}$	+	Distal and mid portion with significant decrease to depletion of epithelial colonic glands without evidence of inflammation. No thickening of colonic wall	70%
Nod2$^{-/-}$	+	Distal and mid portion with decrease to depletion of epithelial colonic glands with mild chronic inflammation. Proximal end with skipping pattern of above change	55%
Q675W/+	-	Epithelial defect with goblet cell depletion	15%
Q675W/+	-	Epithelial erosion with goblet cell depletion and associated lymphoid aggregates, epithelial regeneration and dysplastic changes noted	20%
Q675W/+	-	Epithelial erosion with goblet cell depletion and associated lymphoid aggregates in a skipping pattern, epithelial regeneration and dysplastic changes noted	25%
Q675W/+	-	Distal and mid portions with decrease to depletion of epithelial colonic glands with mild chronic inflammation and lymphoid aggregates; Proximal portion with skipping pattern of above change	40%
Q675W/+	-	Distal and mid portions with decrease to depletion of epithelial colonic glands with mild chronic inflammation and lymphoid aggregates; Proximal portion with skipping pattern of above change	30%
Q675W/+	-	Distal and mid portions with decrease to depletion of epithelial colonic glands with mild chronic inflammation and lymphoid aggregates; Proximal portion with skipping pattern of above change	40%

Q675W/+	-	Distal and mid portions with decrease to depletion of epithelial colonic glands with mild chronic inflammation and lymphoid aggregates; Proximal portion with skipping pattern of above change	50%
Q675W/+	+	Small foci of epithelial erosion with chronic inflammatory cell infiltration	5%
Q675W/+	+	Epithelial erosion with goblet cell depletion and associated lymphoid aggregates, epithelial regeneration and dysplastic changes noted	15%
Q675W/+	+	Tiny focal epithelial erosion with repairment. No acute or chronic inflammation	2%
Q675W/+	+	Within normal range	0%
Q675W/+	+	Epithelial erosion with goblet cell depletion and associated lymphoid aggregates in a skipping pattern	10%
Q675W/+	+	Epithelial erosion with goblet cell depletion and associated lymphoid aggregates in a skipping pattern	20%
Q675W/Q675W	-	Epithelial defects with depletion of epithelial colonic glands with mild chronic inflammation in a skipping pattern	15%
Q675W/Q675W	-	Epithelial defects with depletion of epithelial colonic glands with mild chronic inflammation in a skipping pattern	15%
Q675W/Q675W	-	Epithelial defects with depletion of epithelial colonic glands with mild chronic inflammation and occasional lymphoid aggregate in a skipping pattern	20%
Q675W/Q675W	-	Distal and mid portions with decrease to depletion of epithelial colonic glands with mild chronic inflammation and lymphoid aggregates; Proximal portion with skipping pattern of above change	50%
Q675W/Q675W	-	Epithelial defects with depletion of epithelial colonic glands with mild chronic inflammation and lymphoid aggregates in a skipping pattern	30%
Q675W/Q675W	-	Epithelial defects with depletion of epithelial colonic glands with mild chronic inflammation and lymphoid aggregates in a skipping pattern	40%
Q675W/Q675W	-	Epithelial defects with depletion of epithelial colonic glands with mild chronic inflammation and lymphoid aggregates in a skipping pattern	40%
Q675W/Q675W	+	Extensive decrease to depletion of epithelial colonic glands with mild chronic inflammation and lymphoid aggregates	60%
Q675W/Q675W	+	Distal and mid portions with decrease to depletion of epithelial colonic glands with mild chronic inflammation and lymphoid aggregates; Proximal portion with skipping pattern of above change	50%
Q675W/Q675W	+	Distal and mid portions with decrease to depletion of epithelial colonic glands with mild chronic inflammation and lymphoid aggregates; Proximal portion with skipping pattern of above change	60%
Q675W/Q675W	+	Extensive epithelial defects with depletion of epithelial colonic glands; No evidence of associated acute or chronic inflammation	80%
Q675W/Q675W	+	Extensive epithelial defects with depletion of epithelial colonic glands and associated lymphoid aggregates, epithelial regeneration and dysplastic changes noted	90%
Q675W/Q675W	+	Epithelial defects with depletion of epithelial colonic glands with mild chronic inflammation in a skipping pattern	25%
Q675W/Q675W	+	Epithelial defects with depletion of epithelial colonic glands with mild chronic inflammation in a skipping pattern	15%
Q675W/Q675W	+	Epithelial defects with depletion of epithelial colonic glands with mild chronic inflammation in a skipping pattern	20%

931

932 **Supplemental Table 3. Histological findings of colonic sections from mice receiving DSS.**

933 WT, wild type; *Q675W/+*, *Nod2*$^{Q675W/+}$; *Q675W/Q675W*, *Nod2*$^{Q675W/Q675W}$. WT (post) indicated mice

934 receiving *Efm* after DSS treatment.

935

936 **References**

937 1. Muniz, L.R., Knosp, C., and Yeretssian, G. (2012). Intestinal antimicrobial peptides
938 during homeostasis, infection, and disease. Front Immunol *3*, 310.
939 10.3389/fimmu.2012.00310.
940 2. Bevins, C.L., and Salzman, N.H. (2011). Paneth cells, antimicrobial peptides and
941 maintenance of intestinal homeostasis. Nat Rev Microbiol *9*, 356-368.
942 10.1038/nrmicro2546.
943 3. Ramanan, D., and Cadwell, K. (2016). Intrinsic Defense Mechanisms of the Intestinal
944 Epithelium. Cell Host Microbe *19*, 434-441. 10.1016/j.chom.2016.03.003.
945 4. Okumura, R., Kurakawa, T., Nakano, T., Kayama, H., Kinoshita, M., Motooka, D.,
946 Gotoh, K., Kimura, T., Kamiyama, N., Kusu, T., et al. (2016). Lypd8 promotes the
947 segregation of flagellated microbiota and colonic epithelia. Nature *532*, 117-121.
948 10.1038/nature17406.
949 5. Lehotzky, R.E., Partch, C.L., Mukherjee, S., Cash, H.L., Goldman, W.E., Gardner, K.H.,
950 and Hooper, L.V. (2010). Molecular basis for peptidoglycan recognition by a bactericidal
951 lectin. Proc Natl Acad Sci U S A *107*, 7722-7727. 10.1073/pnas.0909449107.
952 6. Cash, H.L., Whitham, C.V., Behrendt, C.L., and Hooper, L.V. (2006). Symbiotic bacteria
953 direct expression of an intestinal bactericidal lectin. Science *313*, 1126-1130.
954 10.1126/science.1127119.
955 7. Wang, L., Fouts, D.E., Starkel, P., Hartmann, P., Chen, P., Llorente, C., DePew, J.,
956 Moncera, K., Ho, S.B., Brenner, D.A., et al. (2016). Intestinal REG3 Lectins Protect
957 against Alcoholic Steatohepatitis by Reducing Mucosa-Associated Microbiota and
958 Preventing Bacterial Translocation. Cell Host Microbe *19*, 227-239.
959 10.1016/j.chom.2016.01.003.
960 8. Vaishnava, S., Yamamoto, M., Severson, K.M., Ruhn, K.A., Yu, X., Koren, O., Ley, R.,
961 Wakeland, E.K., and Hooper, L.V. (2011). The antibacterial lectin RegIIIgamma
962 promotes the spatial segregation of microbiota and host in the intestine. Science *334*,
963 255-258. 10.1126/science.1209791.
964 9. Brandl, K., Plitas, G., Mihu, C.N., Ubeda, C., Jia, T., Fleisher, M., Schnabl, B.,
965 DeMatteo, R.P., and Pamer, E.G. (2008). Vancomycin-resistant enterococci exploit
966 antibiotic-induced innate immune deficits. Nature *455*, 804-807. 10.1038/nature07250.
967 10. Darnaud, M., Dos Santos, A., Gonzalez, P., Augui, S., Lacoste, C., Desterke, C., De
968 Hertogh, G., Valentino, E., Braun, E., Zheng, J., et al. (2018). Enteric Delivery of
969 Regenerating Family Member 3 alpha Alters the Intestinal Microbiota and Controls
970 Inflammation in Mice With Colitis. Gastroenterology *154*, 1009-1023 e1014.
971 10.1053/j.gastro.2017.11.003.
972 11. Zhao, D., Kim, Y.H., Jeong, S., Greenson, J.K., Chaudhry, M.S., Hoepting, M.,
973 Anderson, E.R., van den Brink, M.R., Peled, J.U., Gomes, A.L., et al. (2018). Survival
974 signal REG3alpha prevents crypt apoptosis to control acute gastrointestinal graft-versus-
975 host disease. J Clin Invest *128*, 4970-4979. 10.1172/JCI99261.
976 12. Yu, S., Balasubramanian, I., Laubitz, D., Tong, K., Bandyopadhyay, S., Lin, X., Flores,
977 J., Singh, R., Liu, Y., Macazana, C., et al. (2020). Paneth Cell-Derived Lysozyme
978 Defines the Composition of Mucolytic Microbiota and the Inflammatory Tone of the
979 Intestine. Immunity *53*, 398-416 e398. 10.1016/j.immuni.2020.07.010.
980 13. Cadwell, K., Liu, J.Y., Brown, S.L., Miyoshi, H., Loh, J., Lennerz, J.K., Kishi, C., Kc,
981 W., Carrero, J.A., Hunt, S., et al. (2008). A key role for autophagy and the autophagy

982 gene Atg16l1 in mouse and human intestinal Paneth cells. Nature *456*, 259-263.
983 10.1038/nature07416.
984 14. Wehkamp, J., Salzman, N.H., Porter, E., Nuding, S., Weichenthal, M., Petras, R.E., Shen,
985 B., Schaeffeler, E., Schwab, M., Linzmeier, R., et al. (2005). Reduced Paneth cell alpha-
986 defensins in ileal Crohn's disease. Proc Natl Acad Sci U S A *102*, 18129-18134.
987 10.1073/pnas.0505256102.
988 15. Koslowski, M.J., Kubler, I., Chamaillard, M., Schaeffeler, E., Reinisch, W., Wang, G.,
989 Beisner, J., Teml, A., Peyrin-Biroulet, L., Winter, S., et al. (2009). Genetic variants of
990 Wnt transcription factor TCF-4 (TCF7L2) putative promoter region are associated with
991 small intestinal Crohn's disease. PLoS One *4*, e4496. 10.1371/journal.pone.0004496.
992 16. Courth, L.F., Ostaff, M.J., Mailander-Sanchez, D., Malek, N.P., Stange, E.F., and
993 Wehkamp, J. (2015). Crohn's disease-derived monocytes fail to induce Paneth cell
994 defensins. Proc Natl Acad Sci U S A *112*, 14000-14005. 10.1073/pnas.1510084112.
995 17. Bel, S., Pendse, M., Wang, Y., Li, Y., Ruhn, K.A., Hassell, B., Leal, T., Winter, S.E.,
996 Xavier, R.J., and Hooper, L.V. (2017). Paneth cells secrete lysozyme via secretory
997 autophagy during bacterial infection of the intestine. Science *357*, 1047-1052.
998 10.1126/science.aal4677.
999 18. Manichanh, C., Borruel, N., Casellas, F., and Guarner, F. (2012). The gut microbiota in
1000 IBD. Nat Rev Gastroenterol Hepatol *9*, 599-608. 10.1038/nrgastro.2012.152.
1001 19. Ni, J., Wu, G.D., Albenberg, L., and Tomov, V.T. (2017). Gut microbiota and IBD:
1002 causation or correlation? Nat Rev Gastroenterol Hepatol *14*, 573-584.
1003 10.1038/nrgastro.2017.88.
1004 20. Wong, S.Y., and Cadwell, K. (2018). There was collusion: Microbes in inflammatory
1005 bowel disease. PLoS Pathog *14*, e1007215. 10.1371/journal.ppat.1007215.
1006 21. Jostins, L., Ripke, S., Weersma, R.K., Duerr, R.H., McGovern, D.P., Hui, K.Y., Lee,
1007 J.C., Schumm, L.P., Sharma, Y., Anderson, C.A., et al. (2012). Host-microbe interactions
1008 have shaped the genetic architecture of inflammatory bowel disease. Nature *491*, 119-
1009 124. 10.1038/nature11582.
1010 22. Knights, D., Lassen, K.G., and Xavier, R.J. (2013). Advances in inflammatory bowel
1011 disease pathogenesis: linking host genetics and the microbiome. Gut *62*, 1505-1510.
1012 10.1136/gutjnl-2012-303954.
1013 23. Cho, J.H., and Abraham, C. (2007). Inflammatory bowel disease genetics: Nod2. Annu
1014 Rev Med *58*, 401-416. 10.1146/annurev.med.58.061705.145024.
1015 24. Bonen, D.K., and Cho, J.H. (2003). The genetics of inflammatory bowel disease.
1016 Gastroenterology *124*, 521-536. 10.1053/gast.2003.50045.
1017 25. Kim, Y.G., Kamada, N., Shaw, M.H., Warner, N., Chen, G.Y., Franchi, L., and Nunez,
1018 G. (2011). The Nod2 sensor promotes intestinal pathogen eradication via the chemokine
1019 CCL2-dependent recruitment of inflammatory monocytes. Immunity *34*, 769-780.
1020 10.1016/j.immuni.2011.04.013.
1021 26. Zhang, Q., Pan, Y., Yan, R., Zeng, B., Wang, H., Zhang, X., Li, W., Wei, H., and Liu, Z.
1022 (2015). Commensal bacteria direct selective cargo sorting to promote symbiosis. Nat
1023 Immunol *16*, 918-926. 10.1038/ni.3233.
1024 27. Petnicki-Ocwieja, T., Hrncir, T., Liu, Y.J., Biswas, A., Hudcovic, T., Tlaskalova-
1025 Hogenova, H., and Kobayashi, K.S. (2009). Nod2 is required for the regulation of
1026 commensal microbiota in the intestine. Proc Natl Acad Sci U S A *106*, 15813-15818.
1027 10.1073/pnas.0907722106.

1028 28. Ramanan, D., Tang, M.S., Bowcutt, R., Loke, P., and Cadwell, K. (2014). Bacterial
1029 sensor Nod2 prevents inflammation of the small intestine by restricting the expansion of
1030 the commensal Bacteroides vulgatus. Immunity *41*, 311-324.
1031 10.1016/j.immuni.2014.06.015.
1032 29. Marchiando, A.M., Ramanan, D., Ding, Y., Gomez, L.E., Hubbard-Lucey, V.M., Maurer,
1033 K., Wang, C., Ziel, J.W., van Rooijen, N., Nunez, G., et al. (2013). A deficiency in the
1034 autophagy gene Atg16L1 enhances resistance to enteric bacterial infection. Cell Host
1035 Microbe *14*, 216-224. 10.1016/j.chom.2013.07.013.
1036 30. Wong, S.Y., Coffre, M., Ramanan, D., Hines, M.J., Gomez, L.E., Peters, L.A., Schadt,
1037 E.E., Koralov, S.B., and Cadwell, K. (2018). B Cell Defects Observed in Nod2 Knockout
1038 Mice Are a Consequence of a Dock2 Mutation Frequently Found in Inbred Strains. J
1039 Immunol *201*, 1442-1451. 10.4049/jimmunol.1800014.
1040 31. de Souza, P.R., Guimaraes, F.R., Sales-Campos, H., Bonfa, G., Nardini, V., Chica, J.E.L.,
1041 Turato, W.M., Silva, J.S., Zamboni, D.S., and Cardoso, C.R.B. (2018). Absence of
1042 NOD2 receptor predisposes to intestinal inflammation by a deregulation in the immune
1043 response in hosts that are unable to control gut dysbiosis. Immunobiology *223*, 577-585.
1044 10.1016/j.imbio.2018.07.003.
1045 32. Robertson, S.J., Geddes, K., Maisonneuve, C., Streutker, C.J., and Philpott, D.J. (2016).
1046 Resilience of the intestinal microbiota following pathogenic bacterial infection is
1047 independent of innate immunity mediated by NOD1 or NOD2. Microbes Infect *18*, 460-
1048 471. 10.1016/j.micinf.2016.03.014.
1049 33. Geddes, K., Rubino, S., Streutker, C., Cho, J.H., Magalhaes, J.G., Le Bourhis, L.,
1050 Selvanantham, T., Girardin, S.E., and Philpott, D.J. (2010). Nod1 and Nod2 regulation of
1051 inflammation in the Salmonella colitis model. Infect Immun *78*, 5107-5115.
1052 10.1128/IAI.00759-10.
1053 34. Couturier-Maillard, A., Secher, T., Rehman, A., Normand, S., De Arcangelis, A.,
1054 Haesler, R., Huot, L., Grandjean, T., Bressenot, A., Delanoye-Crespin, A., et al. (2013).
1055 NOD2-mediated dysbiosis predisposes mice to transmissible colitis and colorectal cancer.
1056 J Clin Invest *123*, 700-711. 10.1172/JCI62236.
1057 35. Wehkamp, J., Harder, J., Weichenthal, M., Schwab, M., Schaffeler, E., Schlee, M.,
1058 Herrlinger, K.R., Stallmach, A., Noack, F., Fritz, P., et al. (2004). NOD2 (CARD15)
1059 mutations in Crohn's disease are associated with diminished mucosal alpha-defensin
1060 expression. Gut *53*, 1658-1664. 10.1136/gut.2003.032805.
1061 36. Bevins, C.L., Stange, E.F., and Wehkamp, J. (2009). Decreased Paneth cell defensin
1062 expression in ileal Crohn's disease is independent of inflammation, but linked to the
1063 NOD2 1007fs genotype. Gut *58*, 882-883; discussion 883-884.
1064 37. VanDussen, K.L., Liu, T.C., Li, D., Towfic, F., Modiano, N., Winter, R., Haritunians, T.,
1065 Taylor, K.D., Dhall, D., Targan, S.R., et al. (2014). Genetic variants synthesize to
1066 produce paneth cell phenotypes that define subtypes of Crohn's disease. Gastroenterology
1067 *146*, 200-209. 10.1053/j.gastro.2013.09.048.
1068 38. van Beelen Granlund, A., Ostvik, A.E., Brenna, O., Torp, S.H., Gustafsson, B.I., and
1069 Sandvik, A.K. (2013). REG gene expression in inflamed and healthy colon mucosa
1070 explored by in situ hybridisation. Cell Tissue Res *352*, 639-646. 10.1007/s00441-013-
1071 1592-z.
1072 39. Ogawa, H., Fukushima, K., Naito, H., Funayama, Y., Unno, M., Takahashi, K.,
1073 Kitayama, T., Matsuno, S., Ohtani, H., Takasawa, S., et al. (2003). Increased expression

1074 of HIP/PAP and regenerating gene III in human inflammatory bowel disease and a
1075 murine bacterial reconstitution model. Inflamm Bowel Dis *9*, 162-170.
1076 10.1097/00054725-200305000-00003.
1077 40. Gao, J., Zhao, X., Hu, S., Huang, Z., Hu, M., Jin, S., Lu, B., Sun, K., Wang, Z., Fu, J., et
1078 al. (2022). Gut microbial DL-endopeptidase alleviates Crohn's disease via the NOD2
1079 pathway. Cell Host Microbe *30*, 1435-1449 e1439. 10.1016/j.chom.2022.08.002.
1080 41. Kim, B., Wang, Y.C., Hespen, C.W., Espinosa, J., Salje, J., Rangan, K.J., Oren, D.A.,
1081 Kang, J.Y., Pedicord, V.A., and Hang, H.C. (2019). Enterococcus faecium secreted
1082 antigen A generates muropeptides to enhance host immunity and limit bacterial
1083 pathogenesis. Elife *8*. 10.7554/eLife.45343.
1084 42. Kim, Y.G., Shaw, M.H., Warner, N., Park, J.H., Chen, F., Ogura, Y., and Nunez, G.
1085 (2011). Cutting edge: Crohn's disease-associated Nod2 mutation limits production of
1086 proinflammatory cytokines to protect the host from Enterococcus faecalis-induced
1087 lethality. J Immunol *187*, 2849-2852. 10.4049/jimmunol.1001854.
1088 43. Garcia-Solache, M., and Rice, L.B. (2019). The Enterococcus: a Model of Adaptability to
1089 Its Environment. Clin Microbiol Rev *32*. 10.1128/CMR.00058-18.
1090 44. Balish, E., and Warner, T. (2002). Enterococcus faecalis induces inflammatory bowel
1091 disease in interleukin-10 knockout mice. Am J Pathol *160*, 2253-2257. 10.1016/S0002-
1092 9440(10)61172-8.
1093 45. Seishima, J., Iida, N., Kitamura, K., Yutani, M., Wang, Z., Seki, A., Yamashita, T.,
1094 Sakai, Y., Honda, M., Yamashita, T., et al. (2019). Gut-derived Enterococcus faecium
1095 from ulcerative colitis patients promotes colitis in a genetically susceptible mouse host.
1096 Genome Biol *20*, 252. 10.1186/s13059-019-1879-9.
1097 46. Ben Braiek, O., and Smaoui, S. (2019). Enterococci: Between Emerging Pathogens and
1098 Potential Probiotics. Biomed Res Int *2019*, 5938210. 10.1155/2019/5938210.
1099 47. Franz, C.M., Huch, M., Abriouel, H., Holzapfel, W., and Galvez, A. (2011). Enterococci
1100 as probiotics and their implications in food safety. Int J Food Microbiol *151*, 125-140.
1101 10.1016/j.ijfoodmicro.2011.08.014.
1102 48. Rangan, K.J., Pedicord, V.A., Wang, Y.C., Kim, B., Lu, Y., Shaham, S., Mucida, D., and
1103 Hang, H.C. (2016). A secreted bacterial peptidoglycan hydrolase enhances tolerance to
1104 enteric pathogens. Science *353*, 1434-1437. 10.1126/science.aaf3552.
1105 49. Pedicord, V.A., Lockhart, A.A.K., Rangan, K.J., Craig, J.W., Loschko, J., Rogoz, A.,
1106 Hang, H.C., and Mucida, D. (2016). Exploiting a host-commensal interaction to promote
1107 intestinal barrier function and enteric pathogen tolerance. Sci Immunol *1*.
1108 10.1126/sciimmunol.aai7732.
1109 50. Griffin, M.E., Espinosa, J., Becker, J.L., Luo, J.D., Carroll, T.S., Jha, J.K., Fanger, G.R.,
1110 and Hang, H.C. (2021). Enterococcus peptidoglycan remodeling promotes checkpoint
1111 inhibitor cancer immunotherapy. Science *373*, 1040-1046. 10.1126/science.abc9113.
1112 51. Wang, Y.C., Westcott, N.P., Griffin, M.E., and Hang, H.C. (2019). Peptidoglycan
1113 Metabolite Photoaffinity Reporters Reveal Direct Binding to Intracellular Pattern
1114 Recognition Receptors and Arf GTPases. ACS Chem Biol *14*, 405-414.
1115 10.1021/acschembio.8b01038.
1116 52. Michot, J.M., Bigenwald, C., Champiat, S., Collins, M., Carbonnel, F., Postel-Vinay, S.,
1117 Berdelou, A., Varga, A., Bahleda, R., Hollebecque, A., et al. (2016). Immune-related
1118 adverse events with immune checkpoint blockade: a comprehensive review. Eur J Cancer
1119 *54*, 139-148. 10.1016/j.ejca.2015.11.016.

1120 53. Parikh, A., Stephan, A.F., and Tzanakakis, E.S. (2012). Regenerating proteins and their
1121 expression, regulation and signaling. Biomol Concepts *3*, 57-70. 10.1515/bmc.2011.055.
1122 54. Wang, W., Wang, Y., Lu, Y., Zhu, J., Tian, X., Wu, B., Du, J., Cai, W., and Xiao, Y.
1123 (2022). Reg4 protects against Salmonella infection-associated intestinal inflammation via
1124 adopting a calcium-dependent lectin-like domain. Int Immunopharmacol *113*, 109310.
1125 10.1016/j.intimp.2022.109310.
1126 55. Qi, H., Wei, J., Gao, Y., Yang, Y., Li, Y., Zhu, H., Su, L., Su, X., Zhang, Y., and Yang,
1127 R. (2020). Reg4 and complement factor D prevent the overgrowth of E. coli in the mouse
1128 gut. Commun Biol *3*, 483. 10.1038/s42003-020-01219-2.
1129 56. Chassaing, B., Srinivasan, G., Delgado, M.A., Young, A.N., Gewirtz, A.T., and Vijay-
1130 Kumar, M. (2012). Fecal lipocalin 2, a sensitive and broadly dynamic non-invasive
1131 biomarker for intestinal inflammation. PLoS One *7*, e44328.
1132 10.1371/journal.pone.0044328.
1133 57. Forster, S.C., Clare, S., Beresford-Jones, B.S., Harcourt, K., Notley, G., Stares, M.D.,
1134 Kumar, N., Soderholm, A.T., Adoum, A., Wong, H., et al. (2022). Identification of gut
1135 microbial species linked with disease variability in a widely used mouse model of colitis.
1136 Nat Microbiol *7*, 590-599. 10.1038/s41564-022-01094-z.
1137 58. Moon, C., Baldridge, M.T., Wallace, M.A., D, C.A., Burnham, Virgin, H.W., and
1138 Stappenbeck, T.S. (2015). Vertically transmitted faecal IgA levels determine extra-
1139 chromosomal phenotypic variation. Nature *521*, 90-93. 10.1038/nature14139.
1140 59. Kommineni, S., Bretl, D.J., Lam, V., Chakraborty, R., Hayward, M., Simpson, P., Cao,
1141 Y., Bousounis, P., Kristich, C.J., and Salzman, N.H. (2015). Bacteriocin production
1142 augments niche competition by enterococci in the mammalian gastrointestinal tract.
1143 Nature *526*, 719-722. 10.1038/nature15524.
1144 60. Teng, F., Kawalec, M., Weinstock, G.M., Hryniewicz, W., and Murray, B.E. (2003). An
1145 Enterococcus faecium secreted antigen, SagA, exhibits broad-spectrum binding to
1146 extracellular matrix proteins and appears essential for E. faecium growth. Infect Immun
1147 *71*, 5033-5041. 10.1128/IAI.71.9.5033-5041.2003.
1148 61. Rakoff-Nahoum, S., Paglino, J., Eslami-Varzaneh, F., Edberg, S., and Medzhitov, R.
1149 (2004). Recognition of commensal microflora by toll-like receptors is required for
1150 intestinal homeostasis. Cell *118*, 229-241. 10.1016/j.cell.2004.07.002.
1151 62. Kernbauer, E., Ding, Y., and Cadwell, K. (2014). An enteric virus can replace the
1152 beneficial function of commensal bacteria. Nature *516*, 94-98. 10.1038/nature13960.
1153 63. Ferrand, A., Al Nabhani, Z., Tapias, N.S., Mas, E., Hugot, J.P., and Barreau, F. (2019).
1154 NOD2 Expression in Intestinal Epithelial Cells Protects Toward the Development of
1155 Inflammation and Associated Carcinogenesis. Cell Mol Gastroenterol Hepatol *7*, 357-
1156 369. 10.1016/j.jcmgh.2018.10.009.
1157 64. Mukherjee, T., Hovingh, E.S., Foerster, E.G., Abdel-Nour, M., Philpott, D.J., and
1158 Girardin, S.E. (2019). NOD1 and NOD2 in inflammation, immunity and disease. Arch
1159 Biochem Biophys *670*, 69-81. 10.1016/j.abb.2018.12.022.
1160 65. Trindade, B.C., and Chen, G.Y. (2020). NOD1 and NOD2 in inflammatory and infectious
1161 diseases. Immunol Rev *297*, 139-161. 10.1111/imr.12902.
1162 66. Neil, J.A., Matsuzawa-Ishimoto, Y., Kernbauer-Holzl, E., Schuster, S.L., Sota, S.,
1163 Venzon, M., Dallari, S., Galvao Neto, A., Hine, A., Hudesman, D., et al. (2019). IFN-I
1164 and IL-22 mediate protective effects of intestinal viral infection. Nat Microbiol *4*, 1737-
1165 1749. 10.1038/s41564-019-0470-1.

1166 67. Sugimoto, K., Ogawa, A., Mizoguchi, E., Shimomura, Y., Andoh, A., Bhan, A.K.,
1167 Blumberg, R.S., Xavier, R.J., and Mizoguchi, A. (2008). IL-22 ameliorates intestinal
1168 inflammation in a mouse model of ulcerative colitis. J Clin Invest *118*, 534-544.
1169 10.1172/JCI33194.
1170 68. Chu, H., Khosravi, A., Kusumawardhani, I.P., Kwon, A.H., Vasconcelos, A.C., Cunha,
1171 L.D., Mayer, A.E., Shen, Y., Wu, W.L., Kambal, A., et al. (2016). Gene-microbiota
1172 interactions contribute to the pathogenesis of inflammatory bowel disease. Science *352*,
1173 1116-1120. 10.1126/science.aad9948.
1174 69. Wu, W.H., Kim, M., Chang, L.C., Assie, A., Saldana-Morales, F.B., Zegarra-Ruiz, D.F.,
1175 Norwood, K., Samuel, B.S., and Diehl, G.E. (2022). Interleukin-1beta secretion induced
1176 by mucosa-associated gut commensal bacteria promotes intestinal barrier repair. Gut
1177 Microbes *14*, 2014772. 10.1080/19490976.2021.2014772.
1178 70. Seo, S.U., Kuffa, P., Kitamoto, S., Nagao-Kitamoto, H., Rousseau, J., Kim, Y.G., Nunez,
1179 G., and Kamada, N. (2015). Intestinal macrophages arising from CCR2(+) monocytes
1180 control pathogen infection by activating innate lymphoid cells. Nat Commun *6*, 8010.
1181 10.1038/ncomms9010.
1182 71. Zhou, L., Chu, C., Teng, F., Bessman, N.J., Goc, J., Santosa, E.K., Putzel, G.G., Kabata,
1183 H., Kelsen, J.R., Baldassano, R.N., et al. (2019). Innate lymphoid cells support regulatory
1184 T cells in the intestine through interleukin-2. Nature *568*, 405-409. 10.1038/s41586-019-
1185 1082-x.
1186 72. Inohara, N., Ogura, Y., Fontalba, A., Gutierrez, O., Pons, F., Crespo, J., Fukase, K.,
1187 Inamura, S., Kusumoto, S., Hashimoto, M., et al. (2003). Host recognition of bacterial
1188 muramyl dipeptide mediated through NOD2. Implications for Crohn's disease. J Biol
1189 Chem *278*, 5509-5512. 10.1074/jbc.C200673200.
1190 73. Hugot, J.P., Chamaillard, M., Zouali, H., Lesage, S., Cezard, J.P., Belaiche, J., Almer, S.,
1191 Tysk, C., O'Morain, C.A., Gassull, M., et al. (2001). Association of NOD2 leucine-rich
1192 repeat variants with susceptibility to Crohn's disease. Nature *411*, 599-603.
1193 10.1038/35079107.
1194 74. Murano, T., Okamoto, R., Ito, G., Nakata, T., Hibiya, S., Shimizu, H., Fujii, S., Kano, Y.,
1195 Mizutani, T., Yui, S., et al. (2014). Hes1 promotes the IL-22-mediated antimicrobial
1196 response by enhancing STAT3-dependent transcription in human intestinal epithelial
1197 cells. Biochem Biophys Res Commun *443*, 840-846. 10.1016/j.bbrc.2013.12.061.
1198 75. Winter, S.E., Winter, M.G., Xavier, M.N., Thiennimitr, P., Poon, V., Keestra, A.M.,
1199 Laughlin, R.C., Gomez, G., Wu, J., Lawhon, S.D., et al. (2013). Host-derived nitrate
1200 boosts growth of E. coli in the inflamed gut. Science *339*, 708-711.
1201 10.1126/science.1232467.
1202 76. Lee, J.Y., Tsolis, R.M., and Baumler, A.J. (2022). The microbiome and gut homeostasis.
1203 Science *377*, eabp9960. 10.1126/science.abp9960.
1204 77. Shouval, D.S., Biswas, A., Kang, Y.H., Griffith, A.E., Konnikova, L., Mascanfroni, I.D.,
1205 Redhu, N.S., Frei, S.M., Field, M., Doty, A.L., et al. (2016). Interleukin 1beta Mediates
1206 Intestinal Inflammation in Mice and Patients With Interleukin 10 Receptor Deficiency.
1207 Gastroenterology *151*, 1100-1104. 10.1053/j.gastro.2016.08.055.
1208 78. Kim, D., Kim, Y.G., Seo, S.U., Kim, D.J., Kamada, N., Prescott, D., Chamaillard, M.,
1209 Philpott, D.J., Rosenstiel, P., Inohara, N., and Nunez, G. (2016). Nod2-mediated
1210 recognition of the microbiota is critical for mucosal adjuvant activity of cholera toxin.
1211 Nat Med *22*, 524-530. 10.1038/nm.4075.

1212 79. Martin, P.K., Marchiando, A., Xu, R., Rudensky, E., Yeung, F., Schuster, S.L.,
1213 Kernbauer, E., and Cadwell, K. (2018). Autophagy proteins suppress protective type I
1214 interferon signalling in response to the murine gut microbiota. Nat Microbiol *3*, 1131-
1215 1141. 10.1038/s41564-018-0229-0.
1216 80. Matsuzawa-Ishimoto, Y., Yao, X., Koide, A., Ueberheide, B.M., Axelrad, J.E., Reis,
1217 B.S., Parsa, R., Neil, J.A., Devlin, J.C., Rudensky, E., et al. (2022). The gammadelta IEL
1218 effector API5 masks genetic susceptibility to Paneth cell death. Nature *610*, 547-554.
1219 10.1038/s41586-022-05259-y.
1220 81. Bokulich, N.A., Kaehler, B.D., Rideout, J.R., Dillon, M., Bolyen, E., Knight, R., Huttley,
1221 G.A., and Gregory Caporaso, J. (2018). Optimizing taxonomic classification of marker-
1222 gene amplicon sequences with QIIME 2's q2-feature-classifier plugin. Microbiome *6*, 90.
1223 10.1186/s40168-018-0470-z.
1224 82. Lozupone, C., Lladser, M.E., Knights, D., Stombaugh, J., and Knight, R. (2011).
1225 UniFrac: an effective distance metric for microbial community comparison. ISME J *5*,
1226 169-172. 10.1038/ismej.2010.133.
1227 83. Vazquez-Baeza, Y., Pirrung, M., Gonzalez, A., and Knight, R. (2013). EMPeror: a tool
1228 for visualizing high-throughput microbial community data. Gigascience *2*, 16.
1229 10.1186/2047-217X-2-16.
1230 84. Dallari, S., Heaney, T., Rosas-Villegas, A., Neil, J.A., Wong, S.Y., Brown, J.J., Urbanek,
1231 K., Herrmann, C., Depledge, D.P., Dermody, T.S., and Cadwell, K. (2021). Enteric
1232 viruses evoke broad host immune responses resembling those elicited by the bacterial
1233 microbiome. Cell Host Microbe *29*, 1014-1029 e1018. 10.1016/j.chom.2021.03.015.
1234 85. Jang, K.K., Kaczmarek, M.E., Dallari, S., Chen, Y.H., Tada, T., Axelrad, J., Landau,
1235 N.R., Stapleford, K.A., and Cadwell, K. (2022). Variable susceptibility of intestinal
1236 organoid-derived monolayers to SARS-CoV-2 infection. PLoS Biol *20*, e3001592.
1237 10.1371/journal.pbio.3001592.
1238

Figure 1

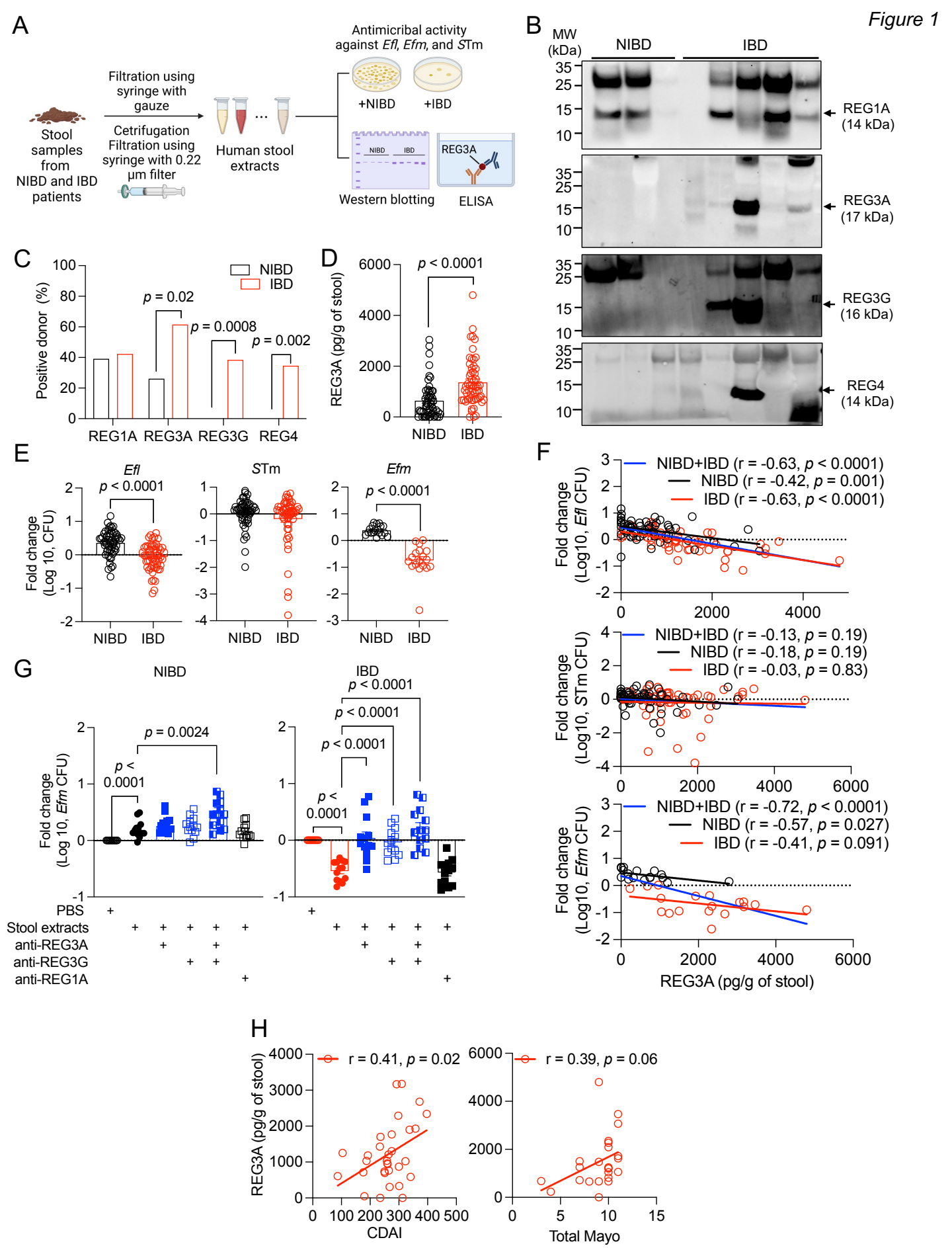
A
Stool samples from NIBD and IBD patients
Filtration using syringe with gauze
Cetrifugation
Filtration using syringe with 0.22 µm filter
Human stool extracts
Antimicribal activity against Efl, Efm, and STm
+NIBD
+IBD
Western blotting
REG3A
ELISA
B
MW (kDa)
NIBD
IBD
REG1A (14 kDa)
REG3A (17 kDa)
REG3G (16 kDa)
REG4 (14 kDa)
C
Positive donor (%)
NIBD
IBD
p = 0.02
p = 0.0008
p = 0.002
REG1A REG3A REG3G REG4
D
REG3A (pg/g of stool)
p < 0.0001
NIBD IBD
E
Efl
STm
Efm
Fold change (Log 10, CFU)
p < 0.0001
NIBD IBD
F
Fold change (Log10, Efl CFU)
NIBD+IBD (r = -0.63, p < 0.0001)
NIBD (r = -0.42, p = 0.001)
IBD (r = -0.63, p < 0.0001)
Fold change (Log10, STm CFU)
NIBD+IBD (r = -0.13, p = 0.19)
NIBD (r = -0.18, p = 0.19)
IBD (r = -0.03, p = 0.83)
Fold change (Log10, Efm CFU)
NIBD+IBD (r = -0.72, p < 0.0001)
NIBD (r = -0.57, p = 0.027)
IBD (r = -0.41, p = 0.091)
REG3A (pg/g of stool)
G
NIBD
IBD
Fold change (Log 10, Efm CFU)
p = 0.0024
p < 0.0001
PBS
Stool extracts
anti-REG3A
anti-REG3G
anti-REG1A
H
REG3A (pg/g of stool)
r = 0.41, p = 0.02
CDAI
r = 0.39, p = 0.06
Total Mayo

Figure 2

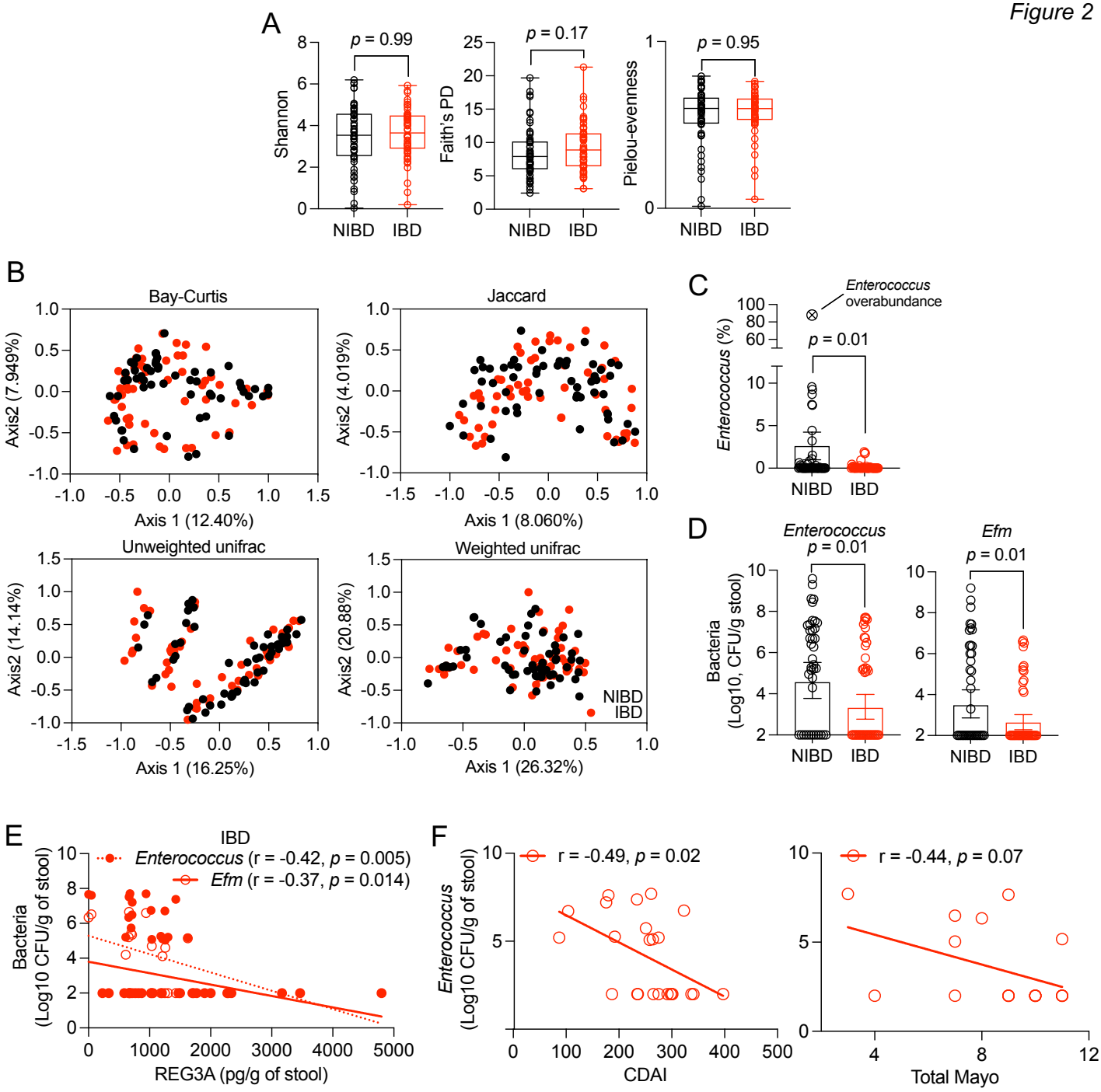
A
Shannon
p = 0.99
Faith's PD
p = 0.17
Pielou-evenness
p = 0.95
NIBD
IBD
B
Bay-Curtis
Jaccard
Unweighted unifrac
Weighted unifrac
Axis2 (7.949%)
Axis 1 (12.40%)
Axis2 (4.019%)
Axis 1 (8.060%)
Axis2 (14.14%)
Axis 1 (16.25%)
Axis2 (20.88%)
Axis 1 (26.32%)
NIBD
IBD
C
Enterococcus overabundance
Enterococcus (%)
p = 0.01
NIBD
IBD
D
Enterococcus
p = 0.01
Efm
p = 0.01
Bacteria (Log10, CFU/g stool)
NIBD
IBD
E
IBD
Enterococcus (r = -0.42, p = 0.005)
Efm (r = -0.37, p = 0.014)
Bacteria (Log10 CFU/g of stool)
REG3A (pg/g of stool)
F
r = -0.49, p = 0.02
Enterococcus (Log10 CFU/g of stool)
CDAI
r = -0.44, p = 0.07
Total Mayo

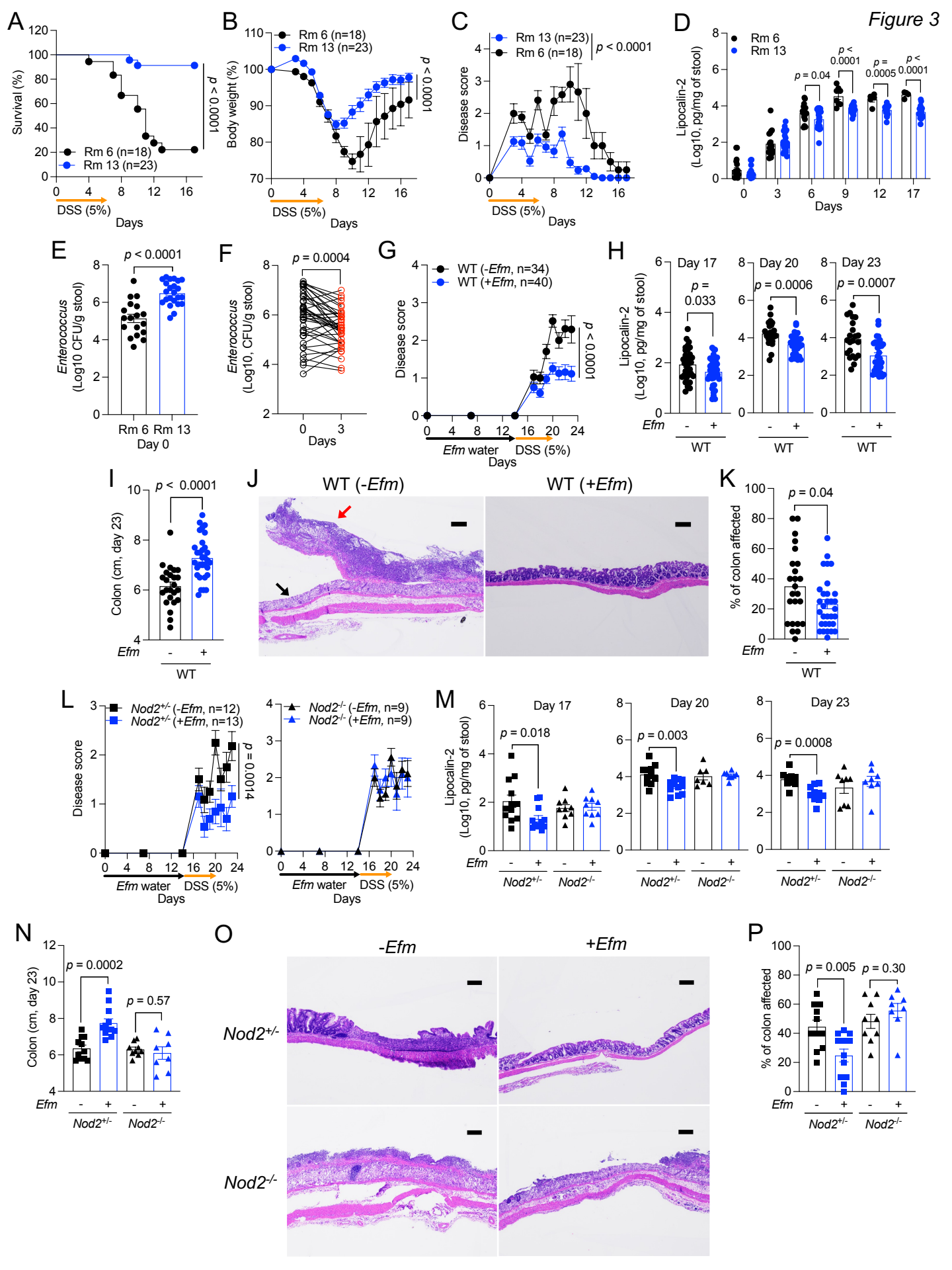
Figure 3
A
Survival (%)
Rm 6 (n=18)
Rm 13 (n=23)
p < 0.0001
DSS (5%)
Days
B
Body weight (%)
Rm 6 (n=18)
Rm 13 (n=23)
p < 0.0001
DSS (5%)
Days
C
Disease score
Rm 13 (n=23)
Rm 6 (n=18)
p < 0.0001
DSS (5%)
Days
D
Lipocalin-2 (Log10, pg/mg of stool)
Rm 6
Rm 13
p = 0.04
p < 0.0001
p = 0.0005
p < 0.0001
Days
E
Enterococcus (Log10 CFU/g stool)
p < 0.0001
Rm 6
Rm 13
Day 0
F
Enterococcus (Log10, CFU/g stool)
p = 0.0004
Days
G
Disease score
WT (-Efm, n=34)
WT (+Efm, n=40)
p < 0.0001
Efm water
DSS (5%)
Days
H
Lipocalin-2 (Log10, pg/mg of stool)
Day 17
Day 20
Day 23
p = 0.033
p = 0.0006
p = 0.0007
Efm
WT
I
Colon (cm, day 23)
p < 0.0001
Efm
WT
J
WT (-Efm)
WT (+Efm)
K
% of colon affected
p = 0.04
Efm
WT
L
Disease score
Nod2+/- (-Efm, n=12)
Nod2+/- (+Efm, n=13)
Nod2-/- (-Efm, n=9)
Nod2-/- (+Efm, n=9)
p = 0.0014
Efm water
DSS (5%)
Days
M
Lipocalin-2 (Log10, pg/mg of stool)
Day 17
Day 20
Day 23
p = 0.018
p = 0.003
p = 0.0008
Efm
Nod2+/-
Nod2-/-
N
Colon (cm, day 23)
p = 0.0002
p = 0.57
Efm
Nod2+/-
Nod2-/-
O
-Efm
+Efm
Nod2+/-
Nod2-/-
P
% of colon affected
p = 0.005
p = 0.30
Efm
Nod2+/-
Nod2-/-

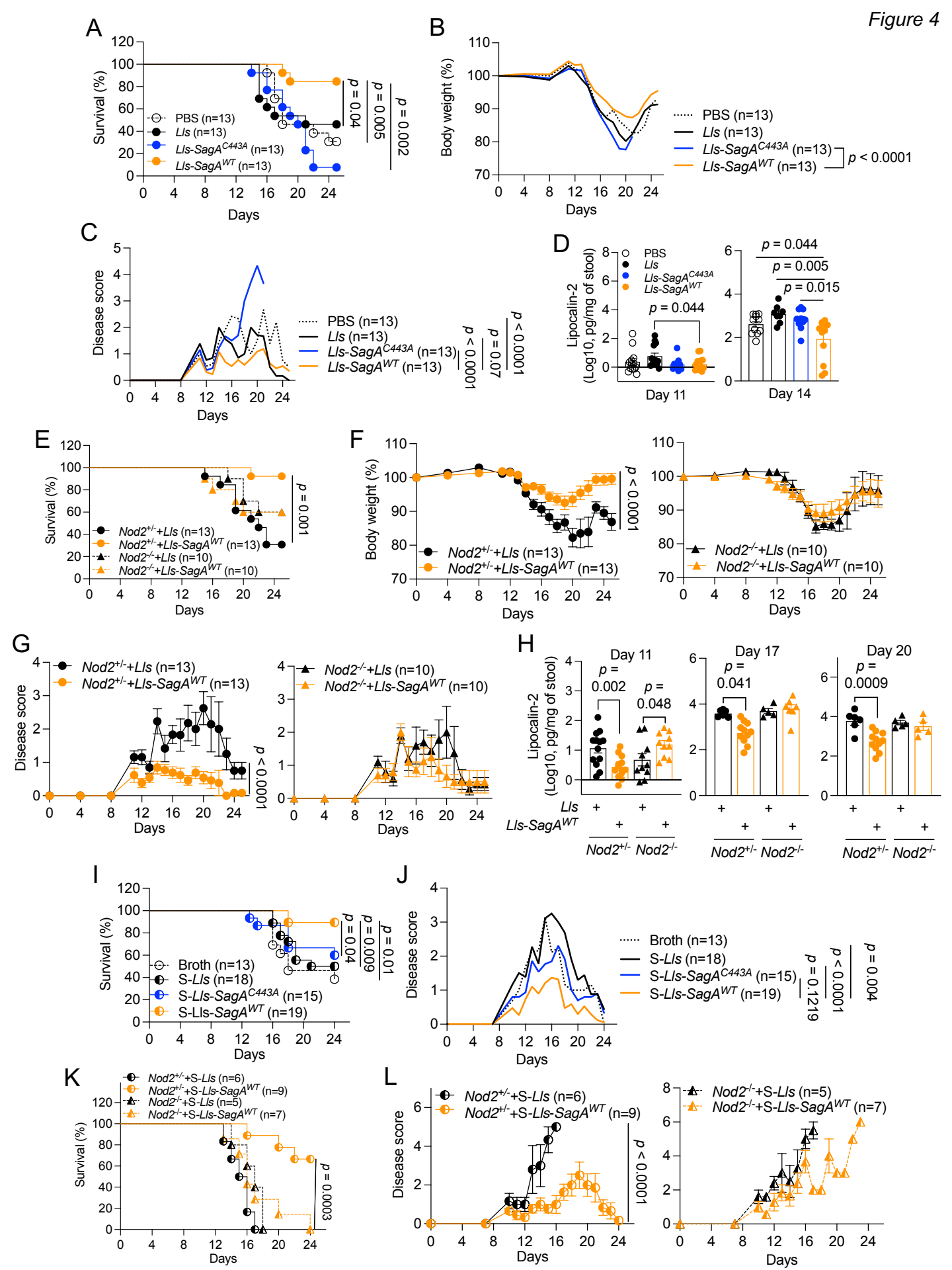
Figure 4
A
Survival (%)
Days
PBS (n=13)
Lls (n=13)
Lls-SagA^C443A (n=13)
Lls-SagA^WT (n=13)
p = 0.04
p = 0.005
p = 0.002
B
Body weight (%)
Days
PBS (n=13)
Lls (n=13)
Lls-SagA^C443A (n=13)
Lls-SagA^WT (n=13)
p < 0.0001
C
Disease score
Days
PBS (n=13)
Lls (n=13)
Lls-SagA^C443A (n=13)
Lls-SagA^WT (n=13)
p < 0.0001
p = 0.07
p < 0.0001
D
Lipocalin-2 (Log10, pg/mg of stool)
PBS
Lls
Lls-SagA^C443A
Lls-SagA^WT
p = 0.044
Day 11
p = 0.044
p = 0.005
p = 0.015
Day 14
E
Survival (%)
Days
Nod2+/-+Lls (n=13)
Nod2+/-+Lls-SagA^WT (n=13)
Nod2-/-+Lls (n=10)
Nod2-/-+Lls-SagA^WT (n=10)
p = 0.001
F
Body weight (%)
Days
Nod2+/-+Lls (n=13)
Nod2+/-+Lls-SagA^WT (n=13)
p < 0.0001
Nod2-/-+Lls (n=10)
Nod2-/-+Lls-SagA^WT (n=10)
G
Disease score
Days
Nod2+/-+Lls (n=13)
Nod2+/-+Lls-SagA^WT (n=13)
p < 0.0001
Nod2-/-+Lls (n=10)
Nod2-/-+Lls-SagA^WT (n=10)
H
Lipocalin-2 (Log10, pg/mg of stool)
Day 11
p = 0.002
p = 0.048
Day 17
p = 0.041
Day 20
p = 0.0009
Lls
Lls-SagA^WT
Nod2+/-
Nod2-/-
I
Survival (%)
Days
Broth (n=13)
S-Lls (n=18)
S-Lls-SagA^C443A (n=15)
S-Lls-SagA^WT (n=19)
p = 0.04
p = 0.009
p = 0.01
J
Disease score
Days
Broth (n=13)
S-Lls (n=18)
S-Lls-SagA^C443A (n=15)
S-Lls-SagA^WT (n=19)
p = 0.1219
p < 0.0001
p = 0.004
K
Survival (%)
Days
Nod2+/-+S-Lls (n=6)
Nod2+/-+S-Lls-SagA^WT (n=9)
Nod2-/-+S-Lls (n=5)
Nod2-/-+S-Lls-SagA^WT (n=7)
p = 0.0003
L
Disease score
Days
Nod2+/-+S-Lls (n=6)
Nod2+/-+S-Lls-SagA^WT (n=9)
p < 0.0001
Nod2-/-+S-Lls (n=5)
Nod2-/-+S-Lls-SagA^WT (n=7)

Figure 5

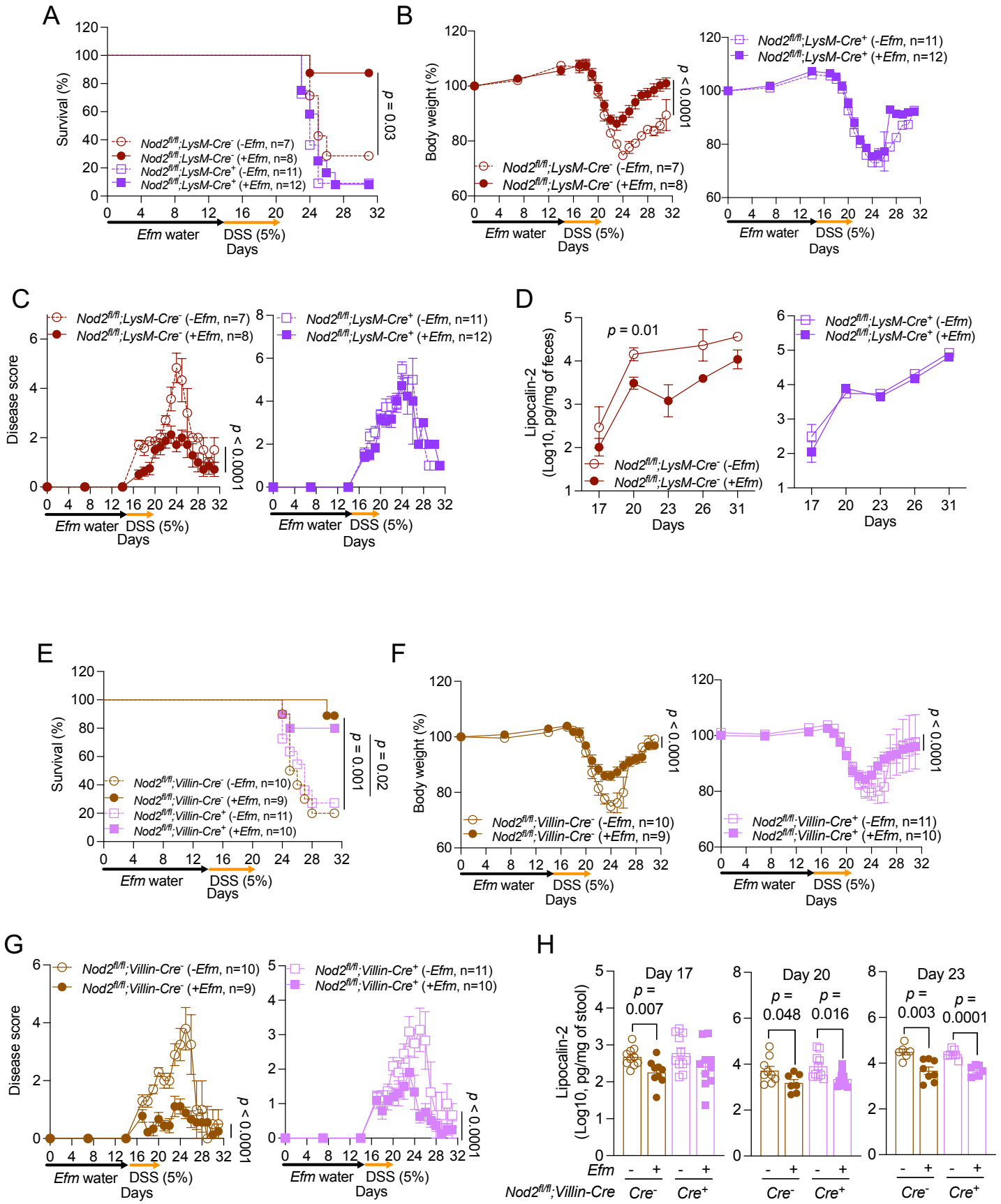
A
Survival (%)
Nod2fl/fl;LysM-Cre- (-Efm, n=7)
Nod2fl/fl;LysM-Cre- (+Efm, n=8)
Nod2fl/fl;LysM-Cre+ (-Efm, n=11)
Nod2fl/fl;LysM-Cre+ (+Efm, n=12)
p = 0.03
Efm water
DSS (5%)
Days
B
Body weight (%)
Nod2fl/fl;LysM-Cre- (-Efm, n=7)
Nod2fl/fl;LysM-Cre- (+Efm, n=8)
p < 0.0001
Nod2fl/fl;LysM-Cre+ (-Efm, n=11)
Nod2fl/fl;LysM-Cre+ (+Efm, n=12)
C
Disease score
Nod2fl/fl;LysM-Cre- (-Efm, n=7)
Nod2fl/fl;LysM-Cre- (+Efm, n=8)
p < 0.0001
Nod2fl/fl;LysM-Cre+ (-Efm, n=11)
Nod2fl/fl;LysM-Cre+ (+Efm, n=12)
D
Lipocalin-2 (Log10, pg/mg of feces)
p = 0.01
Nod2fl/fl;LysM-Cre- (-Efm)
Nod2fl/fl;LysM-Cre- (+Efm)
Nod2fl/fl;LysM-Cre+ (-Efm)
Nod2fl/fl;LysM-Cre+ (+Efm)
E
Survival (%)
Nod2fl/fl;Villin-Cre- (-Efm, n=10)
Nod2fl/fl;Villin-Cre- (+Efm, n=9)
Nod2fl/fl;Villin-Cre+ (-Efm, n=11)
Nod2fl/fl;Villin-Cre+ (+Efm, n=10)
p = 0.001
p = 0.02
F
Body weight (%)
Nod2fl/fl;Villin-Cre- (-Efm, n=10)
Nod2fl/fl;Villin-Cre- (+Efm, n=9)
p < 0.0001
Nod2fl/fl;Villin-Cre+ (-Efm, n=11)
Nod2fl/fl;Villin-Cre+ (+Efm, n=10)
G
Disease score
Nod2fl/fl;Villin-Cre- (-Efm, n=10)
Nod2fl/fl;Villin-Cre- (+Efm, n=9)
p < 0.0001
Nod2fl/fl;Villin-Cre+ (-Efm, n=11)
Nod2fl/fl;Villin-Cre+ (+Efm, n=10)
H
Lipocalin-2 (Log10, pg/mg of stool)
Day 17
p = 0.007
Day 20
p = 0.048
p = 0.016
Day 23
p = 0.003
p = 0.0001
Efm
Nod2fl/fl;Villin-Cre
Cre-
Cre+

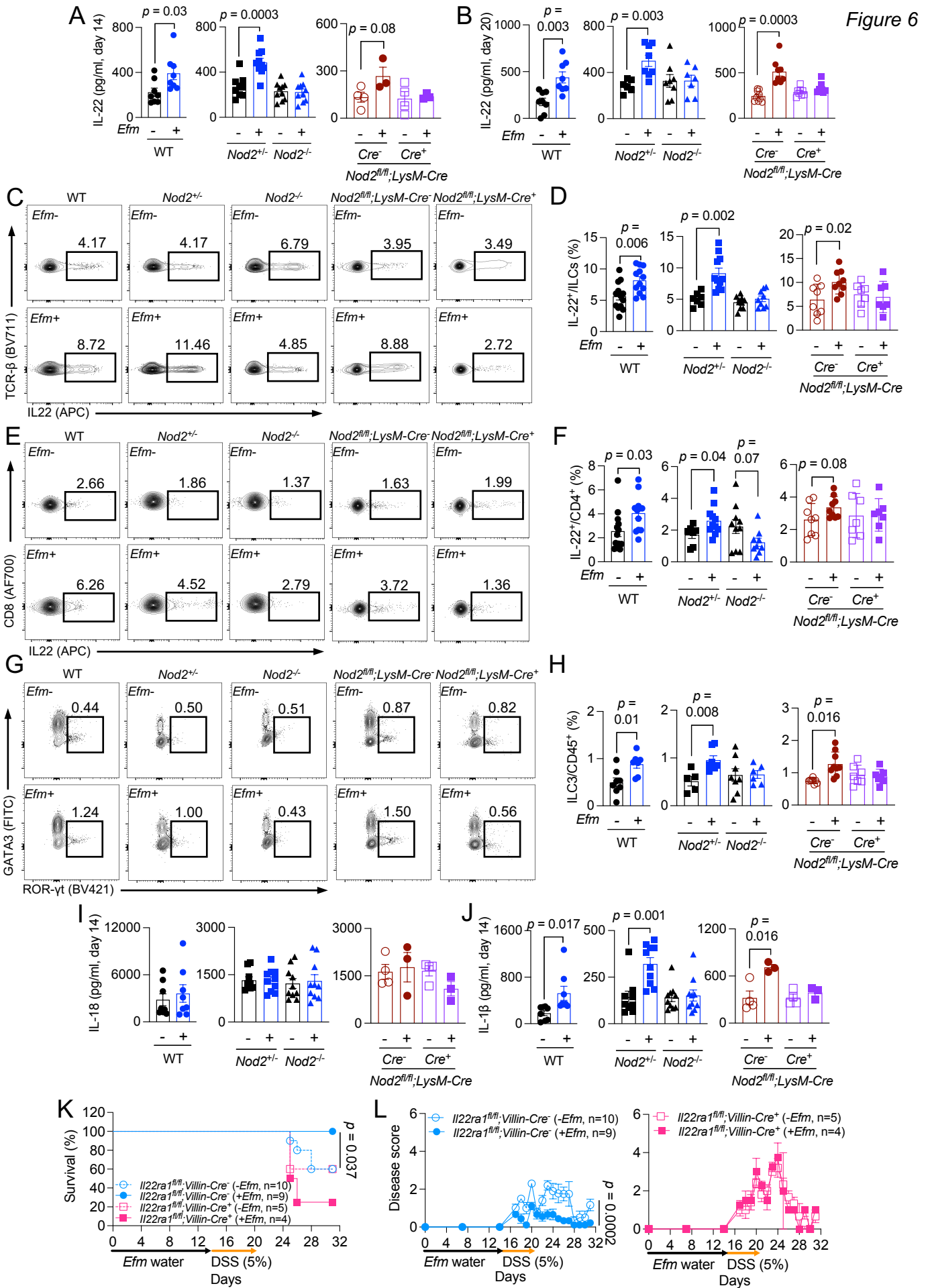
Figure 6
A
IL-22 (pg/ml, day 14)
p = 0.03
p = 0.0003
p = 0.08
Efm
WT
Nod2+/-
Nod2-/-
Cre-
Cre+
Nod2fl/fl;LysM-Cre
B
IL-22 (pg/ml, day 20)
p = 0.003
p = 0.003
p = 0.0003
C
WT
Nod2+/-
Nod2-/-
Nod2fl/fl;LysM-Cre-
Nod2fl/fl;LysM-Cre+
Efm-
Efm+
4.17
4.17
6.79
3.95
3.49
8.72
11.46
4.85
8.88
2.72
TCR-β (BV711)
IL22 (APC)
D
IL-22+/ILCs (%)
p = 0.006
p = 0.002
p = 0.02
E
2.66
1.86
1.37
1.63
1.99
6.26
4.52
2.79
3.72
1.36
CD8 (AF700)
F
IL-22+/CD4+ (%)
p = 0.03
p = 0.04
p = 0.07
p = 0.08
G
0.44
0.50
0.51
0.87
0.82
1.24
1.00
0.43
1.50
0.56
GATA3 (FITC)
ROR-γt (BV421)
H
ILC3/CD45+ (%)
p = 0.01
p = 0.008
p = 0.016
I
IL-18 (pg/ml, day 14)
J
IL-1β (pg/ml, day 14)
p = 0.017
p = 0.001
p = 0.016
K
Survival (%)
Il22ra1fl/fl;Villin-Cre- (-Efm, n=10)
Il22ra1fl/fl;Villin-Cre- (+Efm, n=9)
Il22ra1fl/fl;Villin-Cre+ (-Efm, n=5)
Il22ra1fl/fl;Villin-Cre+ (+Efm, n=4)
p = 0.037
Efm water
DSS (5%)
Days
L
Disease score
Il22ra1fl/fl;Villin-Cre- (-Efm, n=10)
Il22ra1fl/fl;Villin-Cre- (+Efm, n=9)
Il22ra1fl/fl;Villin-Cre+ (-Efm, n=5)
Il22ra1fl/fl;Villin-Cre+ (+Efm, n=4)
p = 0.0002

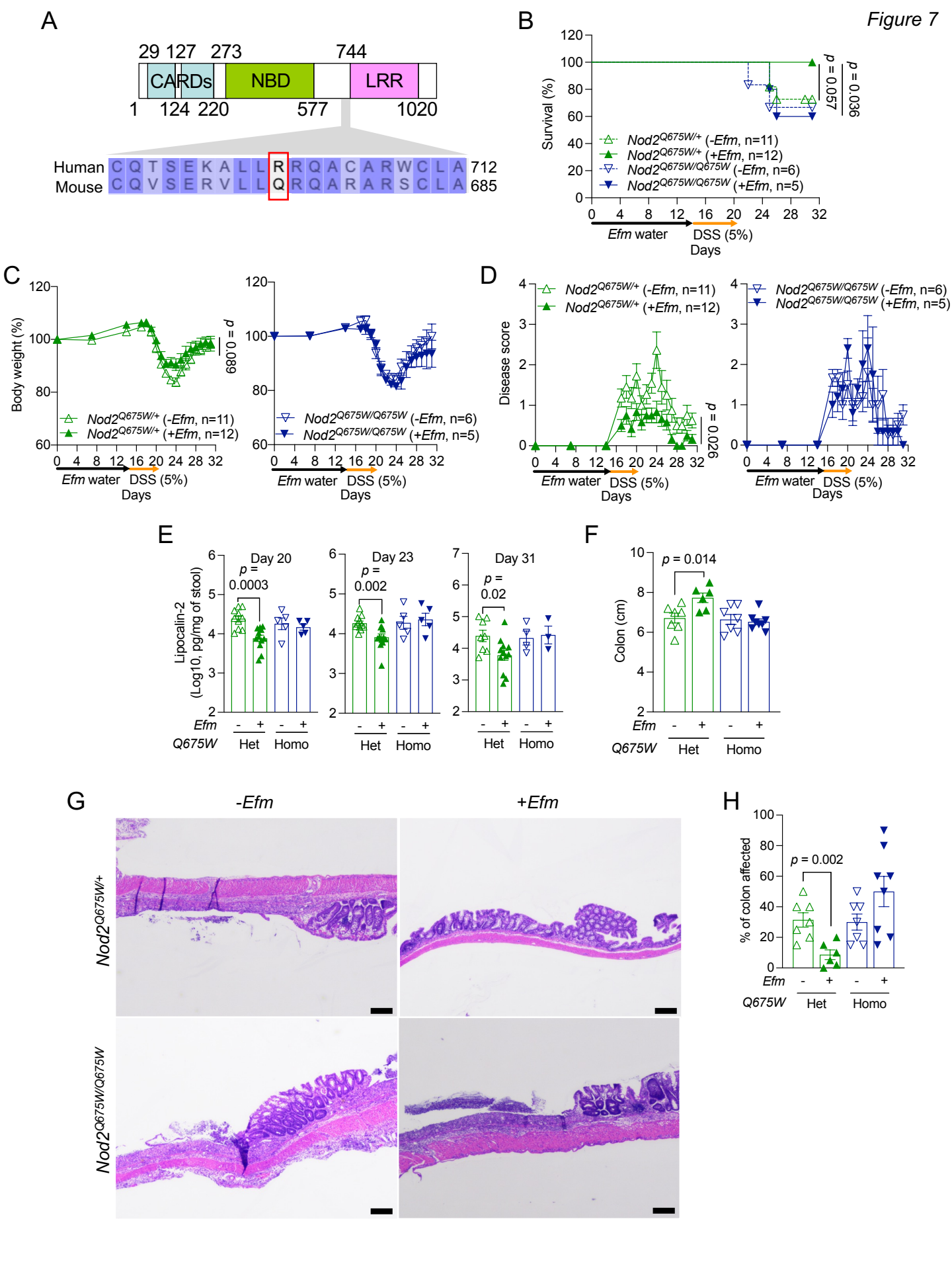
Figure 7
A
29 127 273 744
CARDs
NBD
LRR
1 124 220 577 1020
Human C Q T S E K A L L R R Q A C A R W C L A 712
Mouse C Q V S E R V L L Q R Q A R A R S C L A 685
B
Survival (%)
p = 0.057
p = 0.036
Nod2Q675W/+ (-Efm, n=11)
Nod2Q675W/+ (+Efm, n=12)
Nod2Q675W/Q675W (-Efm, n=6)
Nod2Q675W/Q675W (+Efm, n=5)
Efm water
DSS (5%)
Days
C
Body weight (%)
p = 0.089
Nod2Q675W/+ (-Efm, n=11)
Nod2Q675W/+ (+Efm, n=12)
Nod2Q675W/Q675W (-Efm, n=6)
Nod2Q675W/Q675W (+Efm, n=5)
Efm water
DSS (5%)
Days
D
Disease score
p = 0.026
Nod2Q675W/+ (-Efm, n=11)
Nod2Q675W/+ (+Efm, n=12)
Nod2Q675W/Q675W (-Efm, n=6)
Nod2Q675W/Q675W (+Efm, n=5)
Efm water
DSS (5%)
Days
E
Lipocalin-2 (Log10, pg/mg of stool)
Day 20
p = 0.0003
Day 23
p = 0.002
Day 31
p = 0.02
Efm
Q675W
Het
Homo
F
Colon (cm)
p = 0.014
Efm
Q675W
Het
Homo
G
-Efm
+Efm
Nod2Q675W/+
Nod2Q675W/Q675W
H
% of colon affected
p = 0.002
Efm
Q675W
Het
Homo

Supplemental Figure 1

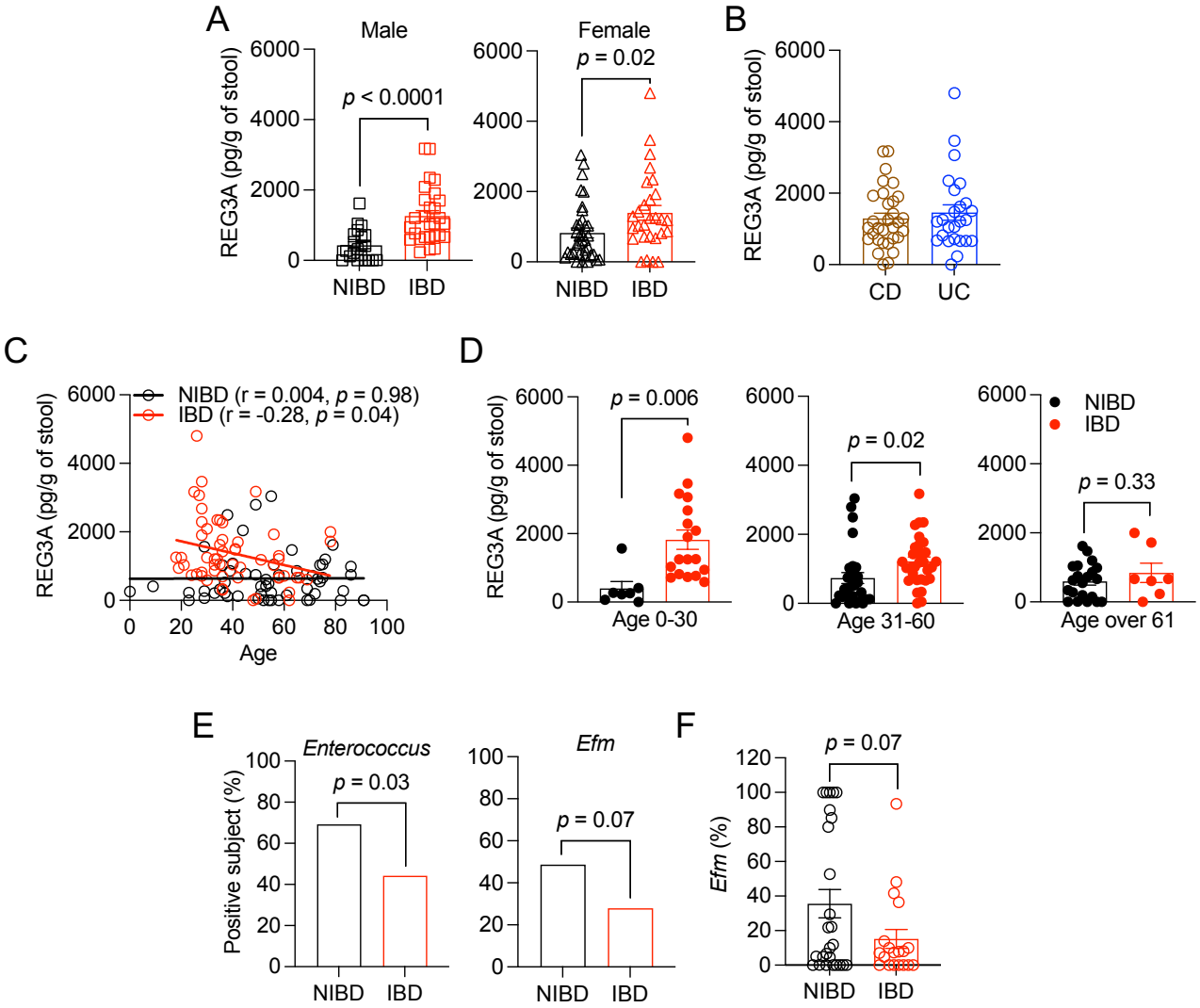

Supplemental Figure 2

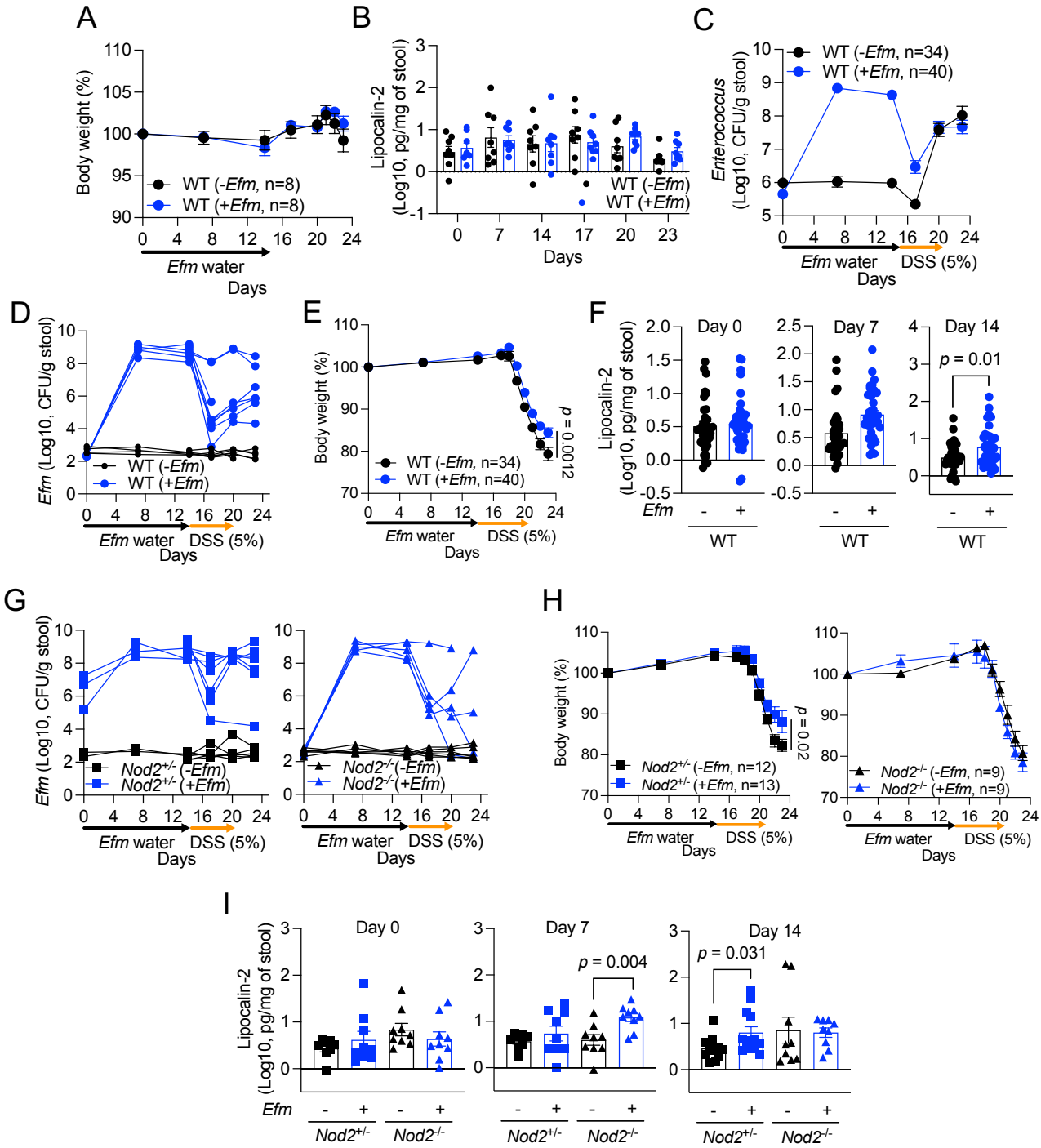

Supplemental Figure 3

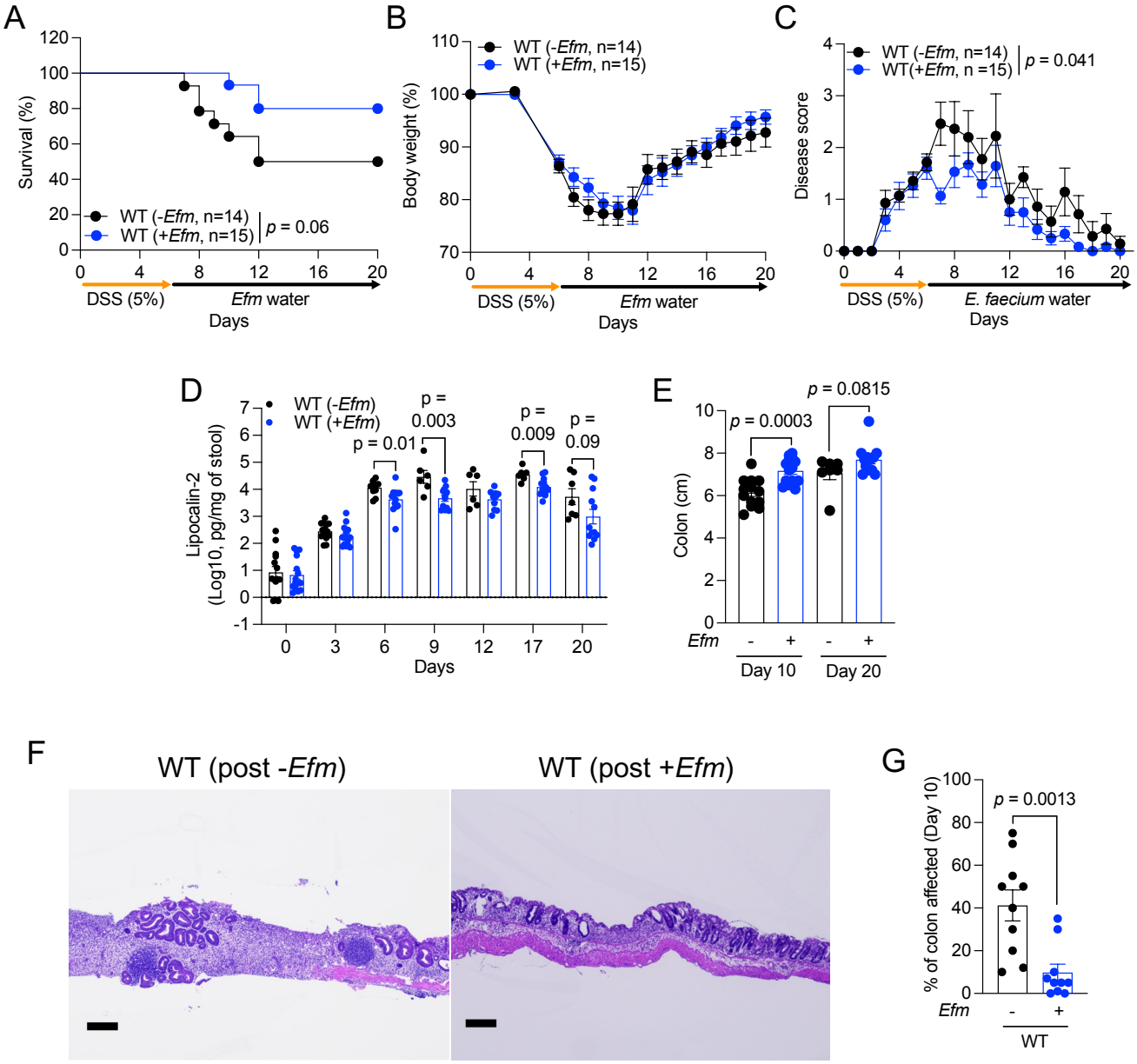

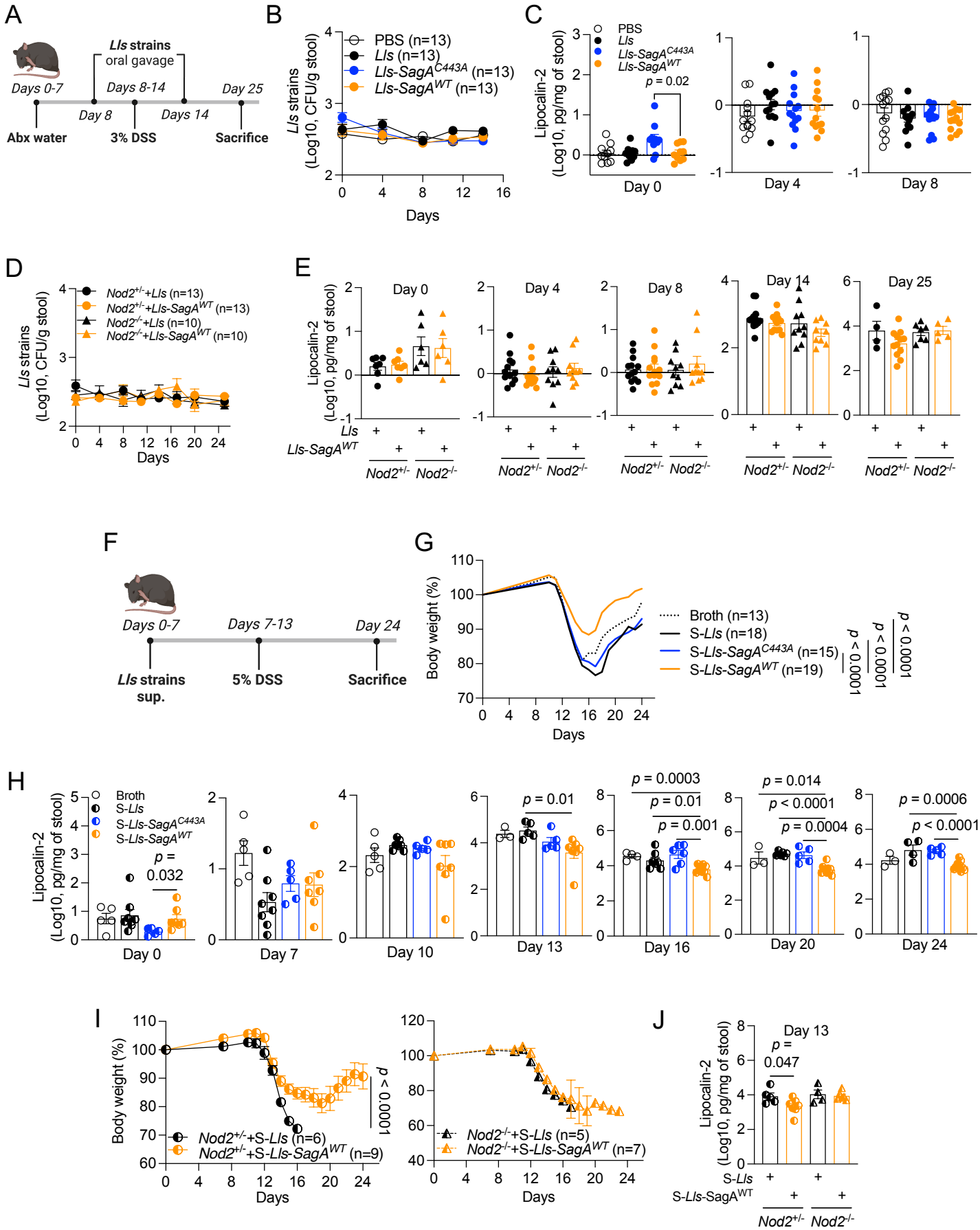
A
Lls strains
oral gavage
Days 0-7
Days 8-14
Day 25
Day 8
Days 14
Abx water
3% DSS
Sacrifice
B
Lls strains (Log10, CFU/g stool)
PBS (n=13)
Lls (n=13)
Lls-SagA^C443A (n=13)
Lls-SagA^WT (n=13)
Days
C
Lipocalin-2 (Log10, pg/mg of stool)
PBS
Lls
Lls-SagA^C443A
Lls-SagA^WT
p = 0.02
Day 0
Day 4
Day 8
D
Lls strains (Log10, CFU/g stool)
Nod2+/-+Lls (n=13)
Nod2+/-+Lls-SagA^WT (n=13)
Nod2-/-+Lls (n=10)
Nod2-/-+Lls-SagA^WT (n=10)
Days
E
Lipocalin-2 (Log10, pg/mg of stool)
Day 0
Day 4
Day 8
Day 14
Day 25
Lls
Lls-SagA^WT
Nod2+/-
Nod2-/-
F
Days 0-7
Days 7-13
Day 24
Lls strains sup.
5% DSS
Sacrifice
G
Body weight (%)
Broth (n=13)
S-Lls (n=18)
S-Lls-SagA^C443A (n=15)
S-Lls-SagA^WT (n=19)
p < 0.0001
p < 0.0001
p < 0.0001
Days
H
Lipocalin-2 (Log10, pg/mg of stool)
Broth
S-Lls
S-Lls-SagA^C443A
S-Lls-SagA^WT
p = 0.032
Day 0
Day 7
Day 10
p = 0.01
Day 13
p = 0.0003
p = 0.01
p = 0.001
Day 16
p = 0.014
p < 0.0001
p = 0.0004
Day 20
p = 0.0006
p < 0.0001
Day 24
I
Body weight (%)
Nod2+/-+S-Lls (n=6)
Nod2+/-+S-Lls-SagA^WT (n=9)
p < 0.0001
Days
Nod2-/-+S-Lls (n=5)
Nod2-/-+S-Lls-SagA^WT (n=7)
Days
J
Lipocalin-2 (Log10, pg/mg of stool)
Day 13
p = 0.047
S-Lls
S-Lls-SagA^WT
Nod2+/-
Nod2-/-

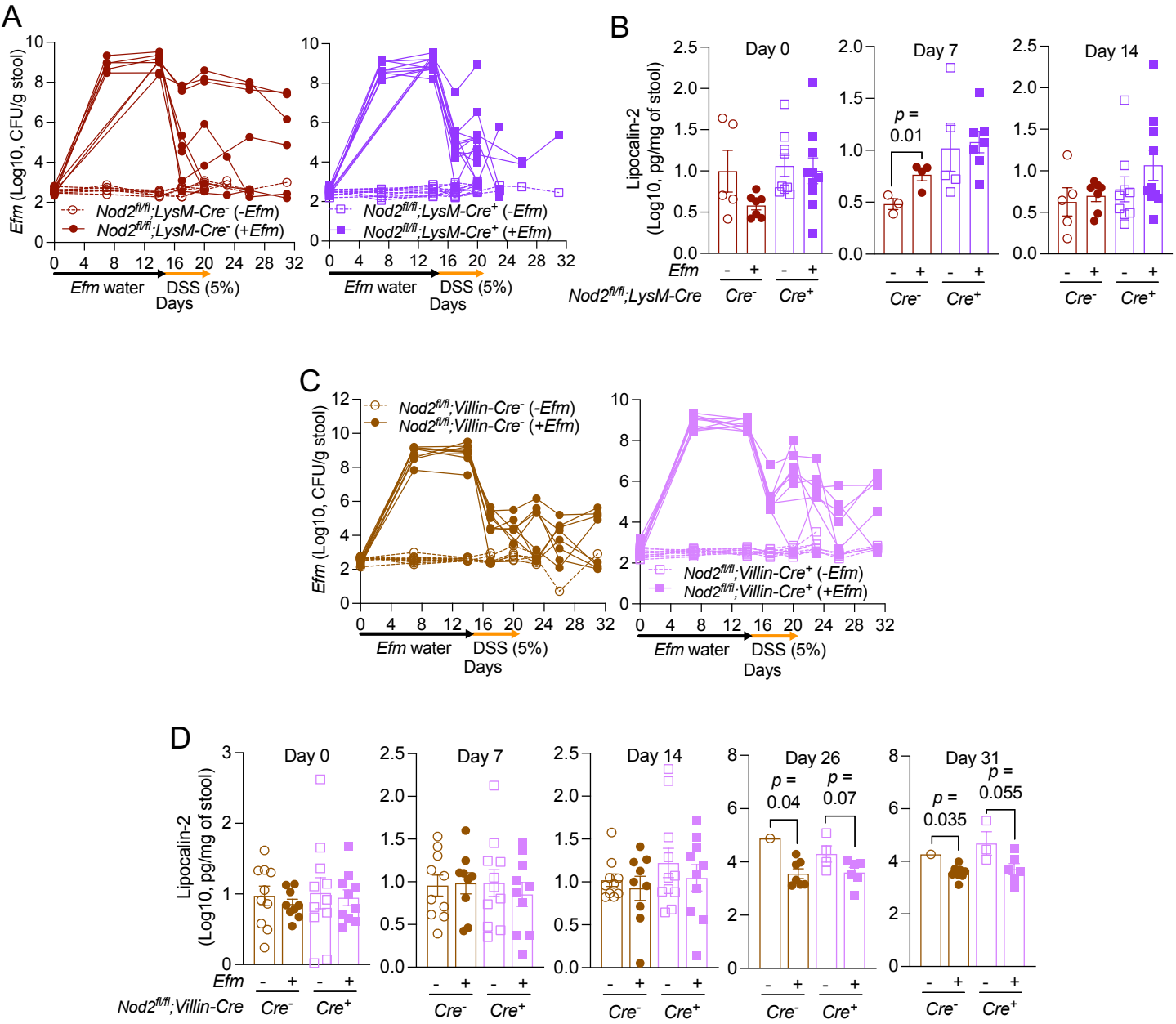
A
Efm (Log10, CFU/g stool)
Nod2fl/fl;LysM-Cre- (-Efm)
Nod2fl/fl;LysM-Cre- (+Efm)
Nod2fl/fl;LysM-Cre+ (-Efm)
Nod2fl/fl;LysM-Cre+ (+Efm)
Efm water
DSS (5%)
Days
B
Lipocalin-2 (Log10, pg/mg of stool)
Day 0
Day 7
Day 14
p = 0.01
Efm
Nod2fl/fl;LysM-Cre
Cre-
Cre+
C
Efm (Log10, CFU/g stool)
Nod2fl/fl;Villin-Cre- (-Efm)
Nod2fl/fl;Villin-Cre- (+Efm)
Nod2fl/fl;Villin-Cre+ (-Efm)
Nod2fl/fl;Villin-Cre+ (+Efm)
Efm water
DSS (5%)
Days
D
Lipocalin-2 (Log10, pg/mg of stool)
Day 0
Day 7
Day 14
Day 26
Day 31
p = 0.04
p = 0.07
p = 0.035
p = 0.055
Efm
Nod2fl/fl;Villin-Cre
Cre-
Cre+

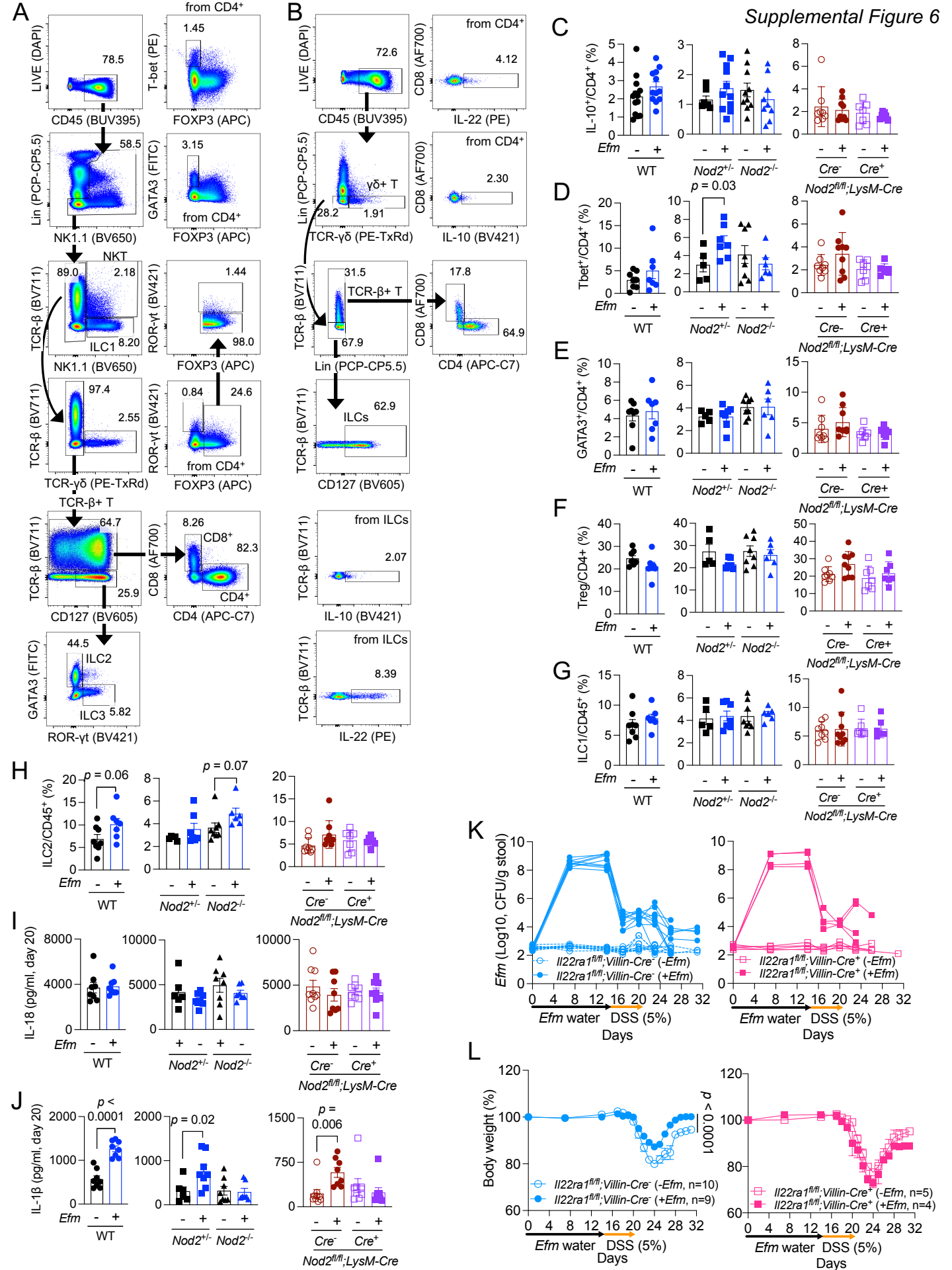
Supplemental Figure 6
A
B
C
D
E
F
G
H
I
J
K
L
LIVE (DAPI)
CD45 (BUV395)
T-bet (PE)
FOXP3 (APC)
Lin (PCP-CP5.5)
NK1.1 (BV650)
GATA3 (FITC)
NKT
ILC1
ILC2
ILC3
TCR-β (BV711)
TCR-γδ (PE-TxRd)
ROR-γt (BV421)
TCR-β+ T
CD8 (AF700)
CD4 (APC-C7)
CD127 (BV605)
IL-22 (PE)
IL-10 (BV421)
γδ+ T
ILCs
from ILCs
from CD4+
IL-10+/CD4+ (%)
Tbet+/CD4+ (%)
GATA3+/CD4+ (%)
Treg/CD4+ (%)
ILC1/CD45+ (%)
ILC2/CD45+ (%)
IL-18 (pg/ml, day 20)
IL-1β (pg/ml, day 20)
Efm
WT
Nod2+/-
Nod2-/-
Cre-
Cre+
Nod2fl/fl;LysM-Cre
p = 0.03
p = 0.06
p = 0.07
p < 0.0001
p = 0.02
p = 0.006
Efm (Log10, CFU/g stool)
Il22ra1fl/fl;Villin-Cre- (-Efm)
Il22ra1fl/fl;Villin-Cre- (+Efm)
Il22ra1fl/fl;Villin-Cre+ (-Efm)
Il22ra1fl/fl;Villin-Cre+ (+Efm)
Efm water
DSS (5%)
Days
Body weight (%)
Il22ra1fl/fl;Villin-Cre- (-Efm, n=10)
Il22ra1fl/fl;Villin-Cre- (+Efm, n=9)
Il22ra1fl/fl;Villin-Cre+ (-Efm, n=5)
Il22ra1fl/fl;Villin-Cre+ (+Efm, n=4)

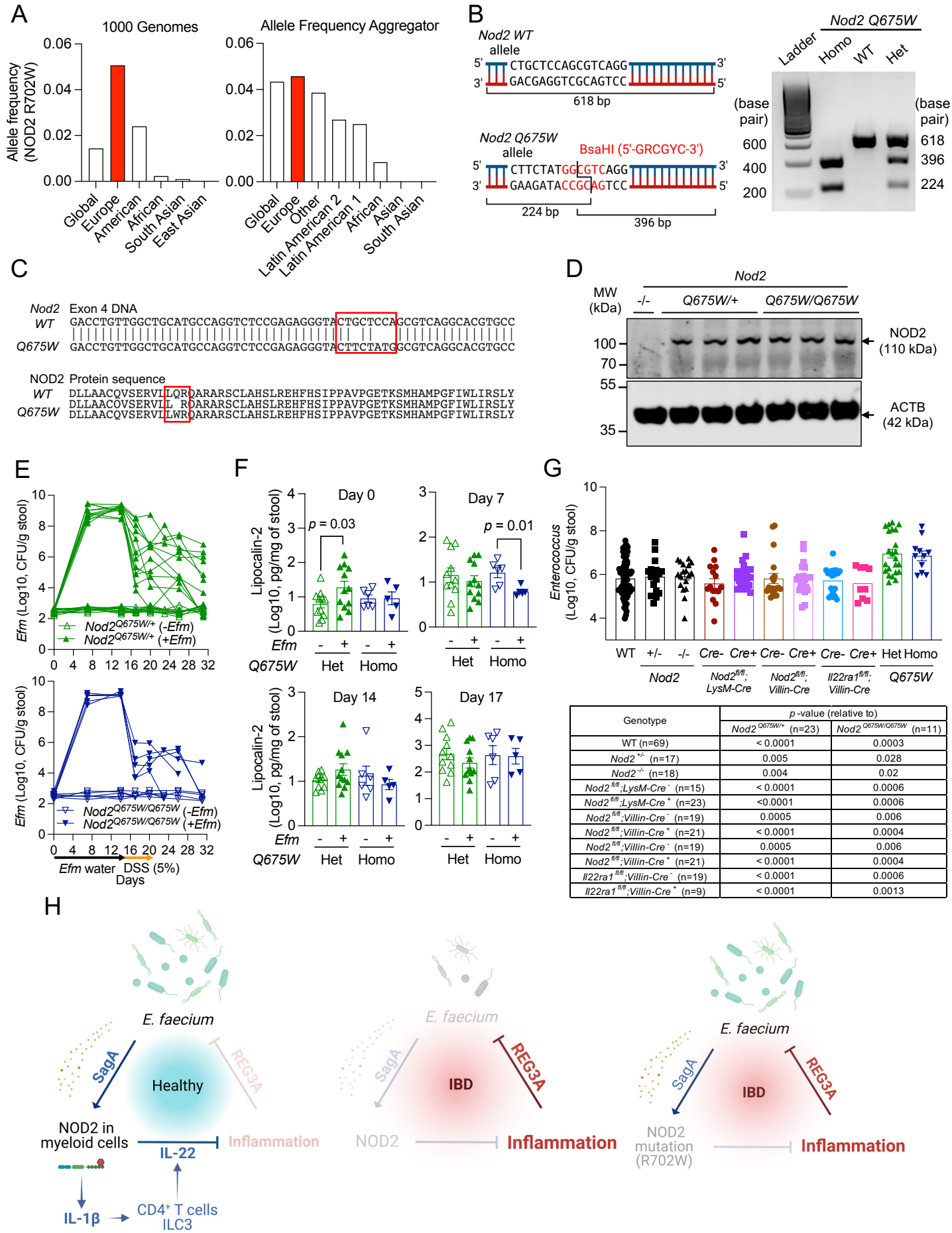

Genotype	*p*-value (relative to)	
	Nod2$^{Q675W/+}$ (n=23)	*Nod2*$^{Q675W/Q675W}$ (n=11)
WT (n=69)	< 0.0001	0.0003
Nod2$^{+/-}$ (n=17)	0.005	0.028
Nod2$^{-/-}$ (n=18)	0.004	0.02
Nod2$^{fl/fl}$;*LysM-Cre*$^{-}$ (n=15)	< 0.0001	0.0006
Nod2$^{fl/fl}$;*LysM-Cre*$^{+}$ (n=23)	<0.0001	0.0006
Nod2$^{fl/fl}$;*Villin-Cre*$^{-}$ (n=19)	0.0005	0.006
Nod2$^{fl/fl}$;*Villin-Cre*$^{+}$ (n=21)	< 0.0001	0.0004
Nod2$^{fl/fl}$;*Villin-Cre*$^{-}$ (n=19)	0.0005	0.006
Nod2$^{fl/fl}$;*Villin-Cre*$^{+}$ (n=21)	< 0.0001	0.0004
Il22ra1$^{fl/fl}$;*Villin-Cre*$^{-}$ (n=19)	< 0.0001	0.0006
Il22ra1$^{fl/fl}$;*Villin-Cre*$^{+}$ (n=9)	< 0.0001	0.0013